

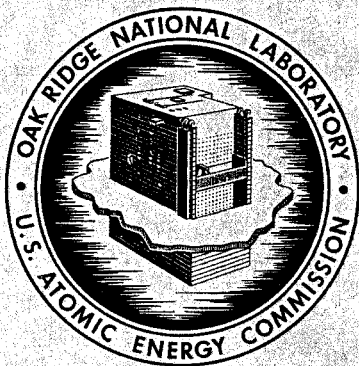
DATE ISSUED: DEC 13 1971

ORNL
MASTER COPY

ORNL-4714 *107*
UC-25 - Metals, Ceramics, and Materials

POSTIRRADIATION EXAMINATION AND
EVALUATION OF THE PERFORMANCE
OF HFIR FUEL ELEMENTS

A. E. Richt
R. W. Knight
G. M. Adamson, Jr.



OAK RIDGE NATIONAL LABORATORY

operated by

UNION CARBIDE CORPORATION

for the

U.S. ATOMIC ENERGY COMMISSION

Printed in the United States of America. Available from
National Technical Information Service
U.S. Department of Commerce
5285 Port Royal Road, Springfield, Virginia 22151
Price: Printed Copy \$3.00; Microfiche \$0.95

This report was prepared as an account of work sponsored by the United States Government. Neither the United States nor the United States Atomic Energy Commission, nor any of their employees, nor any of their contractors, subcontractors, or their employees, makes any warranty, express or implied, or assumes any legal liability or responsibility for the accuracy, completeness or usefulness of any information, apparatus, product or process disclosed, or represents that its use would not infringe privately owned rights.

ORNL-4714

Contract No. W-7405-eng-26

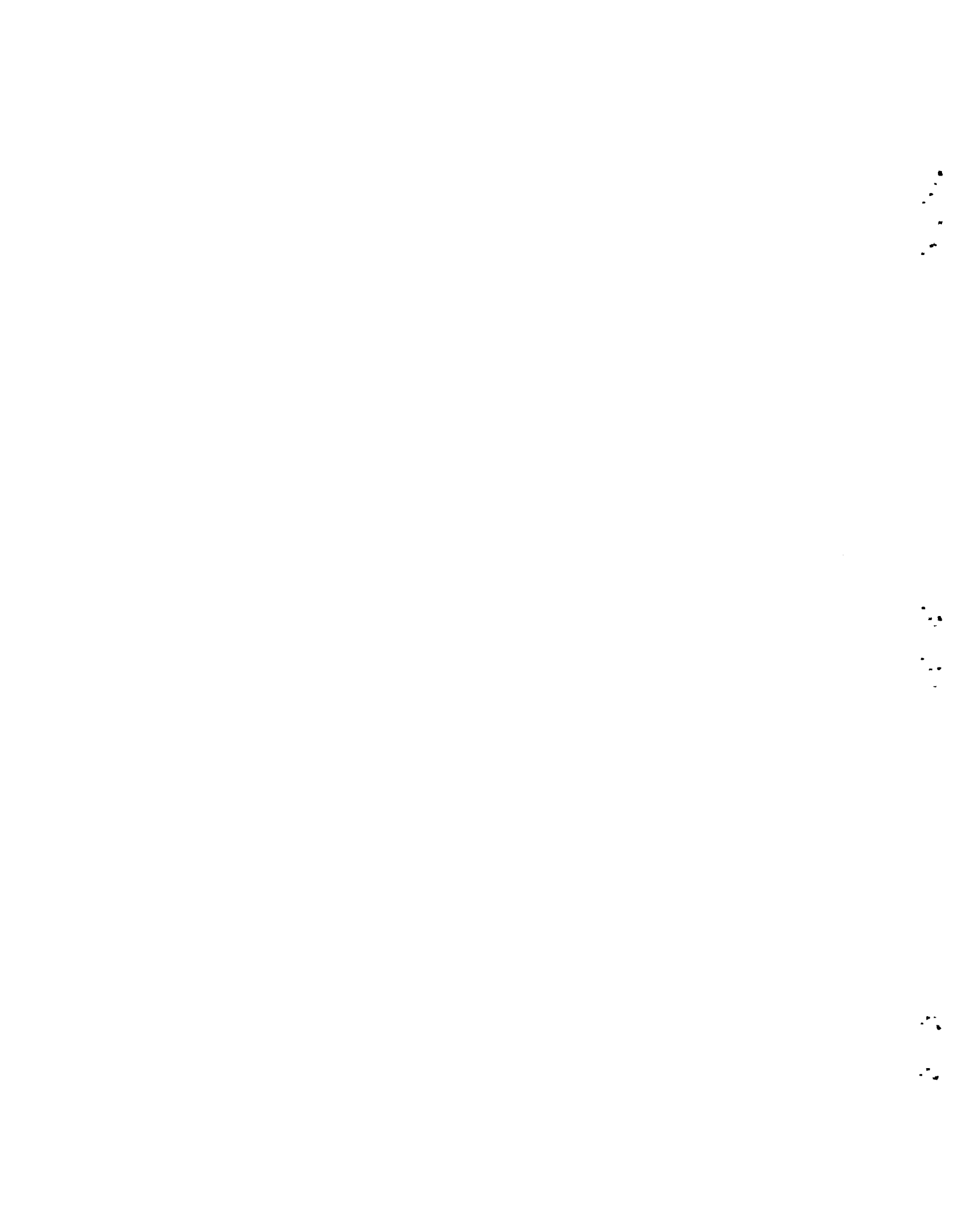
METALS AND CERAMICS DIVISION

POSTIRRADIATION EXAMINATION AND EVALUATION OF THE
PERFORMANCE OF HFIR FUEL ELEMENTS

A. E. Richt R. W. Knight G. M. Adamson, Jr.

DECEMBER 1971

OAK RIDGE NATIONAL LABORATORY
Oak Ridge, Tennessee 37830
operated by
UNION CARBIDE CORPORATION
for the
U.S. ATOMIC ENERGY COMMISSION



CONTENTS

	<u>Page</u>
Abstract	1
Introduction	1
General Description of the HFIR Fuel Elements and Reactor Operating Conditions	3
Selection and Operational History of the Examined HFIR Fuel Elements	12
Postirradiation Examination	15
General Objectives	15
Procedure	16
Results	17
Visual Inspection of the Fuel Assemblies	17
Element Length and Diameter Measurements	21
Fuel Plate Spacing Measurements	21
Fuel Plate Removal	23
Visual Inspection of the Fuel Plates	25
Gamma Scanning Results	32
Fuel Plate Thickness Measurements	34
Fuel-Plate Sectioning and Analytical Burnup Determinations	39
Metallographic Examination	43
Preirradiation Blister-Annealing Tests	55
Discussion	59
Dimensional Stability	59
Structural Integrity	61
Corrosion	61
Additional Comments	63
Conclusions	63
Acknowledgments	64
Appendix A	67
Appendix B	74
Appendix C	77
Appendix D	82
Appendix E	84

10

11

12

POSTIRRADIATION EXAMINATION AND EVALUATION OF THE
PERFORMANCE OF HFIR FUEL ELEMENTS

A. E. Richt R. W. Knight G. M. Adamson, Jr.

ABSTRACT

This report describes the results of the postirradiation examination and evaluation of the prior performance of four spent fuel elements from the High Flux Isotope Reactor. Two elements had been immersed in boiling deionized water for 24 hr before being operated for 2046 MWd. The other two were not pretreated and operated for slightly over 2300 MWd (the normal reactivity lifetime). These elements were examined to determine their overall condition and detect any unexpected problems that might compromise continued operation of the present fuel elements to their full reactivity lifetime.

All four fuel elements were in excellent condition. Gamma scanning and analytical burnup determinations showed the time-integrated power and burnup distribution within these elements to agree very well with design predictions. No significant changes in the dimensions of either the fuel assemblies or the individual fuel plates were indicated. The corrosion-product film on the surfaces of the fuel plates was somewhat thicker than expected, particularly on the pretreated fuel elements. Consequently, this pretreatment of the fuel elements is undesirable. Even with the thicker film, however, the elements appeared to perform quite satisfactorily; extensive visual and metallographic examination of fuel plates from these elements showed no indications of any type of structural damage that could be considered indicative of an actual or incipient failure of the fuel elements.

Since all four elements were in such good condition, we conclude that the current HFIR fuel elements will perform quite satisfactorily throughout their normal lifetime under present operating conditions. The useful lifetime is apparently limited only by nuclear reactivity and not by any irradiation damage.

INTRODUCTION

The High Flux Isotope Reactor (HFIR) currently operating at Oak Ridge National Laboratory was designed and constructed essentially for a single purpose - to produce annually milligram quantities of

various transplutonium isotopes from a rather limited supply of ^{242}Pu feed material. Preliminary analysis of the transplutonium production schemes¹ and studies of possible reactor types^{2,3} indicated that the use of a highly enriched, beryllium-reflected, light-water cooled and moderated, flux-trap reactor having a maximum unperturbed thermal-neutron flux of about 5×10^{15} neutrons $\text{cm}^{-2} \text{sec}^{-1}$ would be an economical and technologically feasible way of achieving the desired production rates. The reactor power required to obtain such a high flux was about 100 MW, which appeared to be consistent with the capital funds available. As the reactor concept was developed, a nominal power level of 100 MW became one of the design criteria; however, since the transplutonium production rates were found to be quite sensitive to the neutron flux level, considerable emphasis was placed upon achieving the highest practical flux level within the flux trap. As a result of these efforts, the present design⁴ of the HFIR represents a significant advancement in increasing the performance capabilities of research and test reactors. For example, at the design power level of 100 MW, the peak thermal and nonthermal neutron fluxes in the fuel region of the HFIR are 2 and 4×10^{15} neutrons $\text{cm}^{-2} \text{sec}^{-1}$, respectively; the maximum power density is 4.26 MW/liter; and the peak heat flux is about 500 W/cm² (1.6×10^6 Btu hr⁻¹ ft⁻²).

Thin, aluminum-base fuel plates for the HFIR fuel elements were selected because minimum development, operating, and capital investment costs were expected. However, HFIR fuel plates would be subjected to heat fluxes, temperatures, and burnup levels considerably higher than those of the more conventional types of research reactors. Moreover,

¹J. A. Lane et al., High Flux Isotope Reactor Preliminary Design Study, ORNL-CF-59-2-65 (March 1959).

²R. D. Cheverton, HFIR Preliminary Physics Report, ORNL-3006 (October 1960).

³N. Hilvety and T. G. Chapman, "Thermal Design of the HFIR Fuel Elements," pp. 138-151 in Research Reactor Fuel Element Conference, September 17-19, 1962, Gatlinburg, Tennessee, TID-7642, Book 1.

⁴F. T. Binford and E. N. Cramer, The High Flux Isotope Reactor, Volume I. Functional Description, ORNL-3572 (May 1964).

in overall design, the HFIR fuel assemblies represented a rather radical departure from those of the other reactor systems.

As of August 1971, over 60 fuel cores have operated at the full design power level of 100 MW to the end of nuclear life without any significant operational problems and with no indications of a fuel element or fuel plate failure. While such an outstanding performance record attests to the satisfactory design of the HFIR fuel elements, we felt that some of the spent fuel assemblies should be subjected to a detailed postoperational examination to more thoroughly evaluate the performance of these elements. The results of the examination of these fuel assemblies are the subject of this report.

GENERAL DESCRIPTION OF THE HFIR FUEL ELEMENTS AND REACTOR OPERATING CONDITIONS

The design and performance characteristics of the HFIR fuel elements differ considerably from those of the more conventional research reactors. The reactor core (Fig. 1) basically consists of four concentric cylindrical regions arranged from inside to out in the following order:

1. the central flux-trap region, which is about 5 in. in diameter, normally contains an assembly of target rods and which initially contained a plutonium dispersion;
2. the fuel region, composed of two concentric, annular fuel assemblies;
3. the control region, consisting of two concentric, cylindrical control elements each about $1/4$ in. thick;
4. the beryllium reflector, which is about 43 in. OD \times 12 in. thick.

During operation the coolant water at 600 psi flows downward through the fuel elements at about 55 ft/sec (13,500 gpm). Under these conditions the pressure drop through the elements is about 105 psi. The coolant inlet temperature is maintained at 110 to 120°F, while the outlet temperature is 150 to 160°F. The pH of the coolant water is maintained at 5.0 by nitric acid additions to minimize corrosion of the aluminum fuel plates. At the design power level of 100 MW, the average and maximum heat fluxes in the fuel assemblies are calculated to be about

ORNL-LR-DWG-65776A

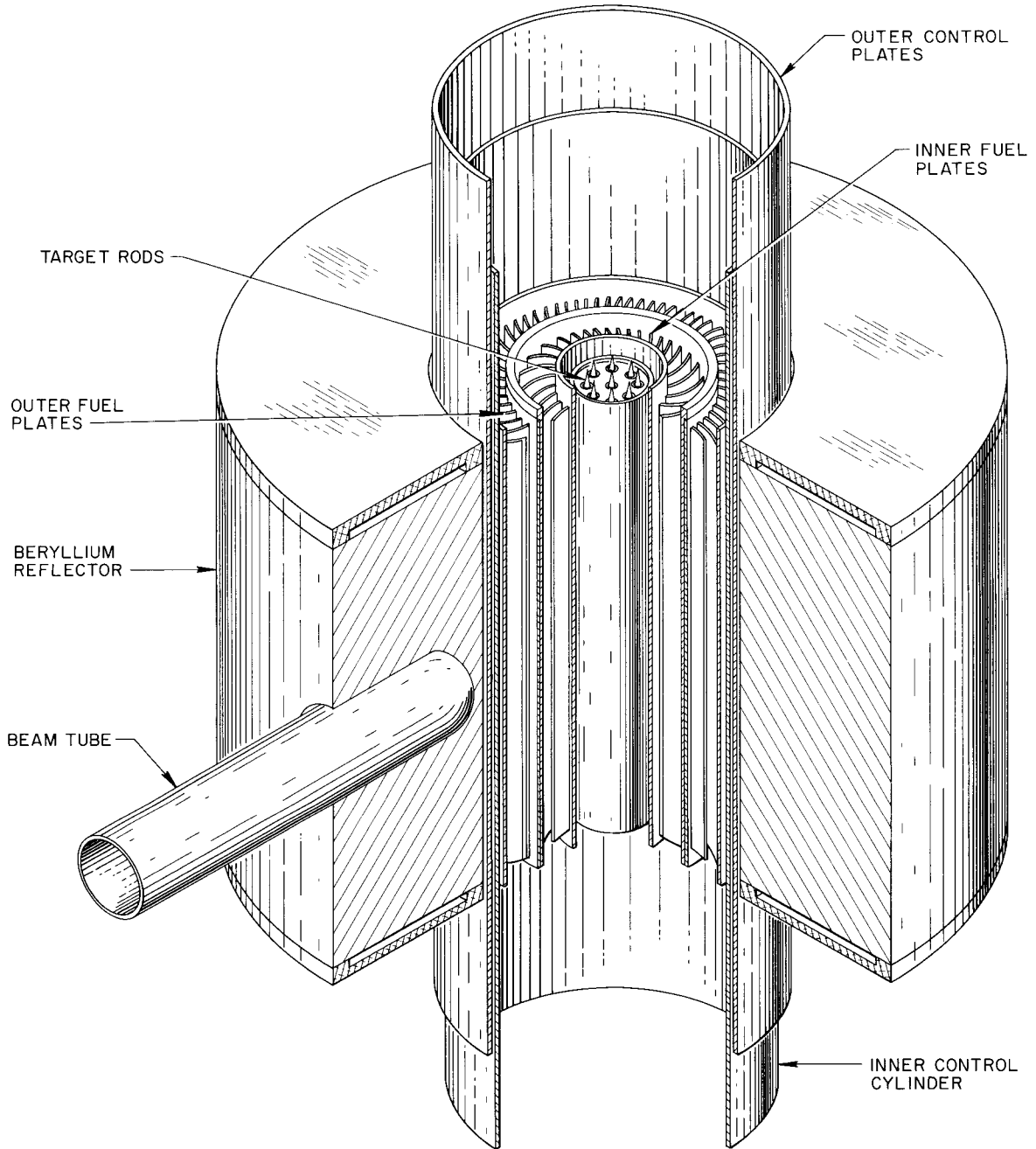


Fig. 1. Schematic Representation of the HFIR Core Components.

0.8 and 1.6×10^6 Btu hr⁻¹ ft⁻², respectively, while the average and maximum power densities are calculated to be 1.92 and 4.26 MW/liter, respectively.

The reactor operating experience has shown that the fuel elements have a useful lifetime of about 23 days (2300 MWD).

The overall design characteristics of the HFIR fuel elements are shown in greater detail in Fig. 2. The inner or outer fuel element consists of an annular array of 0.050-in.-thick aluminum-base fuel plates, which are attached to grooved cylindrical side plates by circumferential TIG weld beads. The fuel plates in both elements are preformed to an involute curvature to maintain a constant 0.050-in. coolant channel spacing between the plates. The fuel plates of both fuel elements are of a sandwich-type construction, consisting of a fuel core composed of a dispersion of U₃O₈ in aluminum, which is clad on all surfaces with aluminum alloy 6061. A unique characteristic of the HFIR fuel plates is the incorporation of a nonlinear fuel gradient across the fuel plate. As shown in Fig. 3, this is achieved by varying the thickness of the fuel core. The purpose of this fuel gradient is apparent when one considers the radial neutron flux distribution in the HFIR. As shown in Fig. 4, the thermal neutron flux peaks very sharply near the inner and outer edges of both fuel elements. If the fuel was uniformly distributed in a radial direction, the power distribution would also peak sharply in these areas. However, if the fuel distribution is varied inversely with the flux profile, the power distribution across the fuel plates can be essentially flattened. Since this reduces the peak-to-average power generation ratio, the fuel plates can then be allowed to operate at a higher average power density. The rather unique control rod system used in HFIR also helps to reduce the peak-to-average power ratio. In normal operation the inner control cylinder moves downward while the outer cylinder simultaneously moves upward to increase reactivity. This maintains axial symmetry of the power density and reduces the power peaking normally encountered at the upper and lower ends of the fuel core.

ORNL-LR-DWG 61472

Outer Annulus, 369 Plates

Inner Annulus, 171 Plates

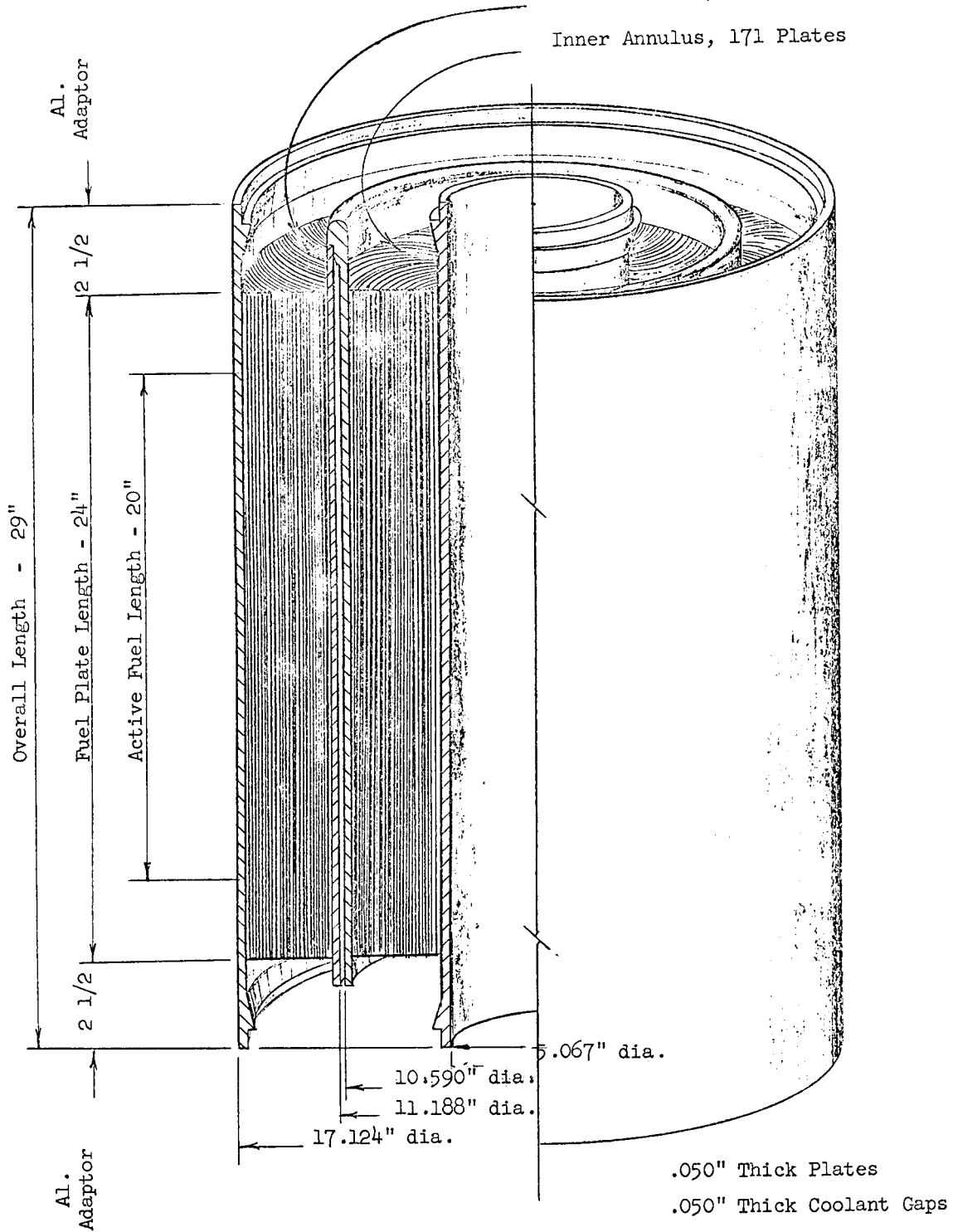


Fig. 2. Sketch of the HFIR Fuel Elements Showing Nominal Dimensions and Overall Configuration.

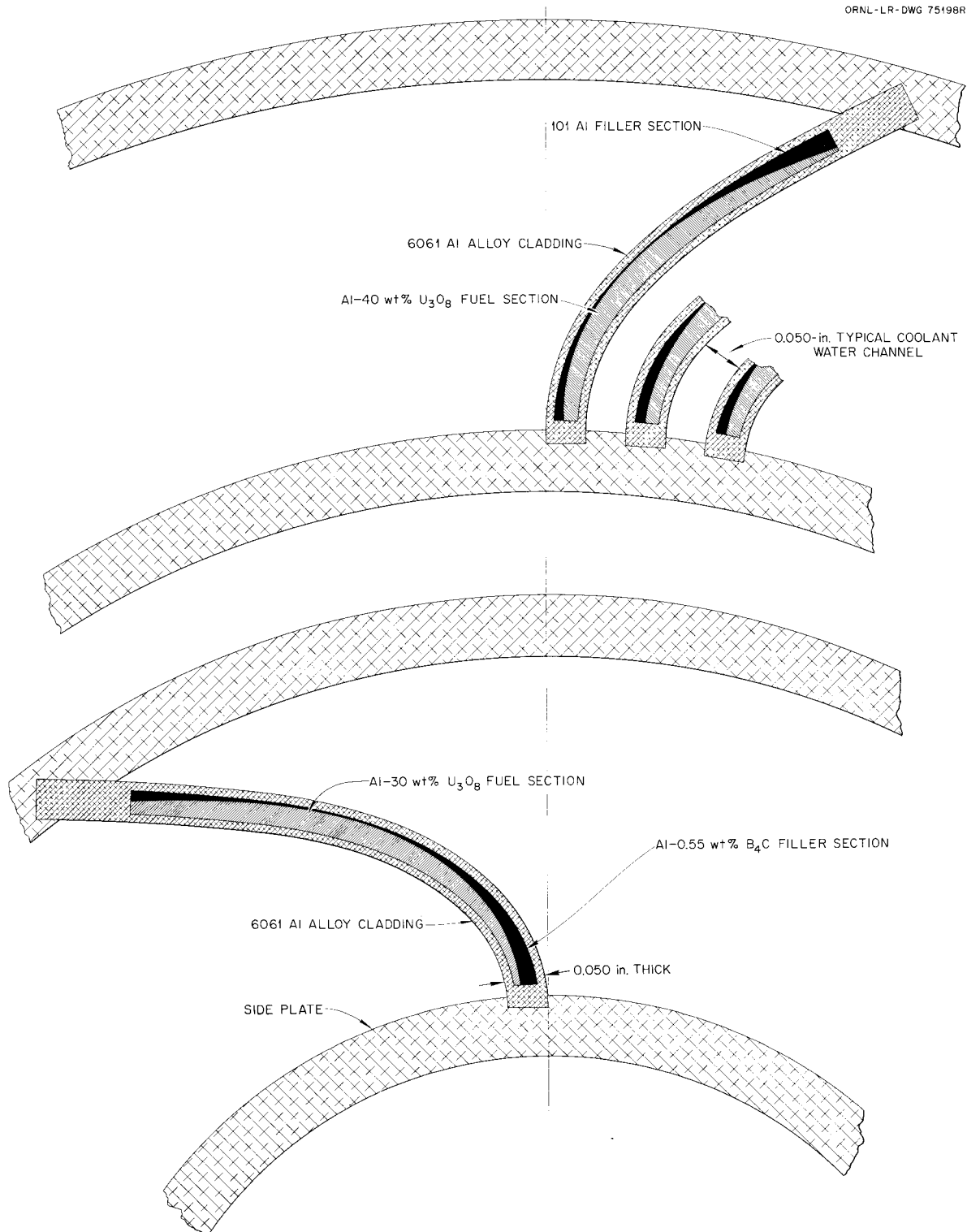


Fig. 3. Schematic Representation of a Horizontal Cross Section Through the HFIR Fuel Elements. Note the variation in thickness of the aluminum- U_3O_8 fuel section across the fuel plates of both inner and outer fuel elements, differences in fuel loading of inner and outer element fuel plates, and that the filler section of the inner element fuel plates contains a small quantity of boron carbide as a burnable poison addition.

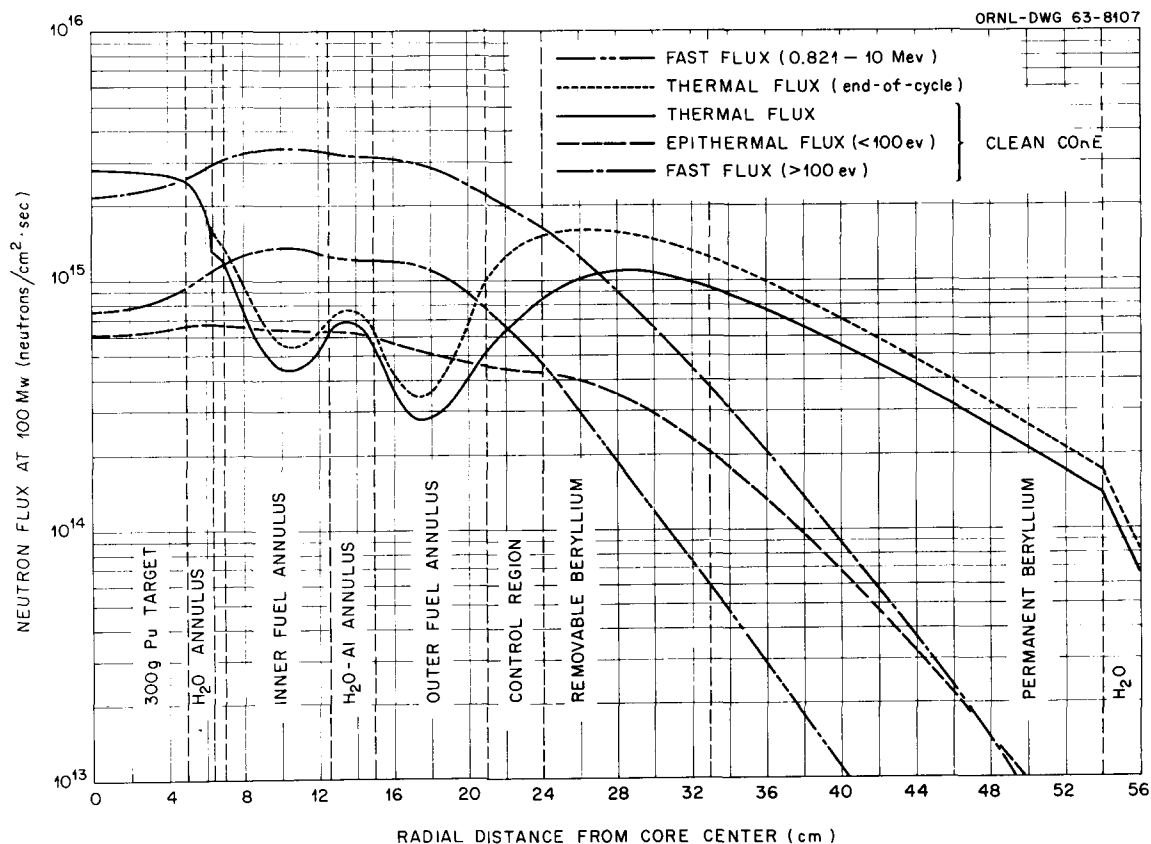


Fig. 4. Typical Radial Flux Distribution in the HFIR.

Although the combination of the reactor control system and the fuel loading gradients flattens the power distribution along and across the fuel plates, the burnup within the fuel dispersion varies almost directly with the axial and radial thermal neutron distribution. Since the thermal neutron flux peaks strongly near the inner and outer edges of the fuel plates, the fuel burnup also peaks strongly in these areas. As shown in Fig. 5, this results in steep burnup gradients across the fuel plates in both the inner and outer fuel elements. It should be noted, however, that the burnup also varies almost inversely with the thickness of the fuel core; that is, the higher burnups occur where the fuel cores are thinnest.

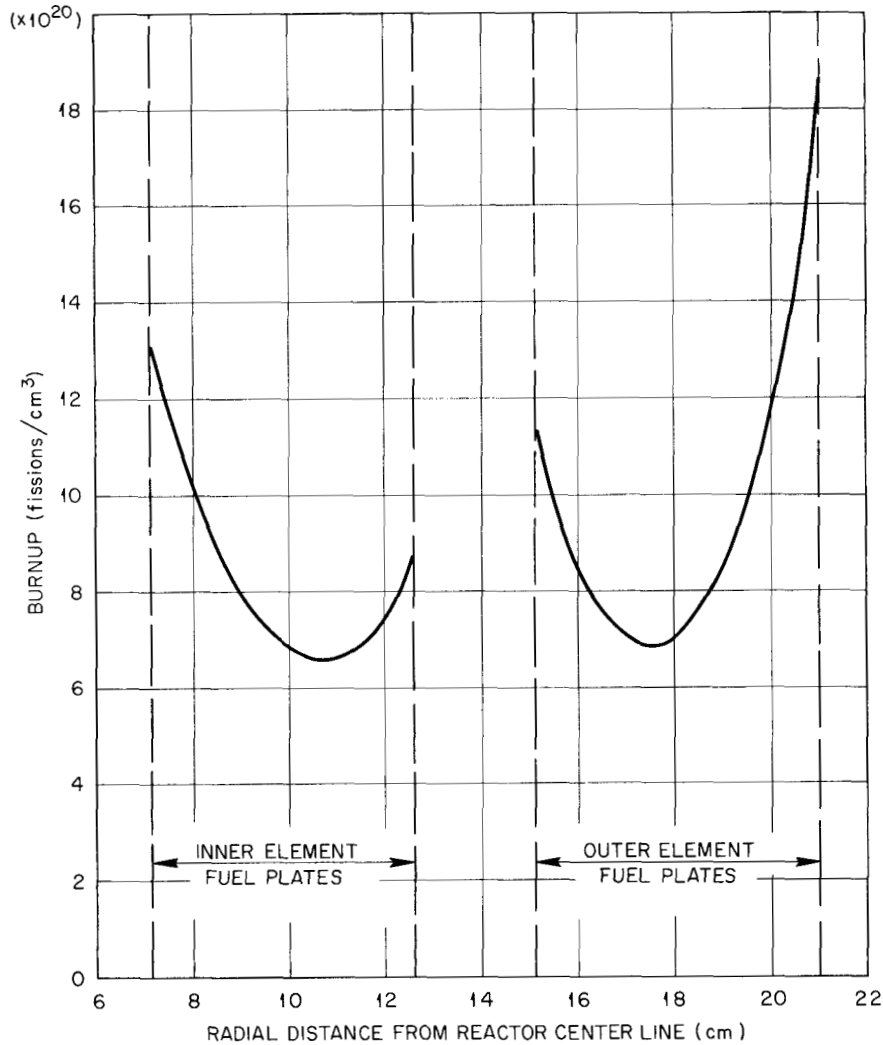


Fig. 5. Calculated Radial Burnup Profiles at the Horizontal Mid-plane of the HFIR after 2300 MWd Operation at 100 MW.

The overall effects of these radial and axial fluence variations upon the burnup distribution within the HFIR fuel plates are more clearly illustrated in Figs. 6 and 7, which show the calculated nominal axial burnup profiles at the inner edge, outer edge, and fuel core hump (i.e., the region of maximum fuel-core thickness) for the inner and outer element fuel plates. The symmetry of the burnup distribution about the horizontal midplane of the reactor and the large differences in burnup across the fuel plates are readily apparent.

The calculated operating temperatures of the fuel plates are also shown in Figs. 6 and 7. Note that the axial temperature profiles are

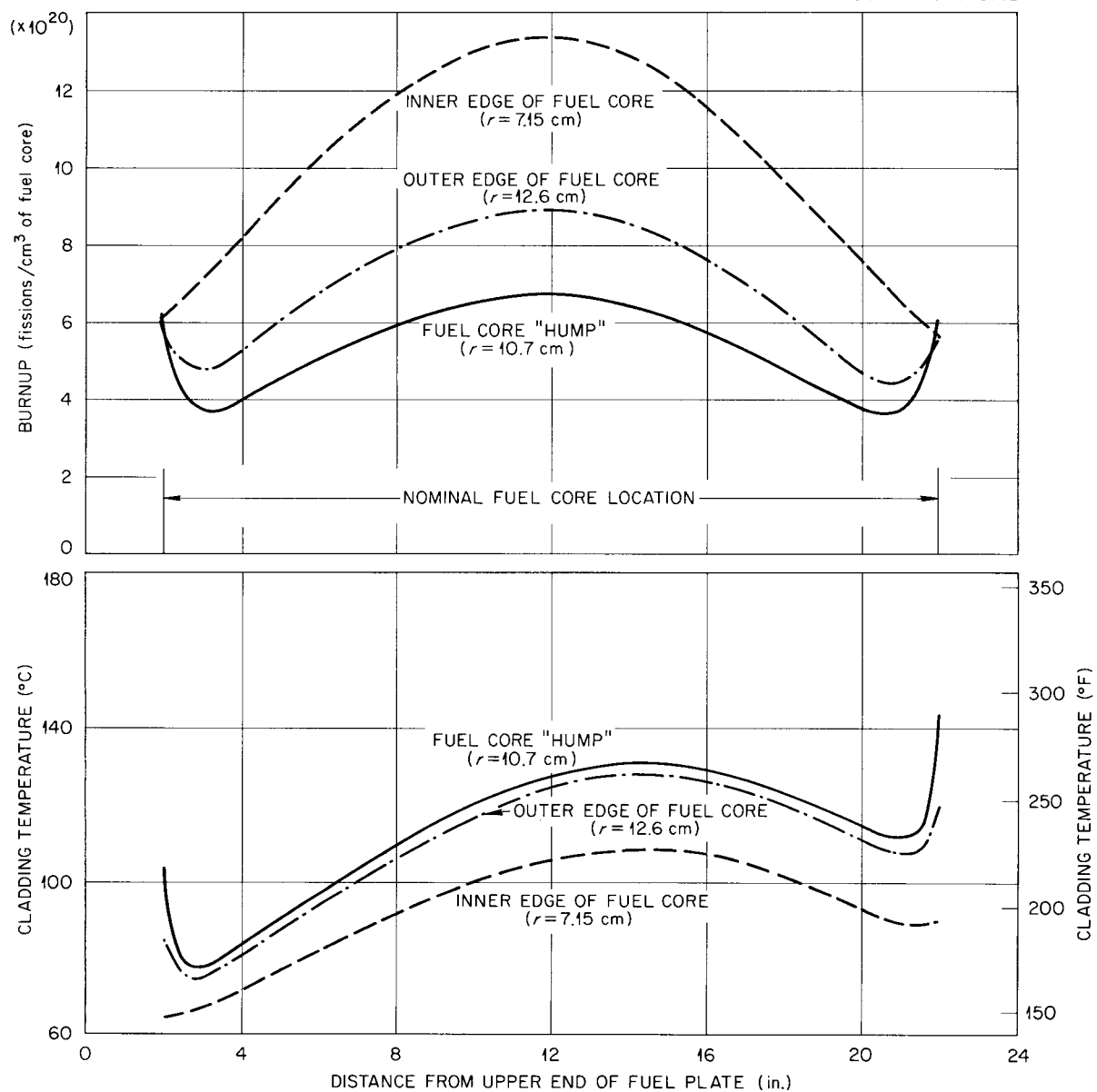


Fig. 6. Nominal Axial Burnup and Irradiation Temperature Profiles for an Inner Annulus HFIR Fuel Plate after 2300 Mwd of Operation.

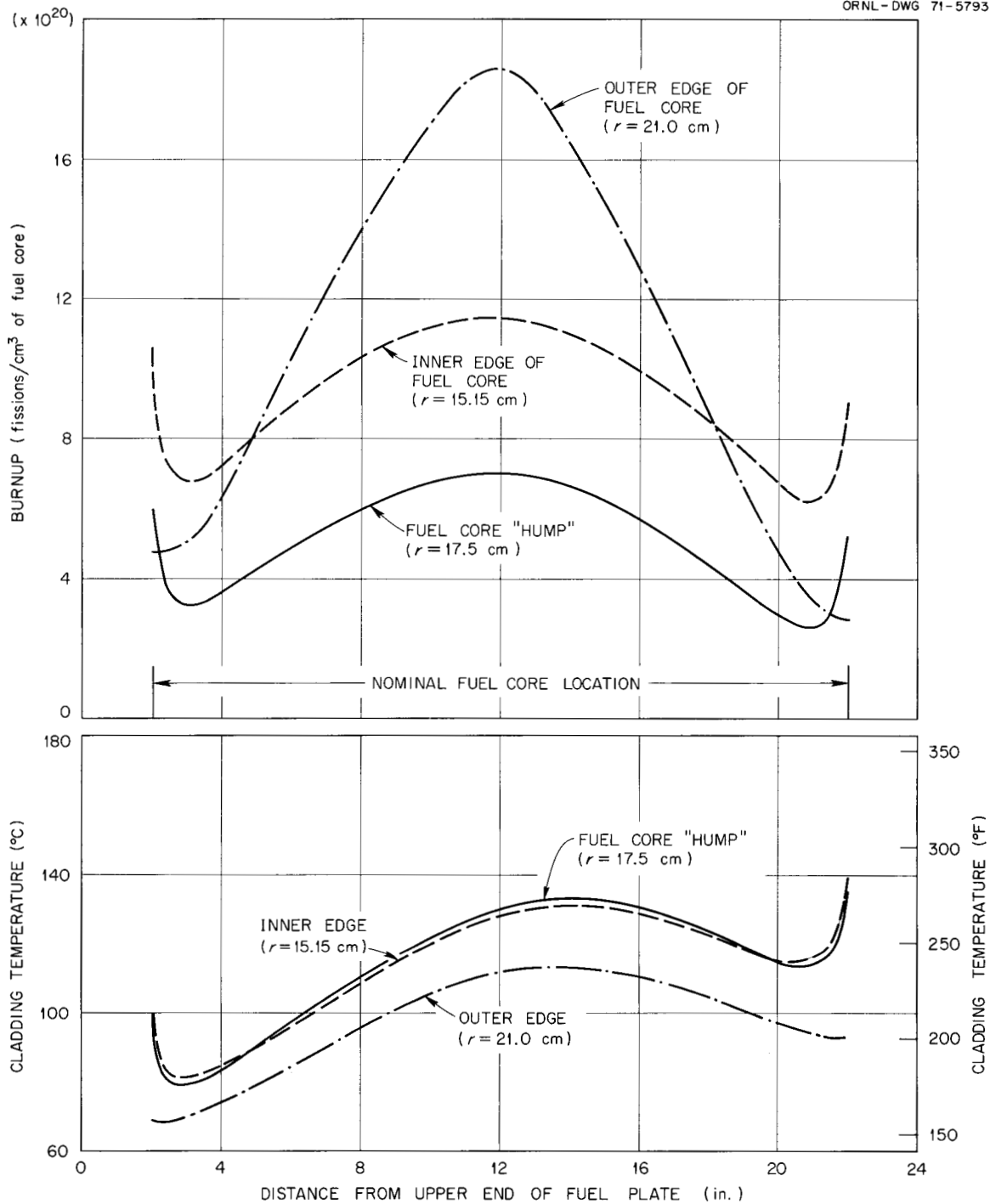


Fig. 7. Nominal Axial Burnup and Irradiation Temperature Profiles for an Outer Annulus HFIR Fuel Plate after 2300 MWd Operation.

not symmetrical about the reactor midplane but are displaced slightly toward the bottom or coolant-outlet end of the fuel plates. It should also be emphasized that corrosion strongly influences the operating temperature of the HFIR fuel plates. As the aluminum cladding corrodes, a film of adherent corrosion products builds up on the surfaces of the fuel plates. Since this film has a relatively low thermal conductivity, the fuel-plate operating temperatures depend strongly upon the thickness and composition of this film. The most recent out-of-reactor experimental data⁵ for the rate of film buildup were used to calculate the temperatures reported herein. However, under reactor operating conditions the film characteristics could differ significantly from those found in the out-of-reactor tests. In fact, the examination of these spent fuel elements showed that the films were thicker and compositionally different from that expected. Thus, one must not assume that the HFIR fuel plates necessarily operated at the temperatures reported here.

A more detailed description of the design, construction, and procedures used in manufacturing the fuel elements has been reported elsewhere.⁶

SELECTION AND OPERATIONAL HISTORY OF THE EXAMINED HFIR FUEL ELEMENTS

The fuel elements examined in the HFIR core evaluation program were identified as fuel elements 5-I, 5-O, 21-O, and 49-I (an "I" or "O" suffix designates an inner or outer annulus fuel element, respectively). Elements 5-I and 5-O were examined primarily because they were used for the first fuel core that operated for an entire core lifetime at the full design power level of 100 MW, and we wanted to ascertain the performance of the HFIR fuel elements as quickly as possible. Later, we

⁵J. C. Griess et al., Effect of Heat Flux on the Corrosion of Aluminum by Water - Part III, ORNL-3230 (June 1961).

⁶R. W. Knight, J. Binns, and G. M. Adamson, Jr., Fabrication Procedures for Manufacturing High Flux Isotope Reactor Fuel Elements, ORNL-4242 (June 1968).

recognized that the in-reactor performance of elements 5-I and 5-O had been slightly affected by a special pretreatment given to fuel elements used in the first few HFIR fuel cores. This pretreatment was intended to increase corrosion resistance during preoperation and low-power runs. Consequently, we decided that other fuel elements should also be examined to ascertain the performance of elements that had been subjected to only normal operating practices. Elements 21-O and 49-I were selected primarily because (1) their in-reactor behavior appeared to be typical of that of the standard, nonpretreated HFIR fuel elements, and (2) they became available for examination during convenient periods for hot cell scheduling. However, element 21-O also contained a few fuel plates that had been accepted on waiver for excessive localized fuel violations (i.e., small areas containing more than 1.27 times the nominal fuel loading), and we thought that the examination of such plates might provide additional data about the performance of fuel plates that did not meet fabrication specifications.

The fuel elements were manufactured by Metals and Controls, Inc.,⁷ under contract 91X-70500. Elements 5-I and 5-O were certified and accepted on March 1, 1966; element 21-O on December 28, 1966; and element 49-I on January 11, 1968. All four elements were accepted on waivers for violation of some of the fabrication specifications; however, except for the few fuel plates with localized excessive fuel contents, these violations were thought to be of no significance to the postirradiation evaluation program.

As mentioned previously, fuel elements 5-I and 5-O were the first fuel core (cycle 4) to operate continuously at full power in the HFIR. These elements were brought to power on September 9, 1966, and operated at 100 MW until September 30, 1966, when a plantwide electrical failure caused a premature shutdown after 2046 Mwd. The fuel elements were then removed from the reactor and stored in the pool until October 12, 1967, when they were transferred to the High Radiation Level Examination Laboratory (HRLLEL) hot cells for examination. High residual heat in the

⁷Metals and Controls, Inc., a Division of Texas Instruments, Inc., Attleboro, Mass.

plates prevented removing them from the pool sooner. Fuel elements 21-I and 21-0 were used during cycle 16 of the HFIR, which was brought to power on December 10, 1967, and operated at 100 MW until January 2, 1968, when loss of reactivity caused a shutdown after 2309 MWd. These elements were then removed from the reactor and stored in the pool until December 16, 1968, when element 21-0 was transferred to the hot cells for examination. Fuel elements 49-I and 49-0 were used during cycle 35 of the HFIR, which was brought to power on May 19, 1969, and operated at 100 MWd until June 11, 1969, when loss of reactivity caused a shutdown after 2319 MWd. These elements were then stored in the pool until February 11, 1970, when element 49-I was transferred to the hot cells for examination.

During the initial stages of the HFIR operation, the fuel elements were often exposed to the reactor pool water for up to three months before being placed into service. This resulted in the formation of a rather thick, gelatinous, corrosion product film on the element surfaces. In an attempt to avoid this condition, initial HFIR fuel cores were pretreated by immersion in boiling deionized water for 24 hr to produce a thin, semiprotective oxide (boehmite, $\text{Al}_2\text{O}_3 \cdot \text{H}_2\text{O}$) film on the surfaces of the elements before they were placed into service. However, once the HFIR operations became routine, pretreatment of the fuel elements was discontinued.

Although this pretreatment was not expected to have any significant effect upon the performance of the HFIR fuel elements, when the reactor used pretreated fuel elements the coolant flow rate generally decreased and the pressure drop across the elements increased during the reactor fuel cycle. No significant variation in either flow rate or pressure drop has been observed when the reactor has operated with non-pretreated fuel elements. Typical examples of the difference in flow rate and pressure drop through pretreated (i.e., elements 5-I and 5-0 during cycle 4) and non-pretreated fuel elements (i.e., elements 21-I and 21-0 during cycle 16) are shown in Fig. 8. These differences appear to result from the buildup of a thicker corrosion product film on the surfaces of the pretreated fuel plates during reactor operation.

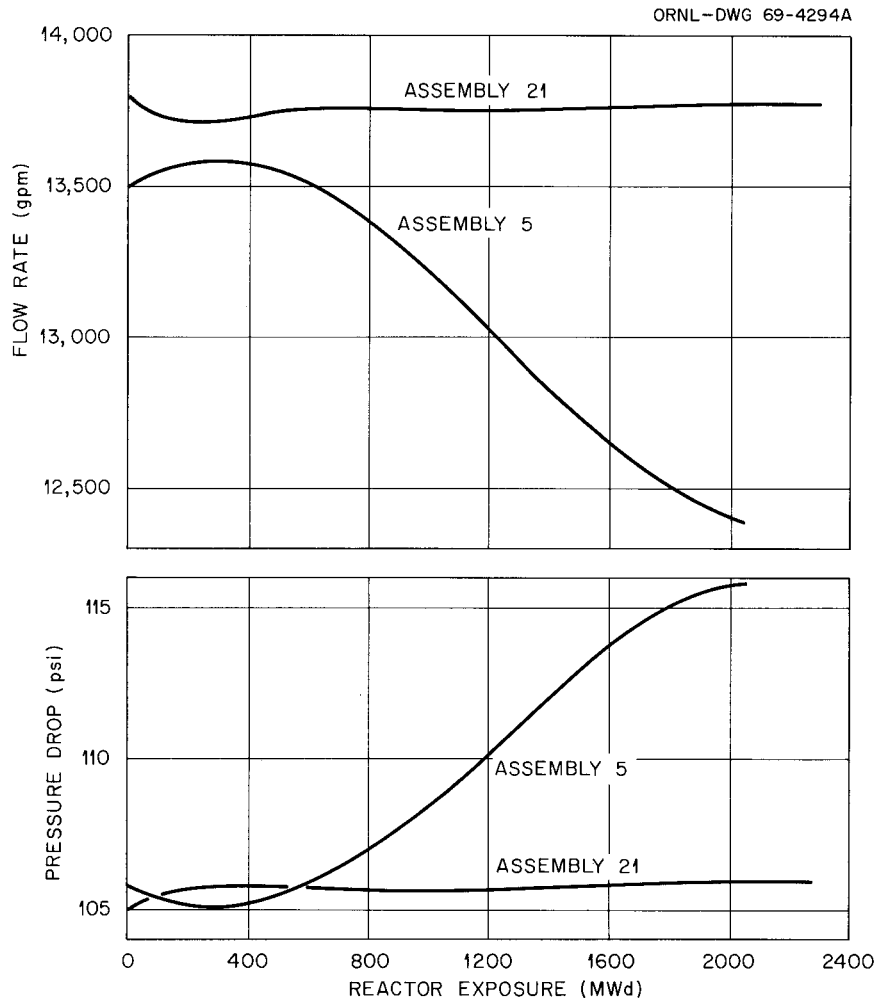


Fig. 8. Coolant Flow Rate and Pressure Drop for HFIR Fuel Assemblies 5 and 21. The inlet temperature was 120°F for assembly 5 and 110°F for assembly 21. The temperature rise was 40°F for both.

POSTIRRADIATION EXAMINATION

General Objectives

The primary objective in the postirradiation examination of the HFIR fuel elements was to ascertain the overall condition of the elements and detect any actual or potential problems that might compromise continued operation of the present elements to their maximum useful lifetime. However, we also wanted to obtain more basic information about specific aspects of the irradiation behavior of these elements to aid in predicting performance capabilities of both the present and advanced

HFIR fuel elements. Although the useful lifetime of the present elements is limited only by loss of reactivity, other factors such as irradiation-induced dimensional instabilities, loss of structural integrity, or excessive corrosion could limit the useful lifetime of any advanced HFIR fuel element design. Consequently, we emphasized the effects of reactor service upon the dimensional stability, structural integrity, and corrosion of the elements.

Procedure

After removal from the reactor core, the spent HFIR fuel elements were transferred to the reactor pool, where they were stored underwater for approximately one year before being transferred to the HRLEL hot cells for examination. This relatively long storage period was necessary to allow the fission products to decay to a level where the beta- and gamma-ray heating would not cause the elements to exceed about 300°F during handling in the hot cells. The postirradiation examination of these elements consisted primarily of visual examination of the element surfaces, measurement of the pertinent element dimensions, gamma scanning, analytical burnup determinations, metallographic examinations, and analysis of the corrosion product films. The elements were first examined visually through the hot-cell windows and with an in-cell periscope at magnifications of up to 4× for evidence of gross damage. The length, inner and outer diameters, and coolant channel spacings were then measured. Four intact fuel plates were then removed from each element for more detailed examinations. These fuel plates were then inspected visually, gamma scanned, and measured for thickness. A fuel plate from each element was then sectioned for analytical burnup determinations and metallographic examination. Some of the fuel plates from three of the fuel elements were also used for postirradiation heat-treatment studies.

The examination of the spent HFIR fuel elements was extremely difficult, complex, and time-consuming. Because of their physical size and configuration, these elements required considerable specialized equipment to handle, inspect, and disassemble them in the hot cells.

In addition, the fuel reprocessors stipulated that these spent elements be essentially reassembled after examination so that they could be handled with the standard reprocessing handling equipment. Since the design, construction, and operation of the specialized equipment was an integral part of the postirradiation examination program, this equipment is briefly described in Appendix A.

Results

Visual Inspection of the Fuel Assemblies

Shortly after unloading the irradiated fuel elements from the shipping cask, we examined the spent fuel assemblies visually through the hot cell windows and with the in-cell periscope system at magnifications up to 4X for evidence of damage. The overall appearance of the four fuel elements is shown in Figs. 9 and 10. In general, all appeared to be in excellent physical condition; no indications of gross warpage or distortion was apparent, and careful inspection of the surfaces revealed no evidence of any type of mechanical or structural damage. The only noticeable effect of irradiation upon the appearance of the elements was a difference in the overall coloration of the fuel assemblies; the as-fabricated HFIR fuel elements normally are bright and shiny, whereas all the irradiated elements were a dull light gray. This coloration appears to be a result of the formation of a thin oxide film on the element surfaces during irradiation or during storage in the HFIR pool. Elements 5-I and 5-0 were slightly darker than elements 49-I and 21-0. This indicates that the oxide film on elements 5-I and 5-0 was slightly thicker. All four elements were slightly darker at the bottom (i.e., the coolant outlet end). This also appears to be a result of slight variation in the thickness of the oxide film along the elements.

The coolant channels of all four elements were also examined visually for evidence of fuel plate warpage or blockage. As shown in Fig. 11, no significant change in coolant channel spacing was apparent; and, except for element 5-I, all channels were free of any blockage or obstructions. As shown in Fig. 12, a soft, white deposit partially

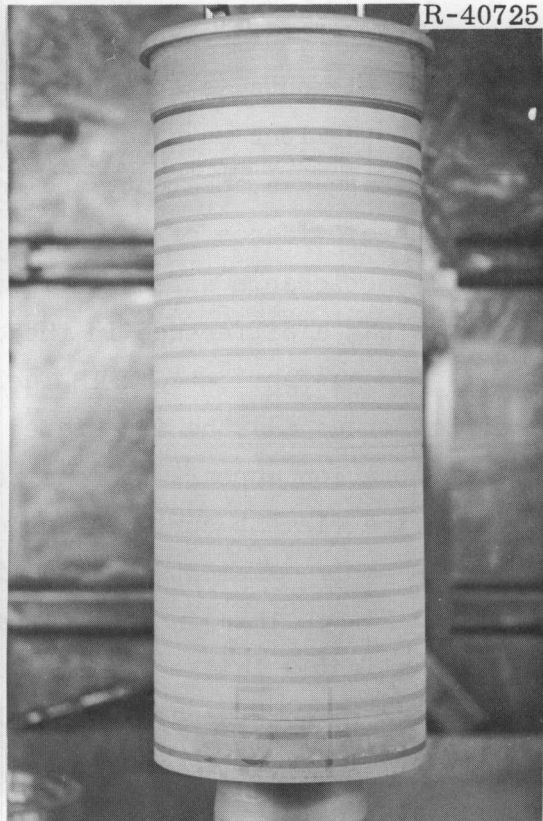
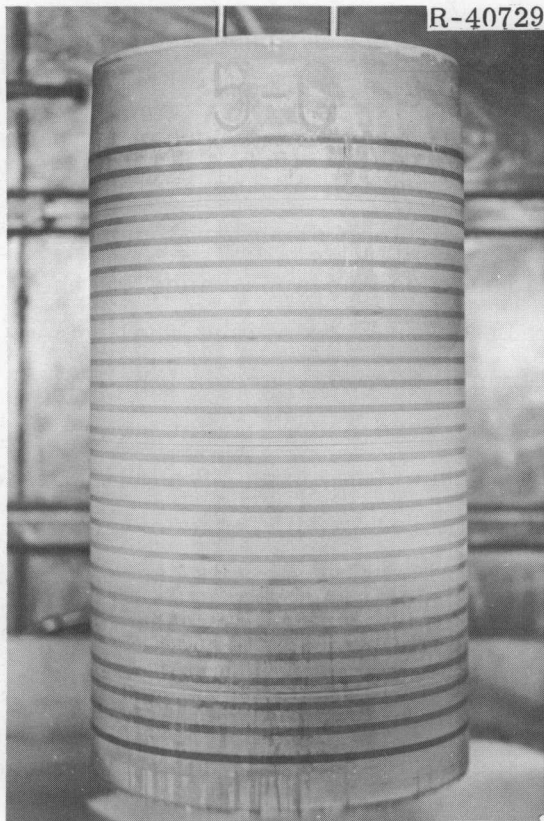
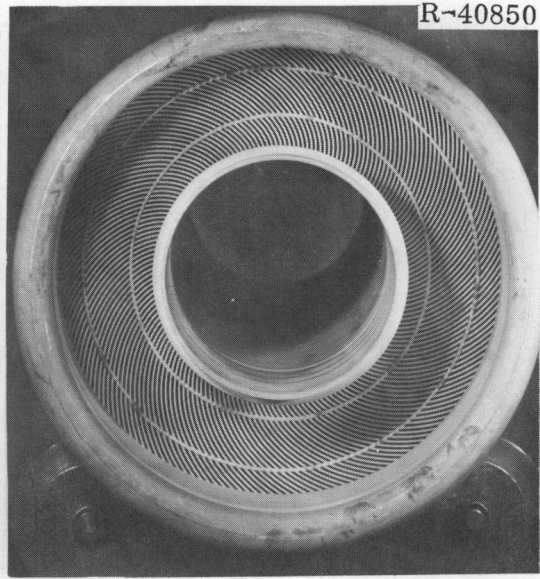
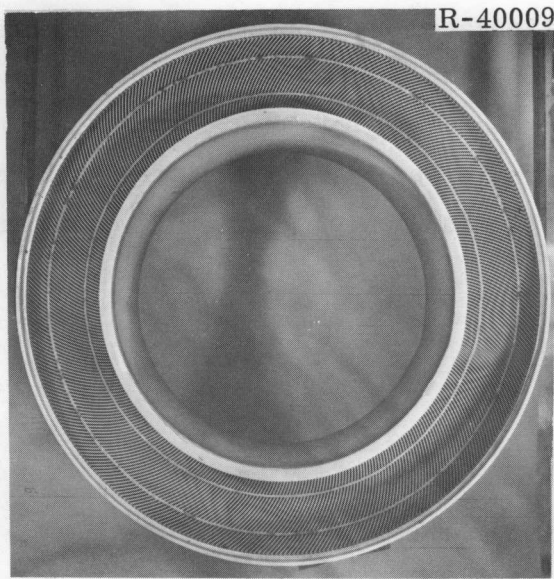


Fig. 9. Fuel Elements 5-I and 5-0 after 2046 MWd of Operation and One Year Storage in the Reactor Pool.

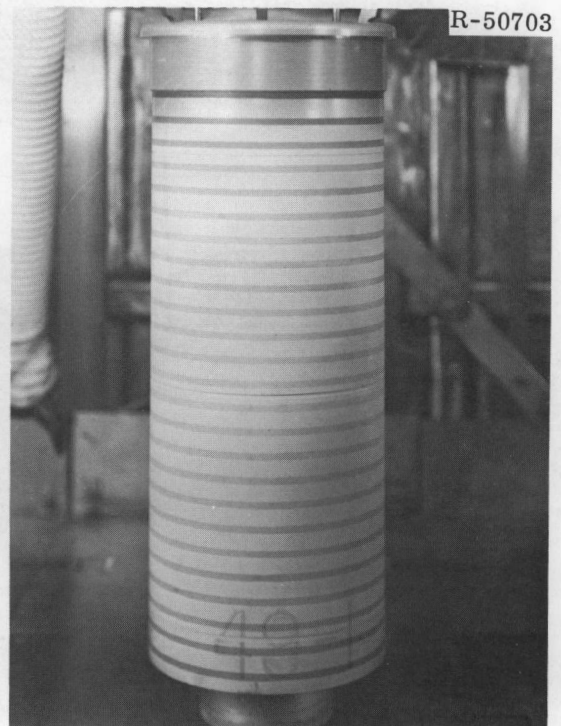
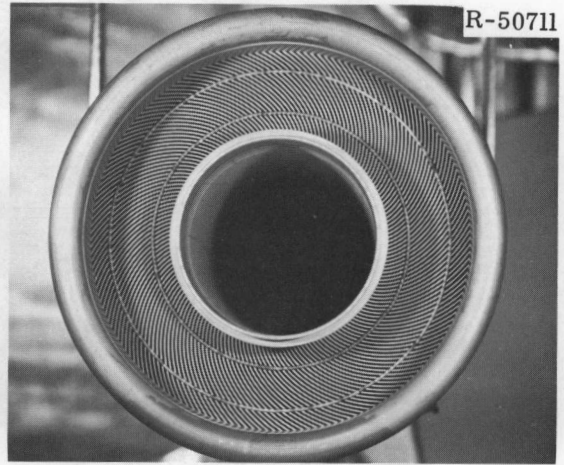
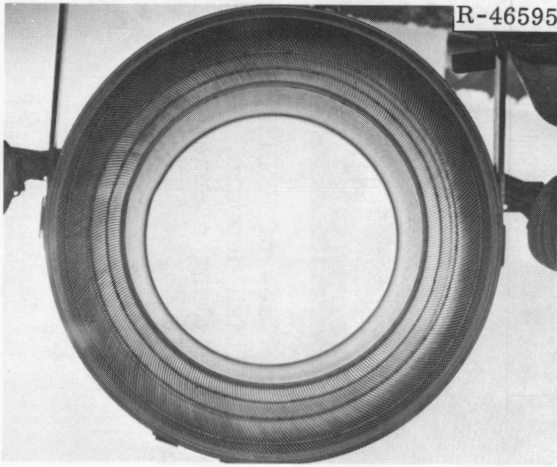


Fig. 10. Fuel Elements 21-0 and 49-I. Reduced 13%.

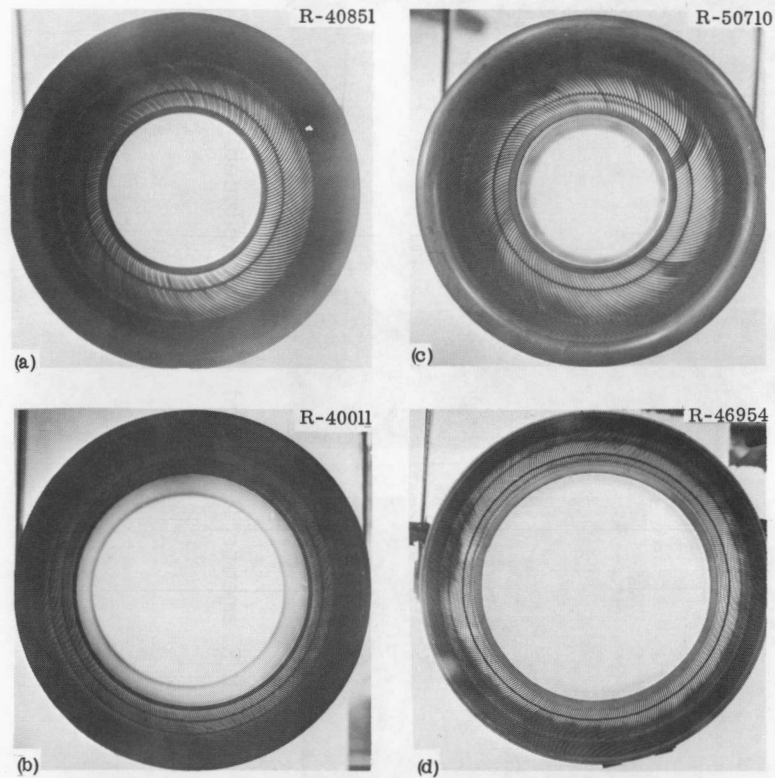


Fig. 11. Backlighted Views Through the Coolant Channels of HFIR Fuel Elements. (a) 5-I, (b) 5-0, (c) 49-I, and (d) 21-0. Reduced 32%.

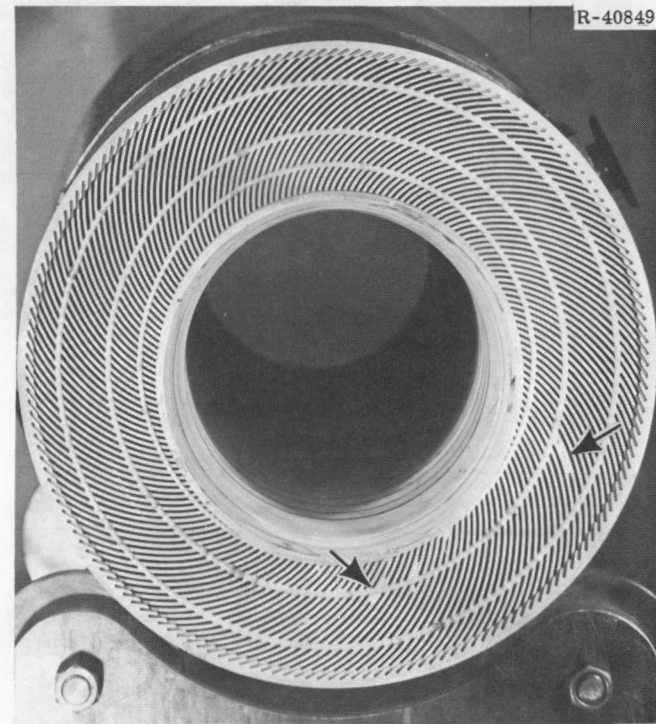


Fig. 12. Bottom View of HFIR Fuel Element 5-I. Arrows show whitish deposit, which partially blocked some of the coolant channels of this element. Reduced 33.5%.

blocked some of the coolant channels at the extreme bottom end of the fuel plates of element 5-I. This whitish material was identified as bayerite ($\beta\text{-Al}_2\text{O}_3 \cdot 3\text{H}_2\text{O}$) by x-ray diffraction. However, it appears unlikely that this friable deposit could have existed during reactor operation because of the high coolant flow rates. As will be discussed in greater detail later, we feel that this partial blockage occurred while these elements were stored.

Element Length and Diameter Measurements

After completion of the visual inspection, the length and inner and outer diameters of the irradiated fuel elements were measured to see if the external dimensions had significantly changed as a result of reactor service. We obtained on each element 12 length measurements (i.e., the shoulder-to-shoulder distance at 30° intervals around the circumference of the outer side plate) and 18 measurements of each diameter (i.e., six positions at 30° intervals around the circumference 9 in. above, 9 in. below, and at the horizontal midplane of the element).

Results of the pre- and postirradiation measurements are summarized in Table 1. In general, the as-measured length and diameters of all four fuel assemblies were slightly greater after irradiation than before irradiation because of thermal expansion. The preirradiation measurements were obtained at 20°C (68°F) in a temperature-controlled inspection area; during the postirradiation measurements, decay heating kept the element surface between 55°C (131°F) and 99°C (210°F). However, by using the measured surface temperatures and the appropriate thermal expansion coefficient for aluminum alloy 6061, we corrected the measurements. As shown in this table, the corrected external dimensions of all four elements are generally well within fabrication specifications and little if any change occurred as a result of irradiation.

Fuel Plate Spacing Measurements

Since the coolant channel spacing is one of the most critical dimensions in the design criteria of the HFIR fuel elements, we wanted to determine if any significant changes in it had occurred as a result

Table 1. Dimensional Measurements on Irradiated HFIR Fuel Elements

Dimension	Measured Value, in.			Indicated Change
	Preirradiation	Postirradiation		
		As-Measured	Corrected ^a	
<u>Element 5-I</u>				
Length	27.934	27.955	27.933	-0.001
Outer diameter				
Upper end	10.591	10.604	10.593	+0.002
Midplane	10.591	10.610	10.599	+0.008
Lower end	10.591	10.607	10.596	+0.005
Inner diameter				
Upper end	5.069	5.074	5.070	+0.001
Midplane	5.069	5.073	5.068	-0.001
Lower end	5.069	5.072	5.068	-0.001
<u>Element 5-0</u>				
Length	29.629	29.629	29.628	-0.001
Outer diameter				
Upper end	17.141	17.160	17.141	0
Midplane	17.141	17.169	17.150	+0.009
Lower end	17.141	17.158	17.139	-0.002
Inner diameter				
Upper end	11.246	11.259	11.247	+0.001
Midplane	11.246	11.262	11.250	+0.004
Lower end	11.246	11.256	11.243	-0.003
<u>Element 21-0</u>				
Length	29.626	29.662	29.632	+0.006
Outer diameter				
Upper end	17.141	17.159	17.142	+0.001
Midplane	17.141	17.162	17.144	+0.003
Lower end	17.141	17.156	17.139	-0.002
Inner diameter				
Upper end	11.246	11.262	11.250	+0.004
Midplane	11.246	11.258	11.247	+0.001
Lower end	11.246	11.257	11.245	-0.001
<u>Element 49-I</u>				
Length	27.937	27.980	27.930	-0.007
Outer diameter				
Upper end	10.592	10.617	10.599	+0.007
Midplane	10.592	10.619	10.599	+0.007
Lower end	10.592	10.616	10.596	+0.004
Inner diameter				
Upper end	5.073	5.086	5.078	+0.005
Midplane	5.073	5.082	5.073	0
Lower end	5.073	5.080	5.071	-0.002

^aCorrected for temperature of irradiated element.

of irradiation. During inspection of the elements after manufacture, the channel spacing is measured by a special five-fingered eddy current probe, which provides a continuous readout of the coolant gap along every channel at five radial locations. A similar one-fingered probe was used to measure the channel spacing of the irradiated fuel elements; however, measurements were restricted to the center of the channels by the end fittings and the combs attached to the upper and lower ends of the fuel plates. Since these measurements proved to be quite tedious and time-consuming, only 20 channels were measured in each of the four irradiated elements. It should also be noted that accuracy of these measurements at a constant temperature and not in a cell is estimated to be about ± 0.001 in.; however, since the irradiated elements were considerably hotter and all handling and measuring were done remotely, the accuracy of the postirradiation measurements may be somewhat less.

As shown in Table 2, results of these measurements suggest that some changes in the coolant channel spacings had occurred. However, it should be emphasized that the differences between the pre- and postirradiation measurements are generally well within the probable accuracy of these measurements. More importantly, the measurements of the four irradiated elements showed that the spacings of 80 channels (i.e., 20 channels/element) were all well within the 0.050 ± 0.006 in. average and the 0.050 ± 0.010 in. local spot fabrication specifications. As will be discussed later, a more detailed analysis of the channel spacing data indicates that the buildup of an oxide film on the surfaces of the fuel plates during irradiation or storage of the elements actually resulted in a small reduction (i.e., < 0.002 in.) in the channel spacing of these fuel elements. In general, however, these measurements conclusively show that no major changes in the coolant channel spacings of the HFIR fuel occurred as a result of irradiation.

Fuel Plate Removal

Following completion of the coolant channel measurements, four fuel plates were cut from fuel elements 5-0, 21-0, and 49-I for further examination. No additional work was done on element 5-I since early

Table 2. Summary of Coolant Channel Spacing Measurements on Irradiated HFIR Fuel Elements

Measurement	Coolant Channel Spacing, in.				
	Average			Local	
	Overall Grand	Maximum Spot	Minimum Spot	Maximum Spot	Minimum Spot
	<u>Element 5-I</u>				
Preirradiation	0.0499	0.0535	0.0445	0.0575	0.0430
Postirradiation	0.0505	0.0523	0.0489		
Difference	+0.0006	-0.0012	+0.0044		
	<u>Element 5-0</u>				
Preirradiation	0.0496	0.0550	0.0460	0.0590	0.0440
Postirradiation	0.0499	0.0519	0.0483		
Difference	+0.0003	-0.0031	+0.0023		
	<u>Element 49-I</u>				
Preirradiation	0.0501	0.0527	0.0476	0.0540	0.0455
Postirradiation	0.0483	0.0508	0.0461		
Difference	-0.0018	-0.0019	+0.0015		
	<u>Element 21-0</u>				
Preirradiation	0.0504	0.0550	0.0460	0.0565	0.0400
Postirradiation	0.0504	0.0515	0.0491		
Difference	0.	-0.0035	+0.0031		

results indicated that the performance of elements 5-I and 5-0 was not typical of most of the HFIR fuel elements and that a detailed examination of fuel plates from 5-0 would be sufficient. One fuel plate was selected from each quadrant of element 5-0; however, the plates removed from elements 21-0 and 49-I were selected from those plates waived for excessive localized fuel loading violations, since this represented what was thought to provide the most severe test.

The individual fuel plates were removed by (1) cutting off the element end adapters, (2) slitting through the inner and outer side plates on each side of the desired fuel plate, (3) milling off the combs at each end of the fuel plate, and (4) slightly spreading the element with a hydraulic jack to permit the fuel plate to slide free. After each plate was removed, a spacer was inserted into the resultant gap and welded to the element side plates. One spacer near each end of both

the inner and outer side plates was used, and a band held the spacers in place during welding. After the last fuel plate was removed, the end adapters were welded into position to complete the reassembly of the element.

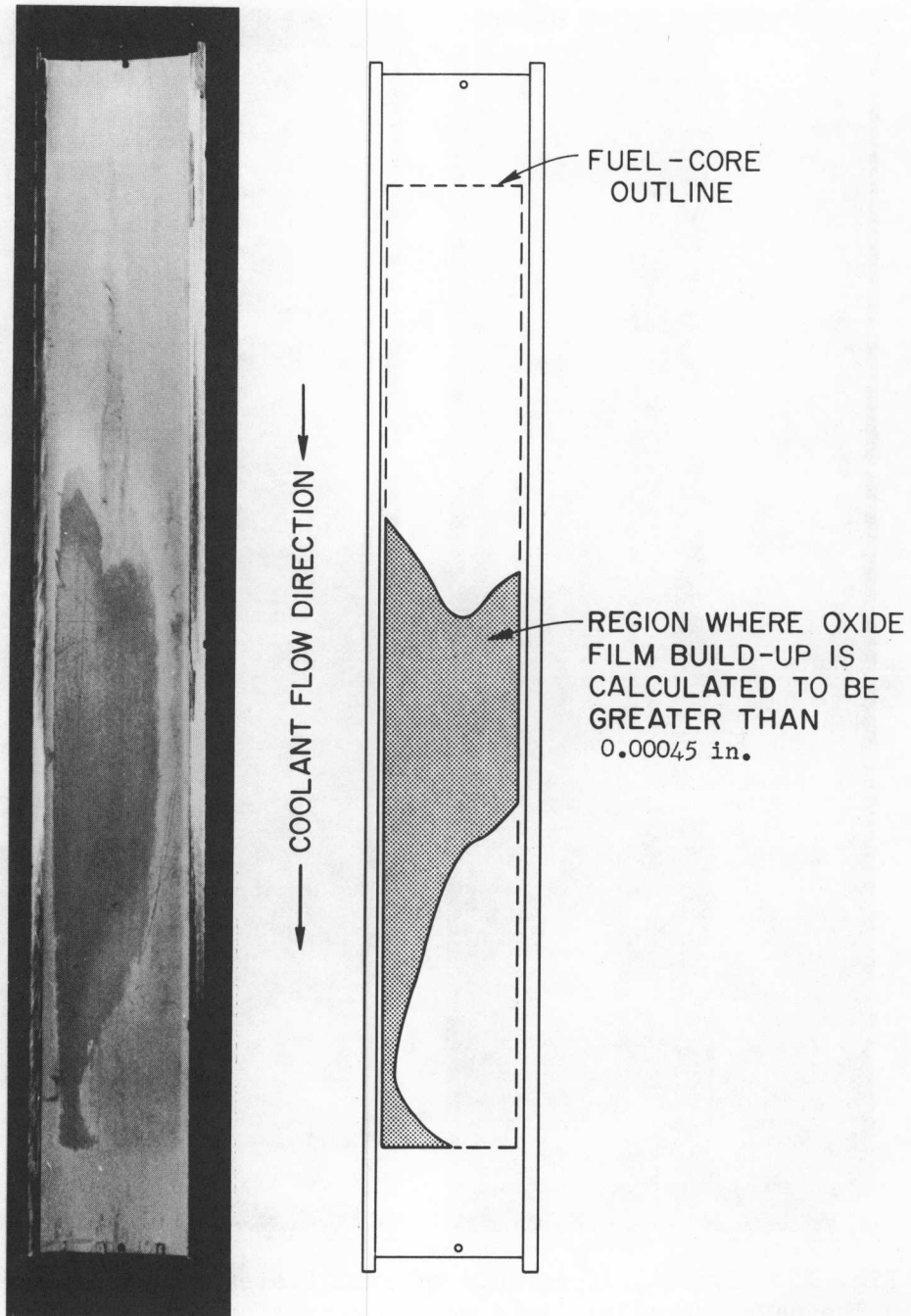
Visual Inspection of the Fuel Plates

The 12 irradiated fuel plates (four plates each from elements 5-0, 21-0, and 49-I) were examined carefully through the hot-cell periscope and stereomicroscope systems at magnifications of up to 20X for evidence of irradiation-induced damage. No indications of cracks, blisters, or any other type of mechanical or structural damage were observed; and, in general all 12 fuel plates appeared to be in excellent physical condition. However, we did observe some rather striking differences in the oxide film on the surfaces of the plates from the three fuel elements. As shown in Fig. 13, the oxide film had spalled from the higher temperature regions of the plates from fuel element 5-0. (Note: Although we did not remove any fuel plates from element 5-I, we could see indications of a similar oxide-spalling pattern on the surfaces of these plates by looking through the coolant channels with a high-power telescope.) As shown in Fig. 14, the oxide-spalling pattern corresponded well with the region where the oxide film would be expected to be thickest; however, later results will show that the film thickness on these fuel plates actually increased to 0.0015 to 0.0020 in. before spalling began. The oxide film on the surfaces of the fuel plates from elements 21-0 and 49-I (Figs. 15 and 16, respectively) generally appeared to be much thinner and showed no indications of spalling.

In general, the film on the surfaces of the fuel plates from all three fuel elements appeared to be quite smooth and virtually featureless. However, as shown in Fig. 17, numerous small blisters were observed over the higher performance regions of the fuel plates from element 49-I and confined to the corrosion product film. These blisters were not apparent when this particular fuel element was first examined in the hot cells (i.e., during inspection of the coolant channels); thus, they probably formed sometime later in the examination program. Since



Fig. 13. Typical Appearance of Fuel Plates from HFIR Fuel Element 5-0. Regions where the oxide film had spalled from plate surfaces are clearly delineated by the large dark irregularly shaped areas. Approximately one-fourth actual size. Coolant flow is downward. (a) Concave surfaces, inner edge of plates at left. (b) Convex surfaces, inner edge of plates at right.



ACTUAL PHOTOGRAPH
OF AN IRRADIATED
HFIR FUEL PLATE

SCHEMATIC REPRESENTATION
OF AN IRRADIATED
HFIR FUEL PLATE

Fig. 14. Comparison Between Oxide Spalling Patterns on Fuel Plates from Element 5-0 with the Predicted Oxide Thickness Pattern for an Outer Annulus HFIR Fuel Plate.

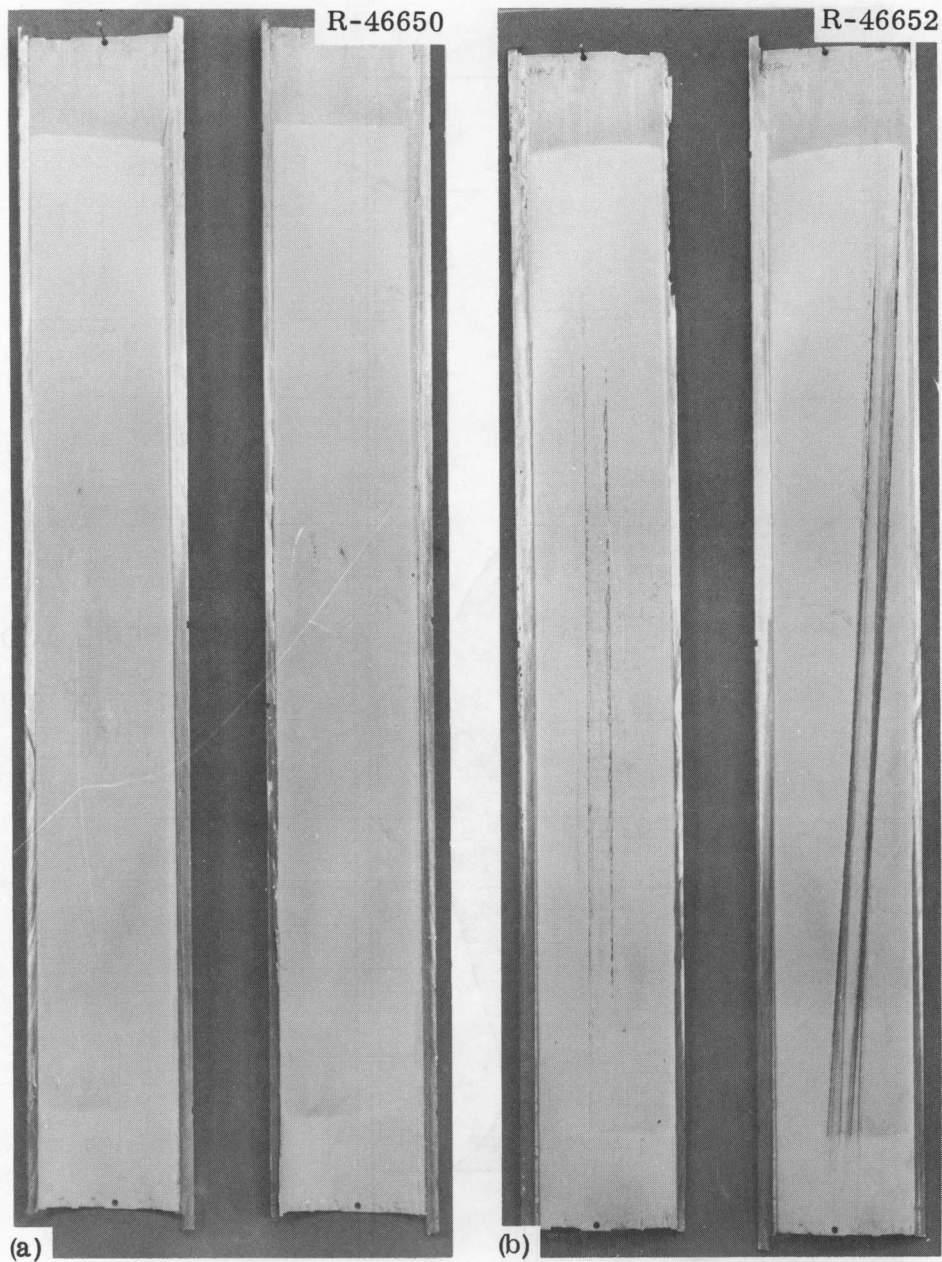


Fig. 15. Typical Appearance of Fuel Plates from HFIR Fuel Element 21-0. The dark, parallel lines on the convex surfaces of these fuel plates are rust stains from sections of a steel tape used as position indicators during disassembly of this fuel element and not an irradiation effect. Approximately one-fourth actual size. Coolant flow is downward. (a) Concave surfaces, inner edge of plates at left. (b) Convex surfaces, inner edge of plates at right.



Fig. 16. Typical Appearance of Fuel Plates from HFIR Fuel Element 49-I. Approximately one-fourth actual size. (a) Convex surfaces, inner edge of plates at left. (b) Concave surfaces, inner edge of plates at right.

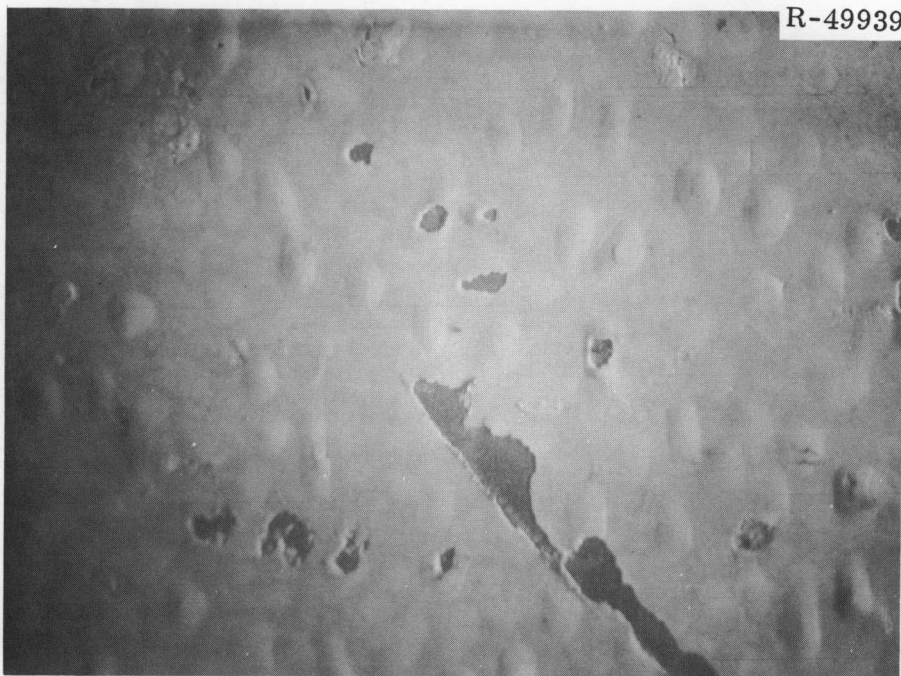


Fig. 17. Blisters in the Oxide Film on the Surfaces of the Fuel Plates from Element 49-I. Dark areas show where the film was accidentally scraped from the surface during hot-cell handling. Approximately 5X.

this particular fuel element was considerably hotter (thermally) than the other two elements, the blisters may have been caused by a partial decomposition of the oxide film as a result of the higher temperatures of these fuel plates while the element was in the hot cells.

Samples of the oxide film were scraped from the surfaces of a fuel plate from each element to identify the type of oxide present. X-ray diffraction results indicated that the oxide on the plates from elements 5-0 and 21-0 was predominantly bayerite ($\beta\text{-Al}_2\text{O}_3 \cdot 3\text{H}_2\text{O}$), whereas that from element 49-I was approximately 50% bayerite and 50% boehmite ($\alpha\text{-Al}_2\text{O}_3 \cdot \text{H}_2\text{O}$). This was surprising, since we expected that only boehmite would form on the surfaces of the HFIR fuel plates during irradiation. Although the initial boehmite film on the surfaces of the fuel plates could have transformed to bayerite during the 9- to 12-month underwater storage period in the HFIR pool, it is equally possible that the film formed during reactor operation could be bayerite, some of which decomposed to boehmite on the surfaces of the plates of element 49-I. This seeming discrepancy in the composition of the oxide film is one of the more perplexing aspects of the postirradiation results.

When the oxide films were chemically stripped from the surfaces of some of the fuel plates, we found numerous pits in their cladding (Fig. 18). Although these pits were not deep enough to be cause for alarm, it is perhaps important to note that they were not apparent until the oxide film was removed from the plate surfaces. Thus, pitting of these fuel plates might not have been discovered if the plates had not been chemically defilmed.

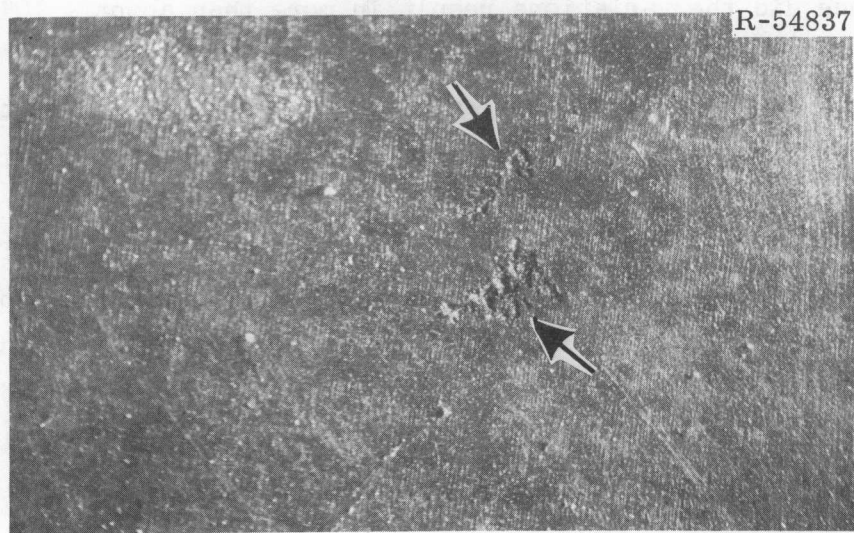


Fig. 18. Typical Appearance of Pits Found in the Cladding of the HFIR Fuel Plates after Removal of the Corrosion Product Films. Approximately 20X.

Gamma Scanning Results

The 12 fuel plates were gamma scanned to determine the relative time-integrated power distribution along and across them. The output of a NaI scintillation detector was recorded upon a strip-chart recorder as the fuel plates were driven at a slow, constant speed past a collimating slit in the detector shielding. A 3/16-in.-diam \times 17-in.-long collimator was used, and the detector circuitry was adjusted to record only gamma rays with energies greater than 0.4 MeV. We made three scans along and five across each fuel plate. The axial scans were made along the center of each plate and just inside the inner and outer edges of the fuel core, whereas the transverse scans were obtained at locations 3, 7.5, 12, 16.5, and 21 in. from the upper end of the 24-in.-long plate.

Typical examples of the axial scans of a fuel plate from each element are shown in Fig. 19 and Appendix B. In general, the scanning results appear to be consistent with the expected axial power distribution. Note, for example, that these activity scans are essentially symmetrical about the axial center line of the fuel plates (i.e., 12 in. from the upper end). The small deviations from a smooth, cosine curve (i.e., the small peaks and valleys) were reproducible and probably indicative of small variations in the fuel loading. Note, however, that in no instance did the variations result in more than about a 10% change in the local gamma activity level. Consequently, these small variations in the fuel loading resulted in less than a 10% deviation in the expected local power distribution over an area approximately 3/16 in. in diameter (i.e., the diameter of the collimator).

Typical examples of the scans across an inner and outer fuel plate at the axial midplane are compared with the predicted radial power distribution in Fig. 20. The agreement between the gamma scanning results and the predicted time-integrated power distribution appears to be excellent and shows that the reactor designers successfully flattened the power distribution across the fuel plates.

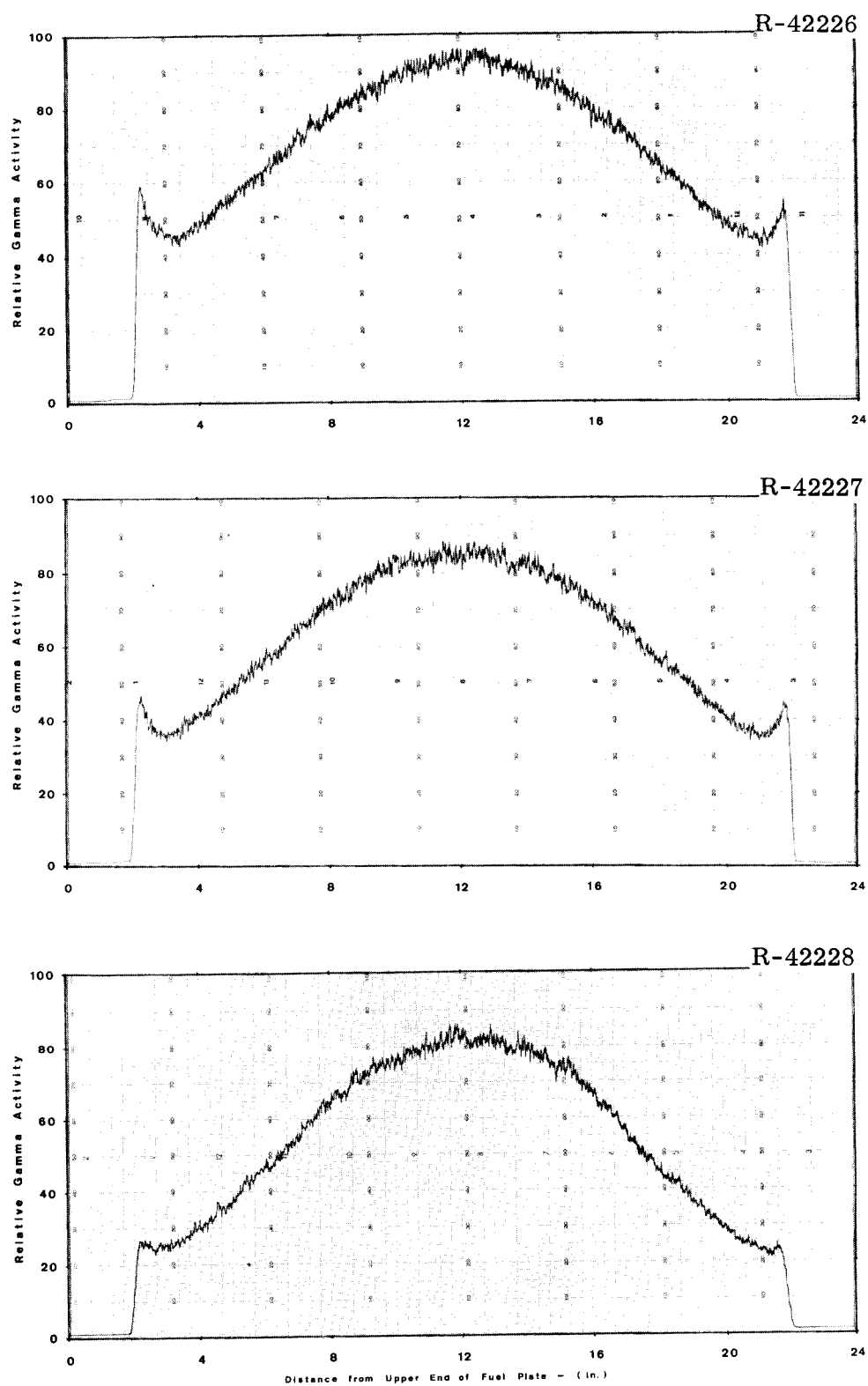


Fig. 19. Typical Axial Gamma Activity Scans of a Fuel Plate from HFIR Fuel Element 5-0. Scans were made at radial positions 16 cm (top), 18.5 cm (center), and 20 cm (bottom) from the core center line.

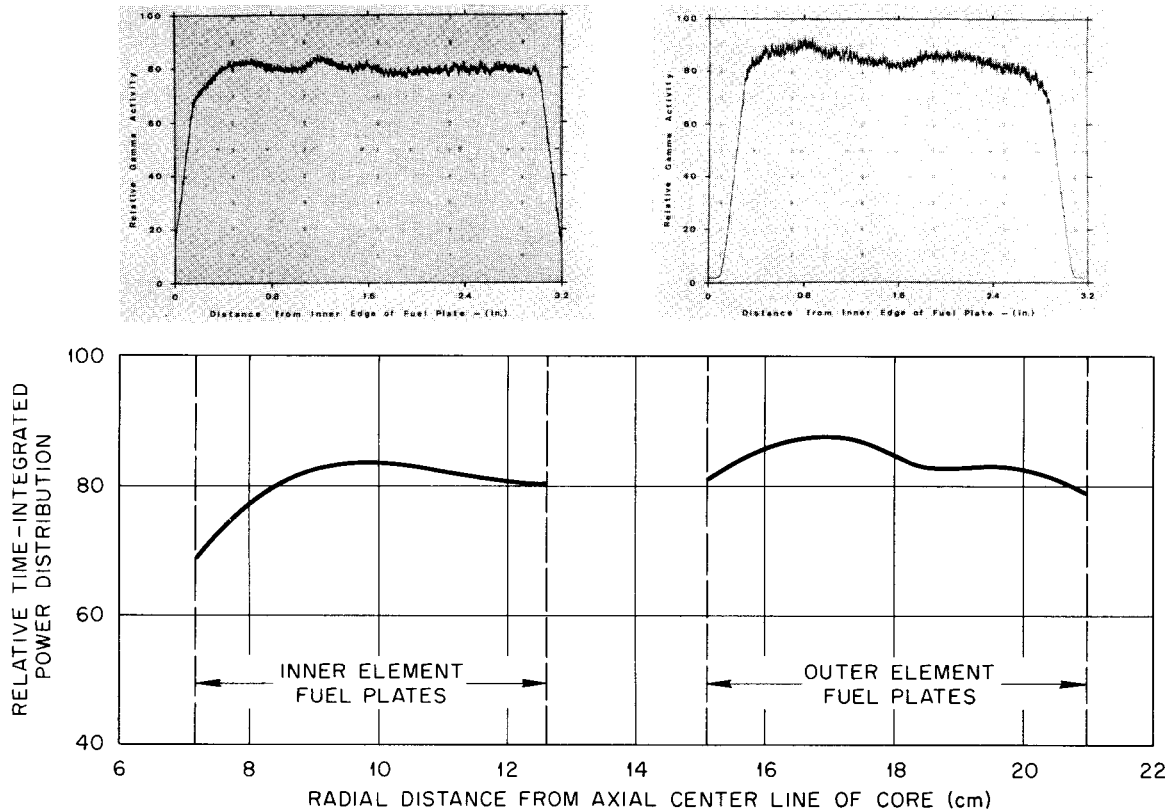


Fig. 20. Comparison Between Transverse Gamma Scanning Results and the Predicted Radial Time-Integrated Power Distribution for the HFIR Fuel Plates. Top-left, transverse gamma scan across axial center line of a fuel plate from element 49-I; top-right, gamma scan across axial center line of a fuel plate from element 21-0; bottom, predicted radial power distribution across both inner and outer fuel plates.

Fuel Plate Thickness Measurements

During reactor operation, one might expect that the HFIR fuel plates would increase in thickness as a result of the combined effects of irradiation-induced swelling of the fuel dispersion and the buildup of an oxide film upon the plate surfaces. This net increase in fuel plate thickness could be an important factor in the performance of the HFIR fuel assemblies, since it could decrease the coolant channel spacing and impede coolant flow. This along with poor heat conduction by an excessive oxide film could cause the plates to operate at an excessively high temperature. Consequently, we measured the thickness of the 12 fuel plates to determine the overall increase in thickness as a result of

exposure to the reactor environment. The oxide film was then chemically stripped from three plates from each element, the plate thicknesses were remeasured, and the oxide film thickness was determined from the thickness differences. Since the fuel burnup and the fuel plate irradiation temperature varied significantly along and across the plates, we measured the thicknesses at 1-in. intervals along each plate at three different radial positions (near the inner edge of the fuel core, at the hump, and near the outer edge).

Results of the thickness measurements on the fuel plates before and after chemical stripping of the oxide film are shown in Appendix C. In general, the fuel plates increased less than about 0.003 in. in thickness. Such small increases have no significant effect upon the satisfactory performance of the HFIR fuel elements.

Results of measurements of the oxide film thickness on the surfaces of fuel plates from the three irradiated HFIR fuel elements are summarized in Figs. 21 through 23. As indicated, metallographic measurements of the film thickness agreed quite well with that indicated from differences in the thickness of the stripped and unstripped fuel plates. In general, the oxide film on the surfaces of the fuel plates from all three elements was thicker than that predicted from calculations based upon Griess' correlation⁸ for the rate of oxide buildup upon aluminum surfaces in out-of-reactor corrosion tests. Note that the oxide thickness on fuel plates from element 5-0 (i.e., one of the pretreated fuel elements) is considerably thicker than that on plates from elements 21-0 and 49-I, even though the later elements were irradiated longer. This suggests that oxide built up more rapidly on the surfaces of the pretreated fuel plates. The actual oxide thickness profiles generally appear to have the same shape as that predicted by these calculations, differing only in absolute magnitude. However, it should be noted that the oxide film may have increased in thickness as a result of additional corrosion or transformation in the oxide after reactor operation. The storage period was much longer than the irradiation period, and since

⁸J. C. Griess et al., Effect of Heat Flux on the Corrosion of Aluminum by Water - Part III, ORNL-3230 (June 1961).

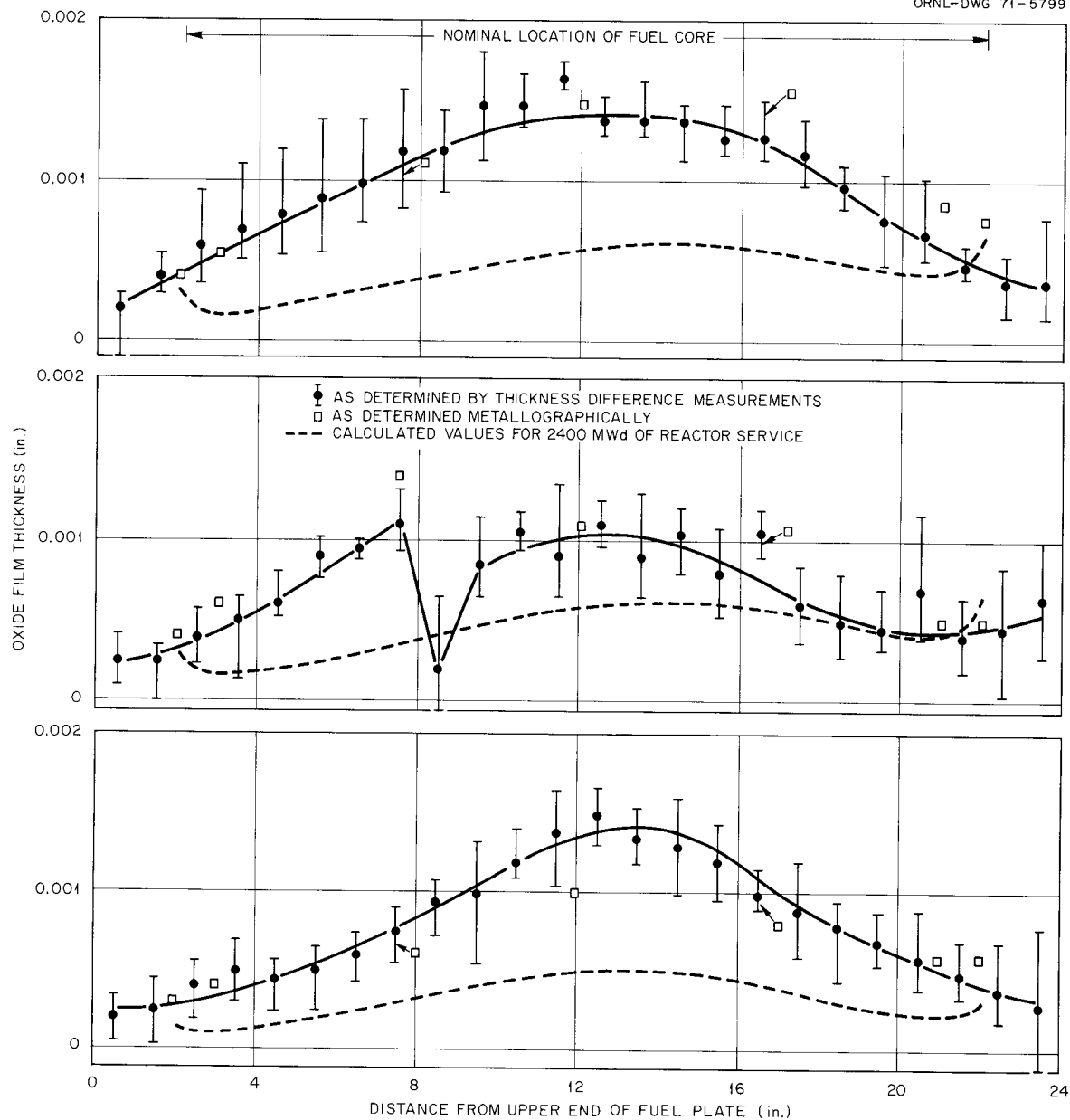


Fig. 21. Axial Film Thickness Profiles on Fuel Plates from HFIR Fuel Element 5-0. Near inner edge (top), over core hump (center), and near outer edge (bottom).

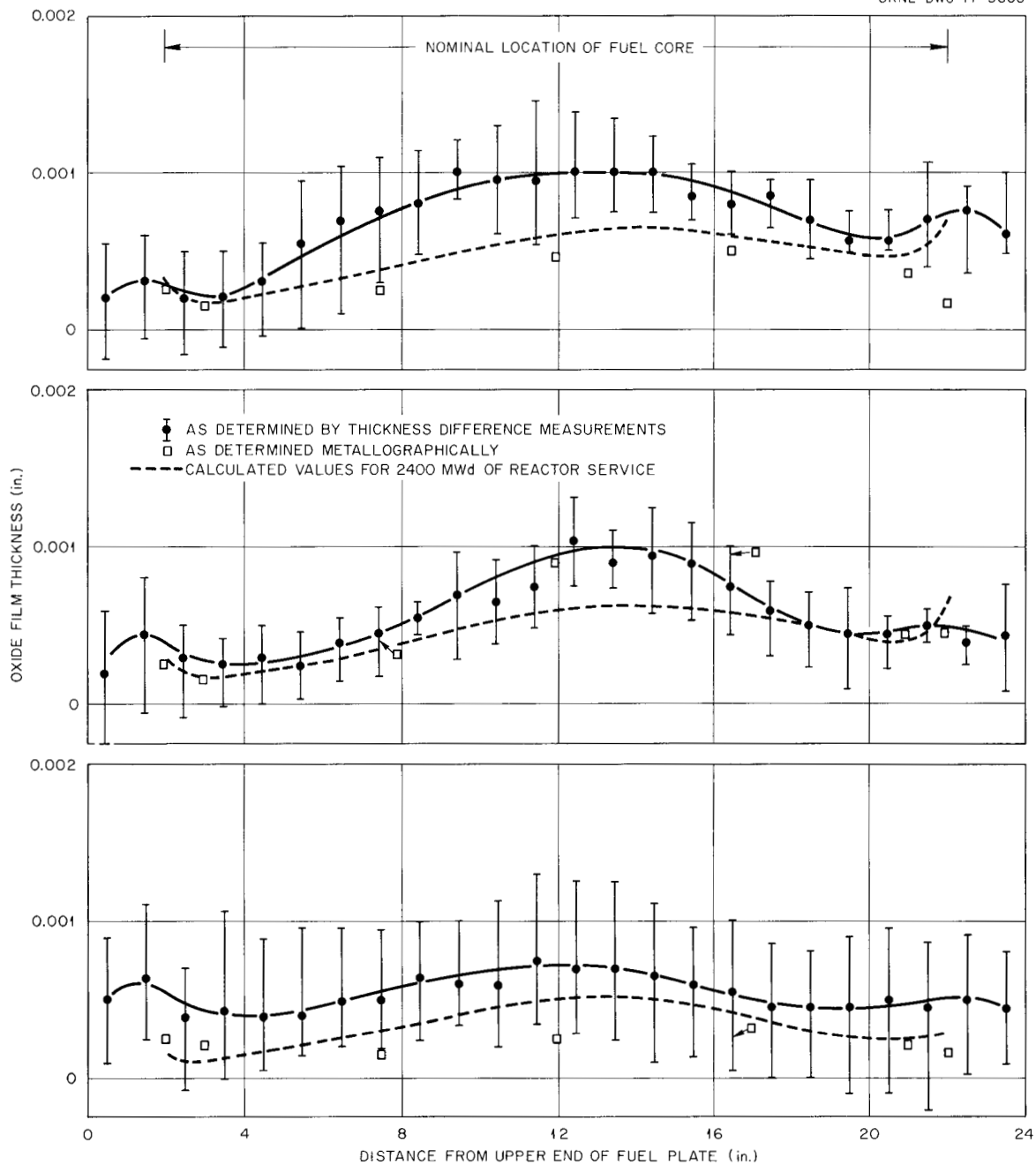


Fig. 22. Axial Film Thickness Profiles on Fuel Plates from HFIR Fuel Element 21-0. Near inner edge of plate (top), over core hump (center), and near outer edge (bottom).

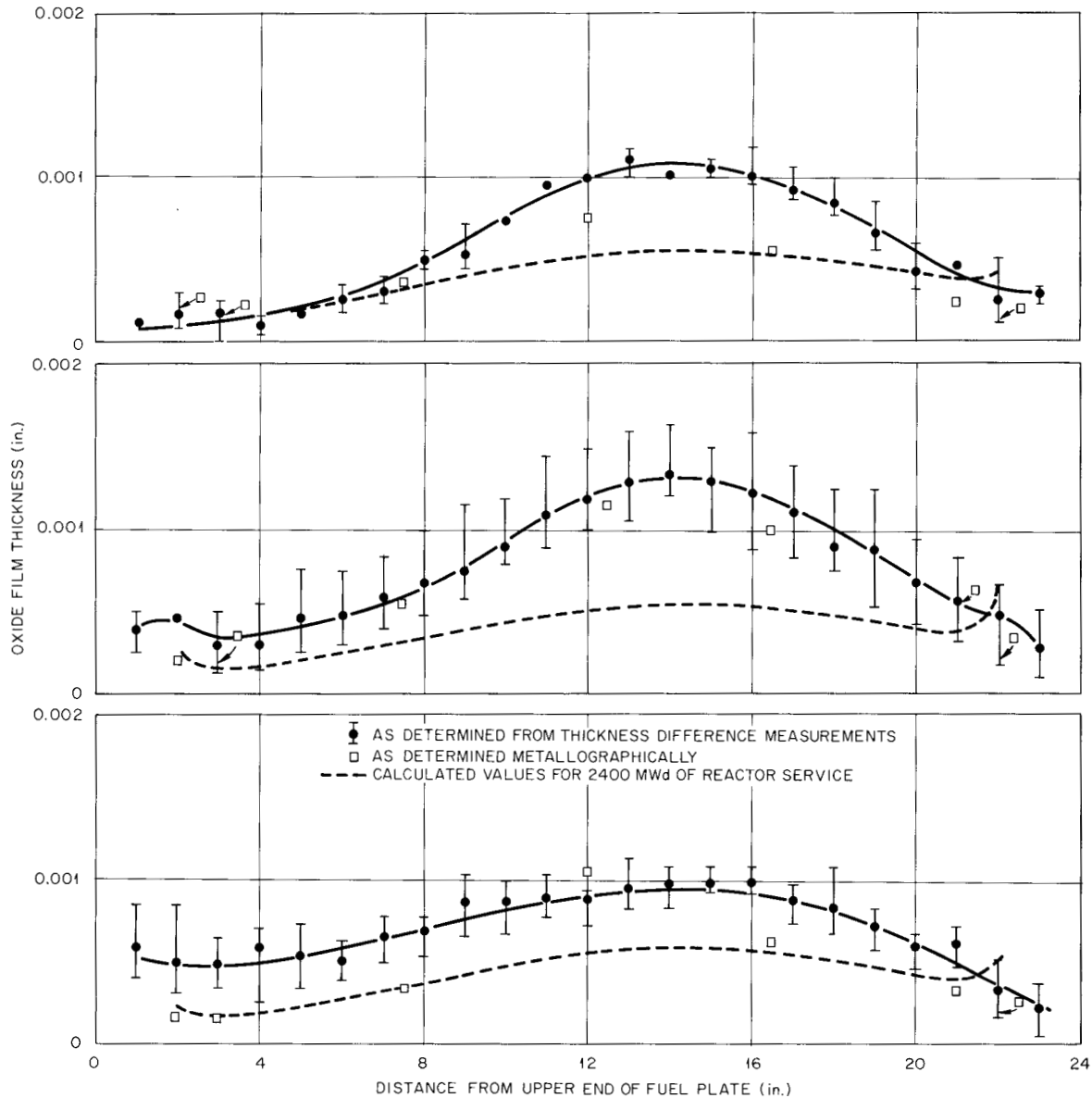


Fig. 23. Axial Film Thickness Profiles on Fuel Plates from HFIR Fuel Element 49-I. Near inner edge of plate (top), over core hump (center), and near outer edge of plate (bottom).

there was no forced circulation, the decay heat kept the fuel plates at temperatures approaching operating values. Another possible source of corrosion is treatment in the hot cells. No longer immersed, the elements became quite hot and were periodically sprayed with water to cool them. The resultant steaming and thermal cycling may have caused more corrosion than operation and storage. The channels gave a characteristic

uncorroded shiny appearance when first unloaded from the carrier; the finish became a dull gray during the weeks of handling in the cells. For these reasons, the measured oxide film thickness may not be indicative of the oxide actually present on the fuel plate surfaces during reactor operation.

Fuel-Plate Sectioning and Analytical Burnup Determinations

Since we saw no significant differences in the overall appearance or condition of the fuel plates from any one particular fuel element, we limited metallographic examination and analytical burnup determinations to sections from one fuel plate from each of the three elements.

The plates selected for metallographic examination and analytical burnup determinations were initially sectioned in the manner shown in Fig. 24 with a water-cooled abrasive cutoff wheel. As indicated, five burnup samples and seven metallographic specimens were cut from each plate. The axial locations of these various specimens were selected to provide metallographic specimens from the extreme upper and lower ends of the fuel core (i.e., specimens M-2 and M-22), the nominal minimum burnup regions (M-3 and M-21), two nominally intermediate burnup regions (M-7.5 and M-16.5), and the nominally maximum burnup region (M-12). The analytical burnup samples were selected similarly, providing samples from two minimum burnup locations, two intermediate burnup locations, and maximum burnup region. To determine the burnup at specific locations within the fuel plates, the five large burnup samples from each fuel plate were cut to provide samples from the inner edge, outer edge, and central region of each large section (Fig. 25).

The individual burnup samples were then submitted for uranium mass-spectrographic analysis, and the atom percent of total uranium fissioned was calculated for each sample from changes in the isotopic composition. The burnup of some of the samples was also determined radiochemically (i.e., from uranium and ^{137}Cs analyses) as a secondary check; generally, excellent agreement was found. The conversion of atom percent of total uranium fissioned to fissions/cm³ of fuel core was based upon the assumption that the cores of the inner and outer plates contained 21.5 and

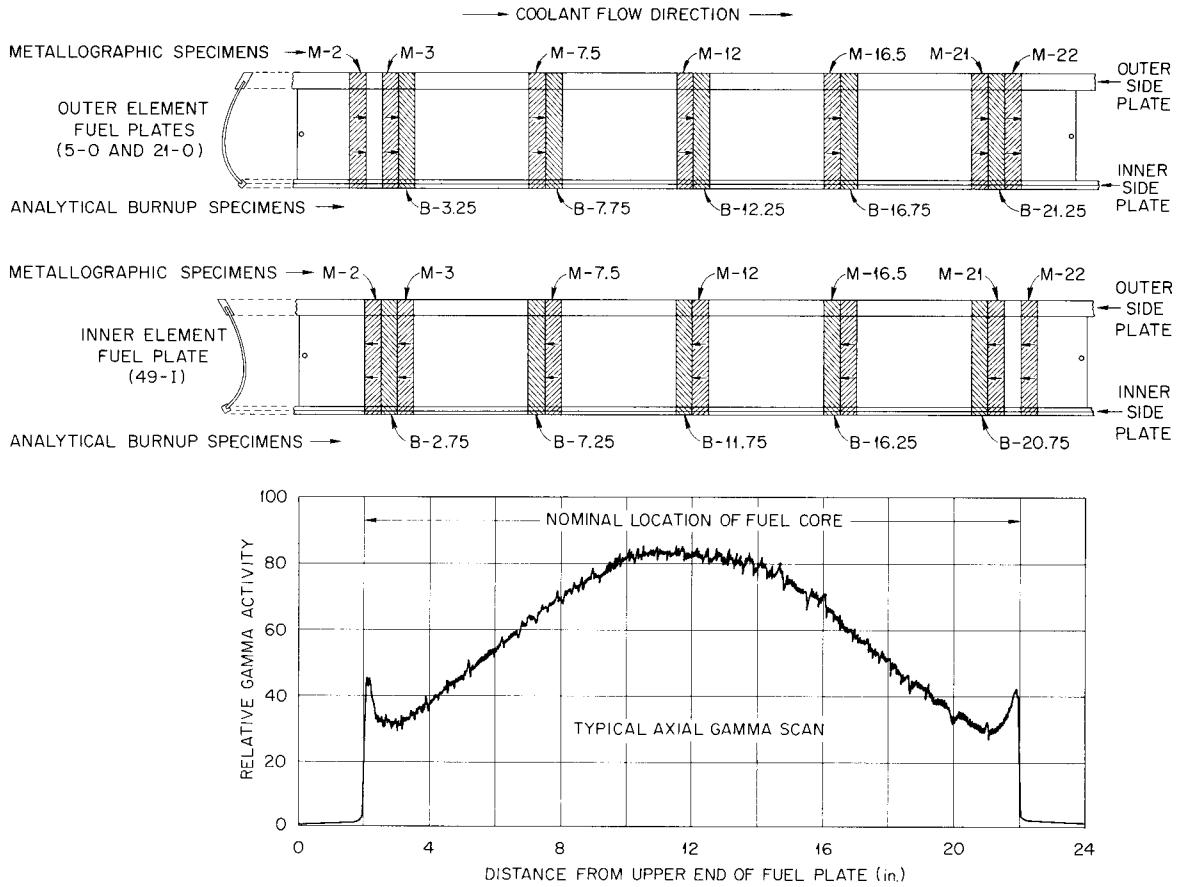


Fig. 24. Axial Location of Specimens Cut from the Irradiated HFIR Fuel Plates for Analytical Burnup Determinations and Metallographic Examination.

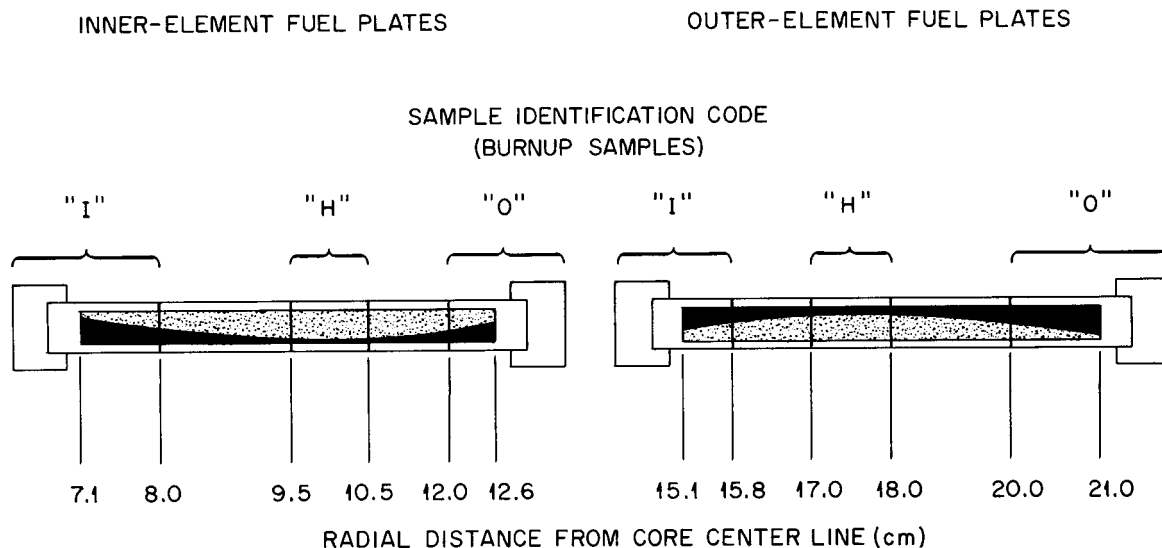


Fig. 25. Radial Locations of Burnup Samples Cut from the Irradiated HFIR Fuel Plates. Note that the sample identification code used can be employed to identify the axial and radial locations of the specimen (i.e., sample B-7.75-0 from a fuel plate from element 21-0 would be from a region 7.5 in. from the upper end of the plate and from 20 to 21 cm from the core center line).

31.2×10^{20} atoms/cm³ of uranium, respectively. These uranium contents were calculated for 30 and 40 wt % dispersions of U₃O₈ in aluminum, respectively, and 97% of theoretical density.

Results of the isotopic analyses and the calculated burnup values for the individual specimens are tabulated in Appendix D. As shown in Figs. 26 and 27, results of the burnup determinations on sections from elements 49-I and 21-0 were in excellent agreement with those predicted. The burnup of sections from the fuel plate from element 5-0 (not shown) was generally about 10% lower than those from element 21-0, as expected from the lower exposure (2046 compared with 2309 Mwd).

Since the analytical burnup determinations and the gamma scanning results were in such good agreement with the calculated burnup and time-integrated power distributions, it appears that the nuclear performance

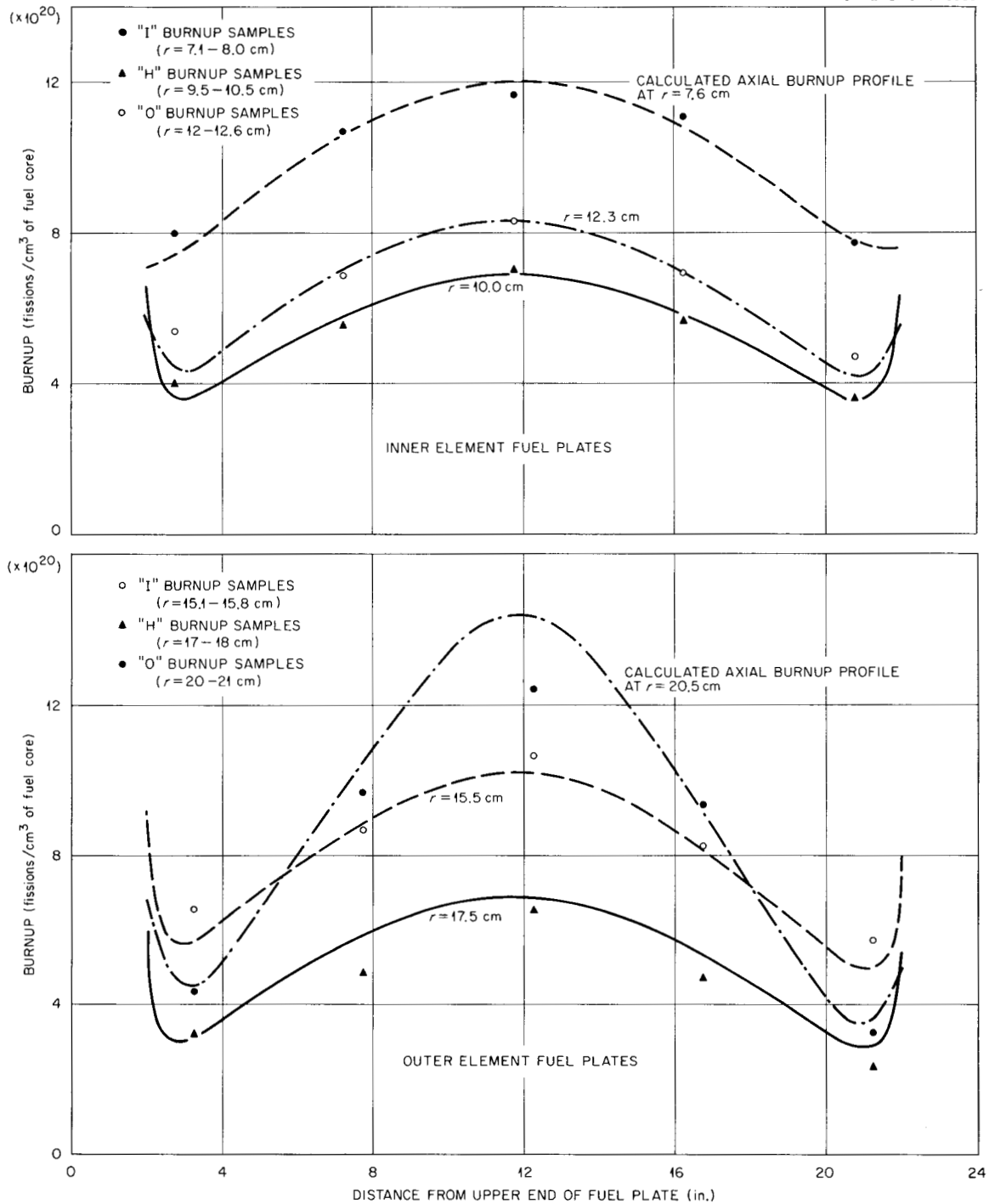


Fig. 26. Comparison of Predicted and Measured Burnup Values Along an Inner and an Outer Fuel Plate. Curves represent the predicted burnup profiles at indicated radial positions; data points represent analytical burnup values obtained on sections of a fuel plate from elements 49-I (top) and 21-0 (bottom).

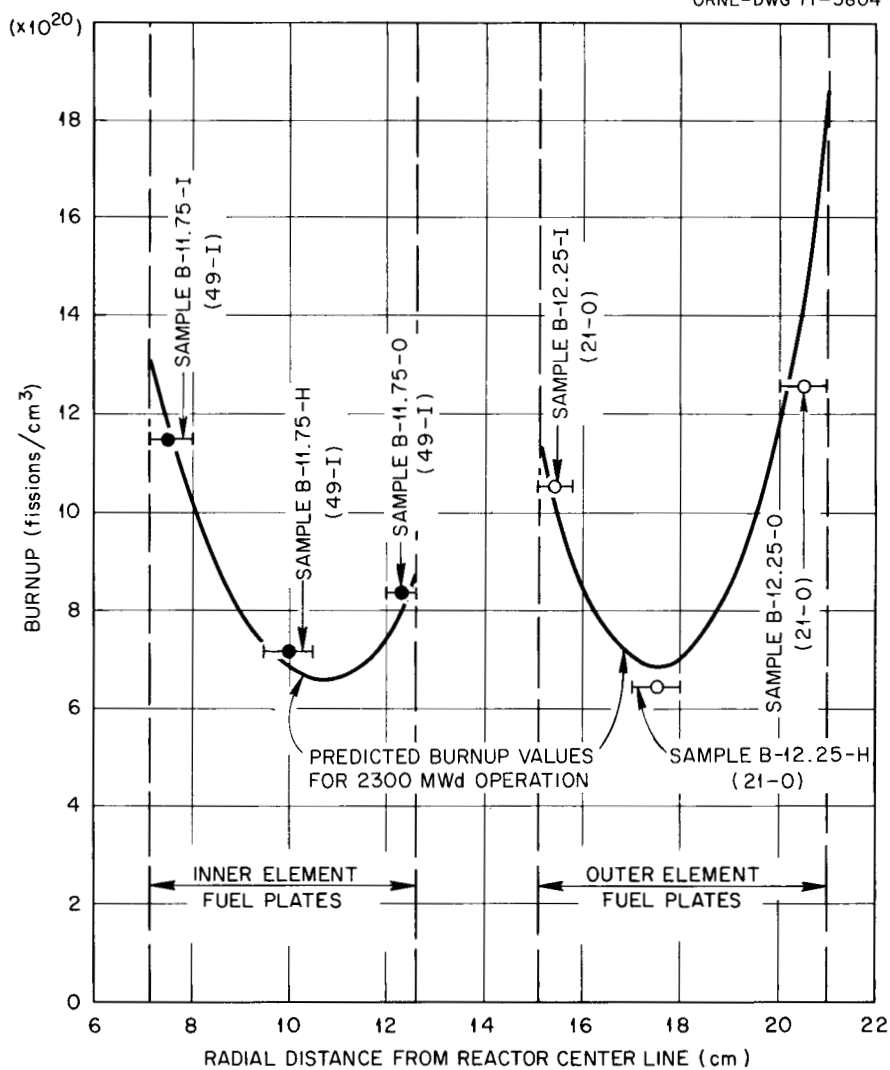


Fig. 27. Comparison of Predicted and Measured Burnup Profiles Across the Horizontal Midplane of the HFIR Fuel Plates.

of the HFIR fuel elements was in excellent agreement with that predicted from the core physics analysis.

Metallographic Examination

As described above, seven complete transverse cross sections were cut from one fuel plate from each of three irradiated fuel elements for metallographic examination. These particular fuel plates had not been chemically defilmed, so the oxide film on the surfaces of the plates was retained for metallographic inspection. Each of the 21 specimens was

next cut into four pieces that would fit into standard 1.25-in.-diam metallographic mounts, mounted in epoxy resin, wet-ground on successively finer grades of silicon carbide abrasive papers, and polished in two stages on Syntron vibratory polishers using diamond and magnesium oxide polishing compounds. All specimens were then examined in both the as-polished and etched conditions for evidence of structural damage and irradiation-induced microstructural changes. Over 450 photomicrographs were taken.

In general, the metallographic examination showed that all sections from the three fuel plates were in excellent condition. Although some indications of slight corrosion of the cladding and changes in the microstructure of the fuel dispersion were apparent, no evidence of any type of damage or defect that could be considered indicative of an actual or incipient failure of the fuel plate was observed in any of the 21 sections from the three fuel plates. The metallographic examination of these specimens revealed that the fuel plates of these three elements performed completely satisfactorily in service and that such fuel plates probably are structurally capable of performing satisfactorily at temperatures and burnup levels higher than can be achieved under normal HFIR operating conditions.

The overall condition of the fuel plates is illustrated in Appendix E with transverse cross sections of each of the three fuel plates at 15 different locations. Although the burnup and irradiation temperature varied from the maximum to the minimum values at the different locations, all sections of these fuel plates are structurally in excellent condition. No indications of cladding cracks, core-cladding separation, fuel core blisters, or any other type of structural defect were observed in any of the 21 complete transverse cross sections from these three fuel plates.

Unfortunately, we had no way to precisely determine how much swelling or corrosion occurred during the irradiation of these fuel plates. However, measurements of the core and cladding thicknesses on metallographic sections from the irradiated and unirradiated (i.e., as-fabricated) fuel plates indicated that neither swelling nor corrosion was excessive. The thickness of the core (fuel plus filler section) on

sections from the three irradiated fuel plates ranged between 0.0265 and 0.0285 in. No direct relationship was apparent between these core thickness values and fuel burnup; in fact, the minimum core thickness values often occurred in the higher burnup regions of the fuel plates. Since the cores of the unirradiated HFIR fuel plates normally range between 0.0260 and 0.0280 in. in thickness, the cores of the three irradiated fuel plates probably increased less than 0.001 in. in thickness as a result of irradiation. We had expected that the cores would swell only slightly.

The thickness of the cladding on sections of the fuel plate from element 5-0 ranged from about 0.0100 to 0.0115 in., and that on sections of the plates from elements 21-0 and 49-I ranged between 0.0105 and 0.0115 in. The cladding of the as-fabricated HFIR fuel plates normally ranges between 0.0110 and 0.0116 in. thick; consequently, corrosion could not have reduced the thickness of the cladding of the irradiated fuel plates by more than 0.0016 in. Actually, however, the cladding of the 5-0 fuel plates was probably reduced in thickness by less than 0.001 in. and that of the 21-0 and 49-I fuel plates by less than 0.0005 in. The greater attack of the element 5-0 fuel plates appears to be a result of the spalling of the oxide film during irradiation. The scalloped surfaces in Fig. E-1 are probably indicative of the heavier attack in regions where the film spalled.

As shown in Fig. 28, the oxide film on the surfaces of all three fuel plates appeared to be composed of two rather distinct layers of approximately equivalent thickness. The films generally appeared to be relatively smooth, tightly adherent, and free of cracks or fissures. However, we did observe some cracks in the oxide near where the film had spalled from the surface of the 5-0 fuel plate. In addition, the two layers had separated in some regions of the 49-I fuel plate to form small blisters (Fig. 29). This separation accounts for the small blisters noted in the visual examination of the element 49-I fuel plates (see Fig. 17, p. 30). However, it should be emphasized that these blisters formed during examination and are within the oxide film, and not within the fuel plate proper.

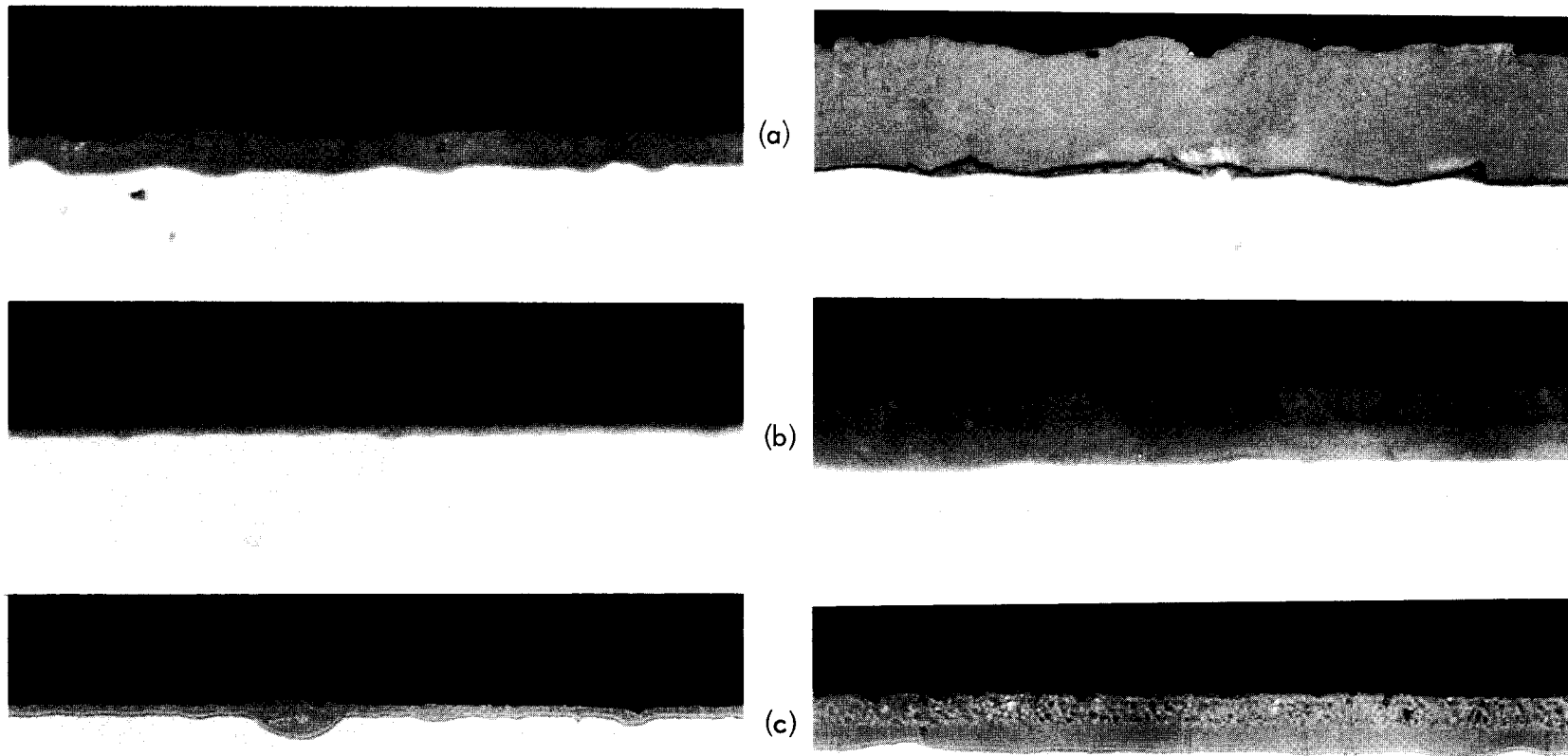


Fig. 28. Comparison of Oxide Films on the Surfaces of the Fuel Plates from HFIR Fuel Elements (a) 5-0, (b) 21-0, and (c) 49-I. These photomicrographs generally show the thinnest (left) and thickest (right) films found in the metallographic examination of a fuel plate from each element. 500X. As polished.



Fig. 29. Typical Blister Found in the Oxide Film on Fuel Plates from HFIR Fuel Element 49-I. 500X. As polished.

As mentioned previously, a number of shallow pits were observed in the surfaces of all fuel plates after chemical removal of the oxide films. Some of these pits were also found during the metallographic examination. Typical examples of these pits are shown in Fig. 30. Note that the oxide film over the surface of the pits is continuous; thus, such pits would not be apparent during visual inspection of the fuel plates until the oxide film had been chemically removed from the plate surfaces. As will be discussed later, the cause of these pits is uncertain; however, they do not appear to be a serious problem since they are relatively shallow (less than 0.003 in. deep).

Although not readily apparent at lower magnifications shown in Appendix E, the microstructure of the U_3O_8 -aluminum fuel dispersion varied considerably along and across each of the three irradiated fuel plates. These differences are perhaps more clearly shown in Fig. 31, which compares the microstructure of the fuel dispersion of an unirradiated HFIR fuel plate with that from the low-burnup, low-temperature and high-burnup, high-temperature regions. These changes in the microstructure of the fuel dispersion appear to result from at least two distinctly different mechanisms: (1) an irradiation-induced change in the microstructure of the U_3O_8 fuel particles proper, and (2) chemical reaction between the U_3O_8 fuel particles and the aluminum matrix material. Note, for example, that the cracks and fractures initially present in the U_3O_8 particles of the as-fabricated dispersion appear to have

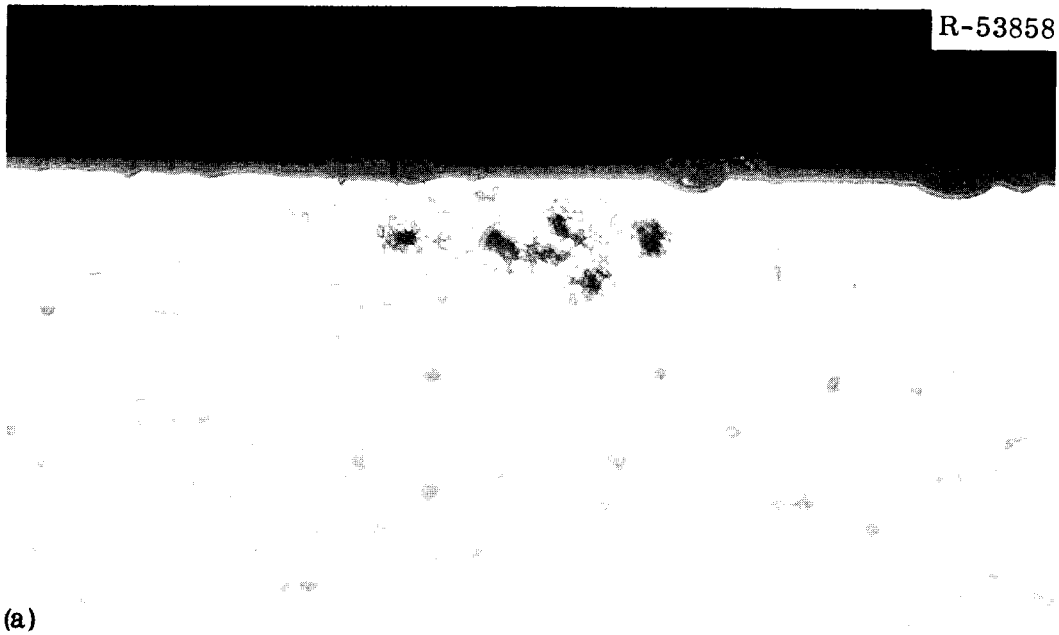


Fig. 30. Microstructural Appearance of Pits Found in the Cladding of the Irradiated HFIR Fuel Plates. 500X. As polished. (a) An early stage of pitting, and (b) fully developed pit.

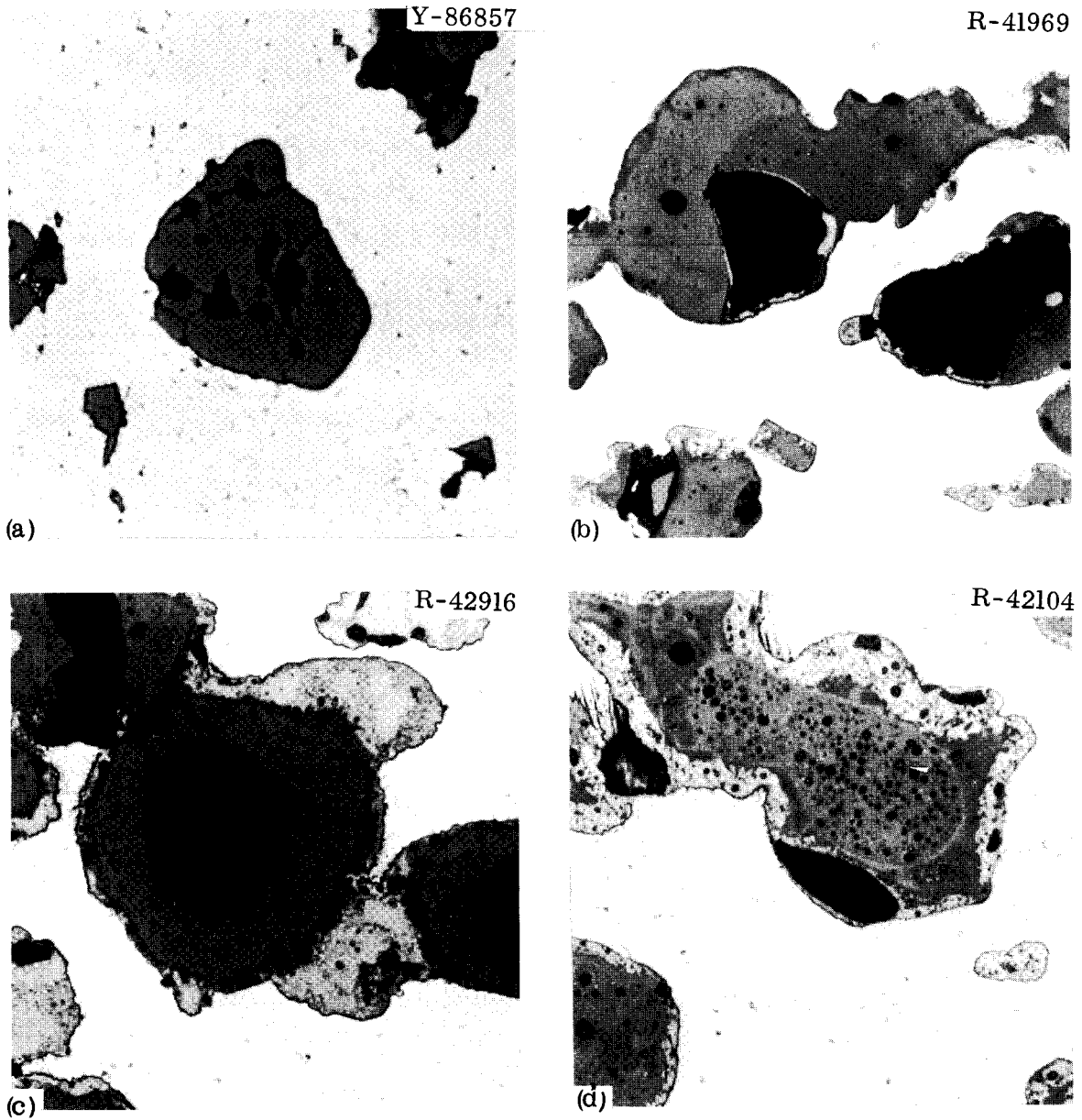


Fig. 31. Typical Microstructures of Fuel Cores of the HFIR Fuel Plates. As polished. 500X. (a) Unirradiated, (b) from a low-burnup, low-irradiation temperature region, (c) from an intermediate-burnup, high-irradiation temperature region, and (d) from a high-burnup, intermediate-irradiation temperature region.

healed or sintered even at the lowest burnup. Also, the numerous small voids and cracks have agglomerated to form rather large voids or pores. At higher burnup levels, these large voids generally appear to decrease somewhat in size; however, an increasing number of small, spherical voids (or perhaps fission-gas bubbles) begin to appear. In many respects, these changes appear to be somewhat analogous to the fuel restructuring often observed in bulk-oxide fuel pins for power reactors.

Since it has been known for some time that U_3O_8 is thermodynamically unstable in contact with aluminum, we were not surprised to find evidence of reaction between the fuel particles and the matrix. Although reaction between these two materials is generally quite sluggish even at 500 to 600°C in the absence of irradiation,⁹ extensive reaction has been observed¹⁰ in such dispersions after irradiation at temperatures as low as 100°C. On the basis of some early irradiation testing results of U_3O_8 -aluminum dispersions, Graber et al.¹¹ concluded that the extent of reaction was a function of both the fuel burnup and the irradiation temperature. As indicated in Fig. 31, the extent of reaction at higher burnup and higher irradiation temperature was significantly greater than at lower burnup and temperature. However, comparing the microstructure of the dispersion at other locations within the three fuel plates indicated that the extent of reaction might be a function of only the irradiation temperature and relatively independent of the fuel burnup in the range experienced by the fuel elements. For example, in regions of the fuel plates irradiated to the same burnup level but at different temperatures, as seen in Fig. 32(a) and (b), the reaction is greater in the region irradiated at the higher temperature. However, regions irradiated at the same temperature but to different burnup levels - compare Fig. 32(b) and (c) - show little difference in the extent of reaction.

⁹R. C. Waugh, The Reaction and Growth of Uranium Oxide-Aluminum Fuel Plates and Compacts, ORNL-2701 (March 9, 1959).

¹⁰A. E. Richt, C. F. Leitten, Jr., and R. J. Beaver, "Radiation Performance and Induced Transformations in Aluminum-Base Fuels," pp. 469-488 in Research Reactor Fuel Element Conference, September 17-19, 1962, Gatlinburg, Tennessee, TID-7642, Book 2 (1963).

¹¹M. J. Graber et al., Results of ATR Sample Fuel Plate Irradiation Experiment, IDO-16958 (March 1964), pp. 36-41.

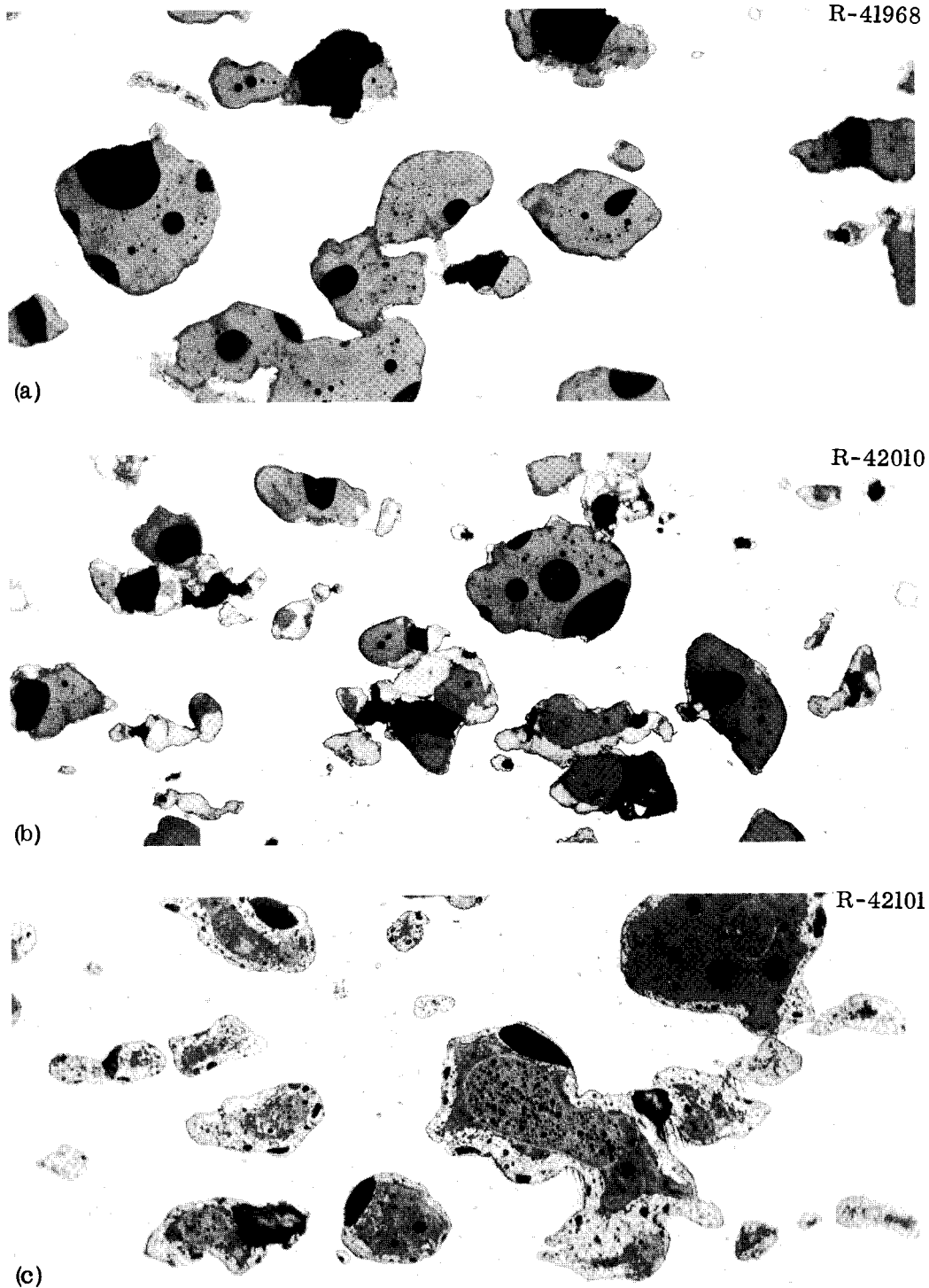


Fig. 32. Comparison of the Extent of Reaction in Regions of a Fuel Plate from Element 5-0 to the Same Burnup at Different Temperatures or Different Burnups at the Same Temperature. (a) 3×10^{20} fissions/cm³ at 80°C; (b) 3×10^{20} fissions/cm³ at 115°C; (c) 16×10^{20} fissions/cm³ at 115°C. As polished. White, aluminum matrix; black, voids; dark gray, U₃O₈; light gray, reaction products. Reduced 6%.

To check on this hypothesis, we attempted to estimate the extent of reaction in various regions of the three irradiated fuel plates by determining the volume fraction of aluminum remaining within the dispersion by areal analysis of the photomicrographs. Since aluminum is consumed during reaction with the U_3O_8 , the volume fraction of aluminum within the fuel dispersion should decrease with increasing amounts of reaction. The results of these measurements were then plotted as a function of the estimated fuel-core irradiation temperature. As shown in Fig. 33, the results clearly show that the extent of reaction between U_3O_8 and aluminum is primarily a function of the irradiation temperature and relatively insensitive to the fuel burnup, which is shown in parentheses by each point.

One other interesting aspect of the metallographic examination was the observation of zones showing fission-product-recoil damage around the individual fuel particles (Fig. 34). Although recoil-damaged zones have been previously observed around the fuel particles of irradiated dispersions of UO_2 in stainless steel,¹² to our knowledge these are the first photomicrographs to clearly show the recoil-damaged zones in an aluminum-base fuel dispersion. In these fuel plates, the width of the damaged zone appeared to be about 15 μm , which is in excellent agreement with the average accepted range of 13.8 μm for fission fragments in aluminum.

Measurements on sections from the irradiated and unirradiated HFIR fuel plates indicated that the hardness of the cladding and filler sections increased significantly as a result of irradiation. The hardness of the alloy 6061 cladding increased from 30 ± 1 to 64 ± 3 DPH, while that of the Alcoa 101 filler section increased from 24 ± 2 to 46 ± 4 DPH. In spite of the wide variations in fluence and irradiation temperature, we found little difference in the hardness of either the cladding or filler sections in the various regions of the three irradiated fuel plates. Such hardness increases are probably primarily a result of fast neutron displacement-type damage. These hardness increases are probably

¹²W. K. Barney and B. D. Wemple, Metallography of Irradiated UO_2 -Containing Fuel Elements, KAPL-1836 (June 1956).

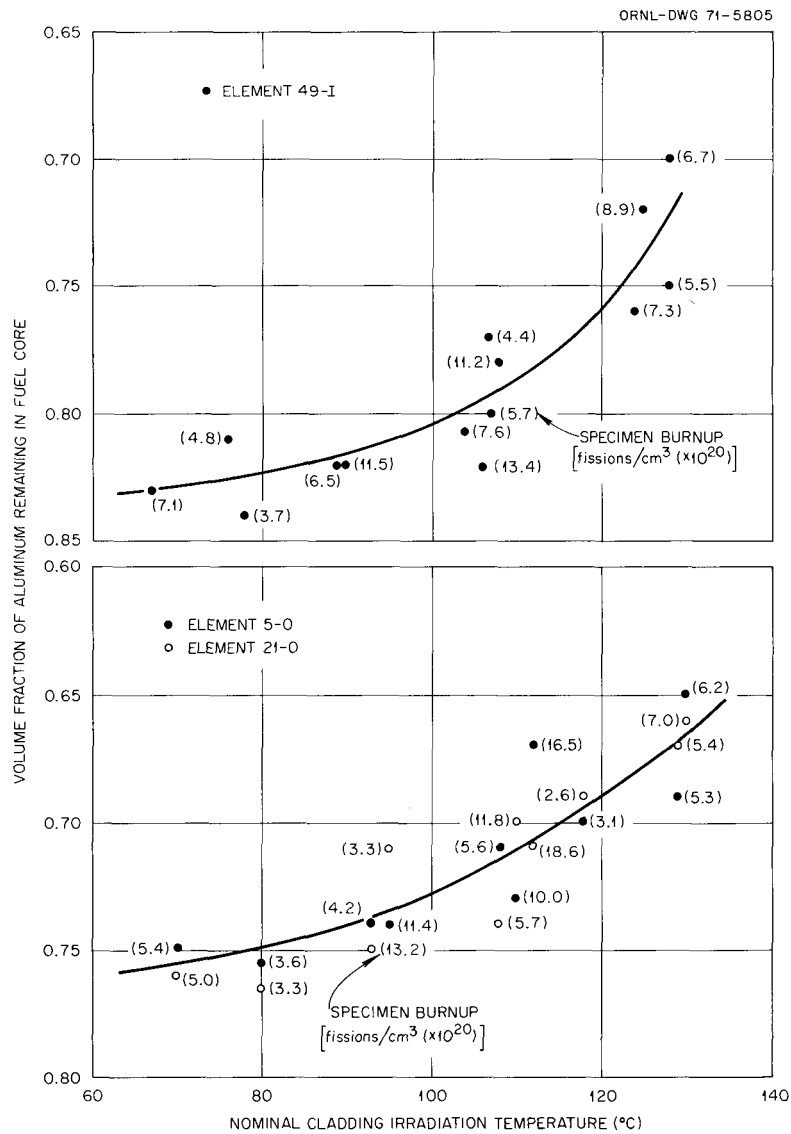


Fig. 33. Effect of Irradiation Temperature upon the Extent of Reaction in the Cores of the Inner (Top) and Outer (Bottom) Annulus HFIR Fuel Plates.

accompanied by corresponding increases in the yield strength and decreases in the overall ductility of the fuel plates proper. While such changes in the mechanical properties of the fuel plates could be considered as evidence of irradiation-induced damage, they could actually be advantageous for the HFIR fuel elements. In particular, the increase in the yield strength of the aluminum would make the fuel plates less susceptible to distortion by thermal or hydraulic forces during reactor operation.

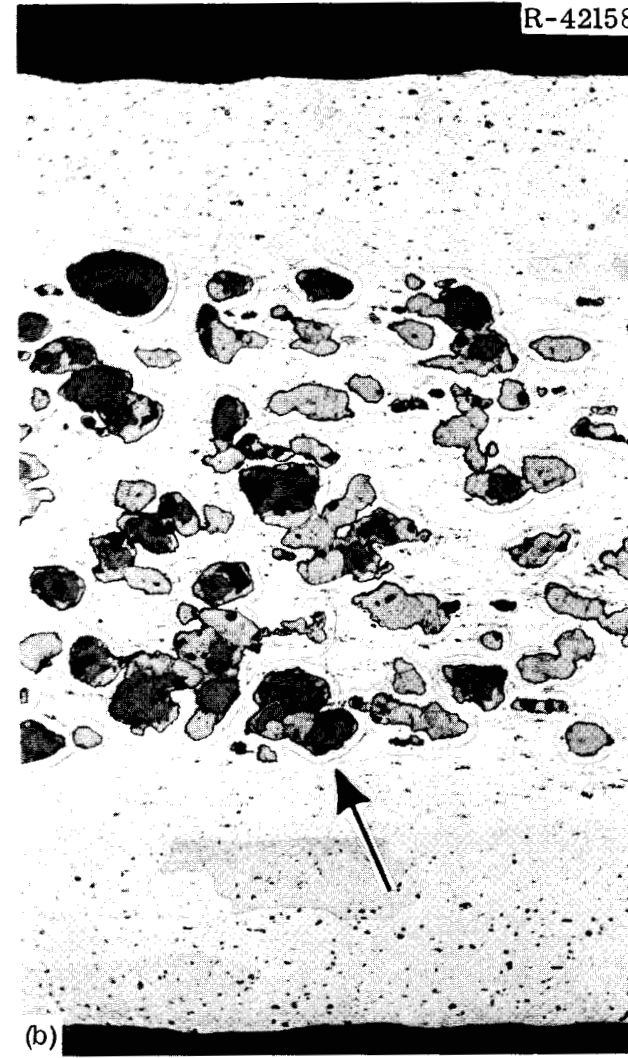
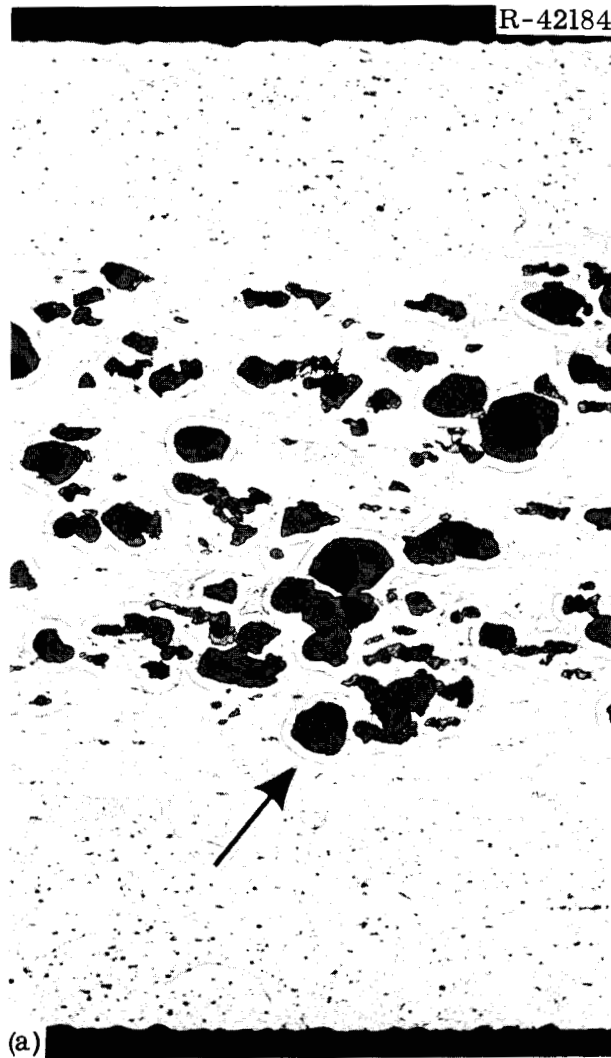


Fig. 34. Zones of Fission-Product Recoil Damage Surrounding Fuel Particles in the Irradiated HFIR Fuel Plates. 100X. Etched with 30% KOH. (a) Typical low-burnup, low-temperature region. (b) Typical high-burnup, high-temperature region.

Postirradiation Blister-Annealing Tests

Even though the present HFIR fuel elements have performed quite satisfactorily in reactor service, there is an economic incentive to develop fuel elements with longer nuclear lifetime. Such elements, of course, would contain a higher fuel loading and would also operate at somewhat higher temperatures and to significantly higher burnups. However, since the burnup and temperature limitations of the U_3O_8 -aluminum fuel dispersion have not really been established, some uncertainty remains whether such an advanced HFIR fuel element would perform satisfactorily under these more severe operating conditions. Workers at the Idaho Nuclear Corporation have suggested, however, that one can establish the burnup-temperature limitations of aluminum-base fuel materials from studies of the blistering behavior of irradiated fuel plates during post-irradiation heat treatments.¹³ In these so-called blister-annealing tests, sections of fuel plates that have been irradiated to various known burnup levels are heat treated at successively higher temperatures until the fuel plate blisters. The postirradiation blistering temperatures are then plotted as a function of burnup to obtain a curve that supposedly delineates the in-reactor burnup-temperature capabilities of that particular fuel material. Since the performance limitations of U_3O_8 -aluminum fuel dispersions are of considerable interest to the development of advanced HFIR fuel elements, we decided to conduct similar blister-annealing studies on plates from each of the three irradiated fuel elements.

As shown in Fig. 35, the postirradiation blistering temperature of the outer fuel plates was significantly higher than that of the inner plate. The blistering temperature of the inner plate appears to agree reasonably well with that reported¹³ for other U_3O_8 -aluminum dispersions, but that of the outer plates appears to be about 100°C higher.

¹³M. F. Marchbanks, W. C. Francis, and M. L. Griebenow, Reactor Engineering Branch Annual Report Fiscal Year 1969, IN-1335 (November 1969), pp. 49-52.

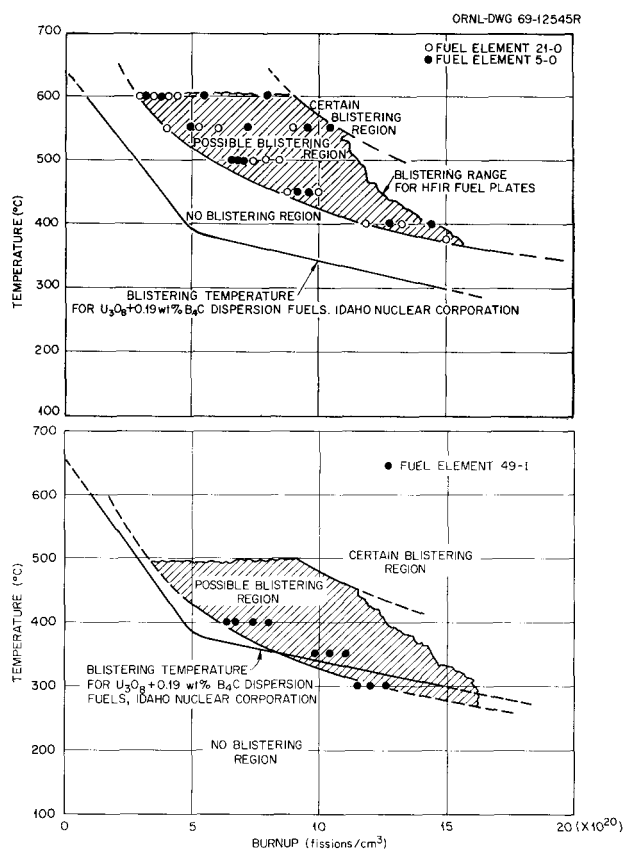


Fig. 35. Postirradiation Blistering Temperatures of Outer (Top) and Inner (Bottom) HFIR Fuel Plates. Idaho Nuclear Corporation results are from Marchbanks et al.¹³

At present, we have no completely satisfactory explanation for these differences in the postirradiation blistering of these fuel plates. However, the postirradiation blistering temperature of the U_3O_8 -aluminum fuel dispersions is apparently not strictly a function of the fuel core fission density. Differences in the blistering behavior of the inner and outer HFIR fuel plates might be attributed to the differences in the fuel loading of these plates (the cores of the inner plates contain a 30 wt % U_3O_8 dispersion and those of the outer plates contain a 40 wt % U_3O_8 dispersion). If this is true, one would expect the post-irradiation blistering temperature of the advanced HFIR fuel plates, which would contain approximately 25% higher fuel loadings, to be significantly different from that of the present elements. Consequently,

one could not use the blistering temperature curves for the present HFIR fuel plates to establish the performance limitations of the advanced fuel plates.

Proper interpretation of the value of these postirradiation blister-annealing tests is further clouded by the fact that the blistering temperature of both the inner and outer HFIR fuel plates appeared to depend not only upon the fission density and fuel loading but also upon the irradiation temperature. In regions of the plates exposed to equivalent fission densities, areas irradiated at the higher operating temperatures consistently exhibited higher blistering temperatures. An example of this behavior is given in Fig. 36, which shows two sections of the fuel plate from element 21-0 after the 1 hr heat treatment at 600°C. The section from the upper end (coolant inlet) was irradiated at less than 100°C and achieved a burnup of 3.5 to 10×10^{20} fissions/cm³. The other section was cut from the axial midplane of the fuel plate, where the irradiation temperatures ranged from 115 to 130°C and the burnups ranged between 6.0 and 18.5×10^{20} fissions/cm³. Blisters are apparent over the entire fueled region of the upper section of this plate, even over the regions of very low burnup (i.e., 3.5×10^{20} fissions/cm³). Blistering is also apparent in the higher burnup regions of the other section of this plate, but there are no blisters over a relatively large area near the center of this section. The burnup in this unblistered area ranged between 6.0 and 9.0×10^{20} fissions/cm³. This apparent dependence upon the irradiation temperature may account for the relatively large "possible-blistering" bands in Fig. 35. More importantly, it raises considerable questions as to the validity of using postirradiation blister-annealing data to establish the in-reactor performance limitations or capabilities of any U₃O₈-aluminum fuel plates. For example, one might logically expect that the blister resistance of a given fuel plate would decrease if the irradiation temperature was increased. These blister-annealing results, however, suggest that the blister resistance of that same fuel plate increases with increasing irradiation temperature. We therefore feel that these blister-annealing results are of little value in attempting to establish the performance capabilities of either the present or advanced HFIR fuel plates.

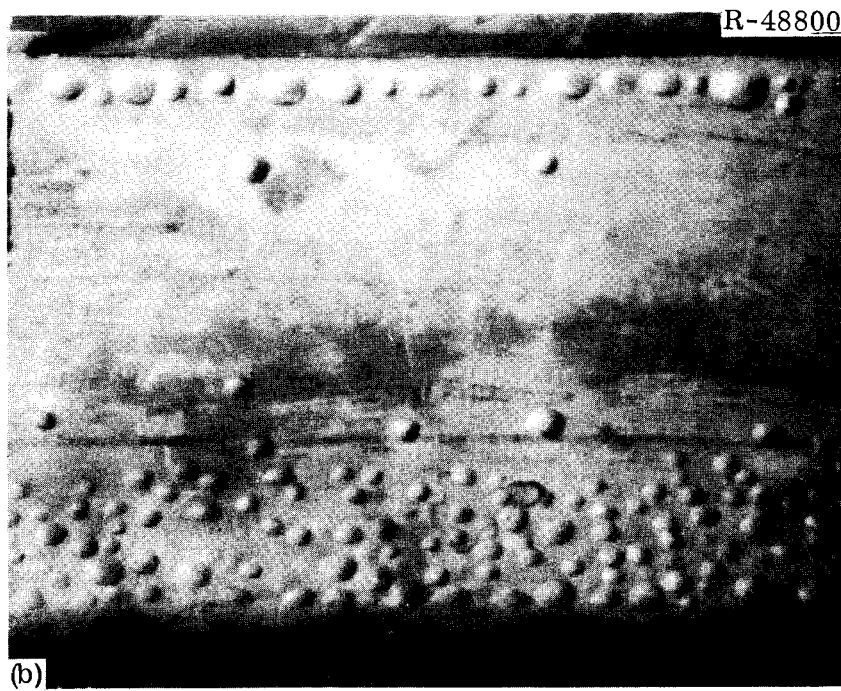
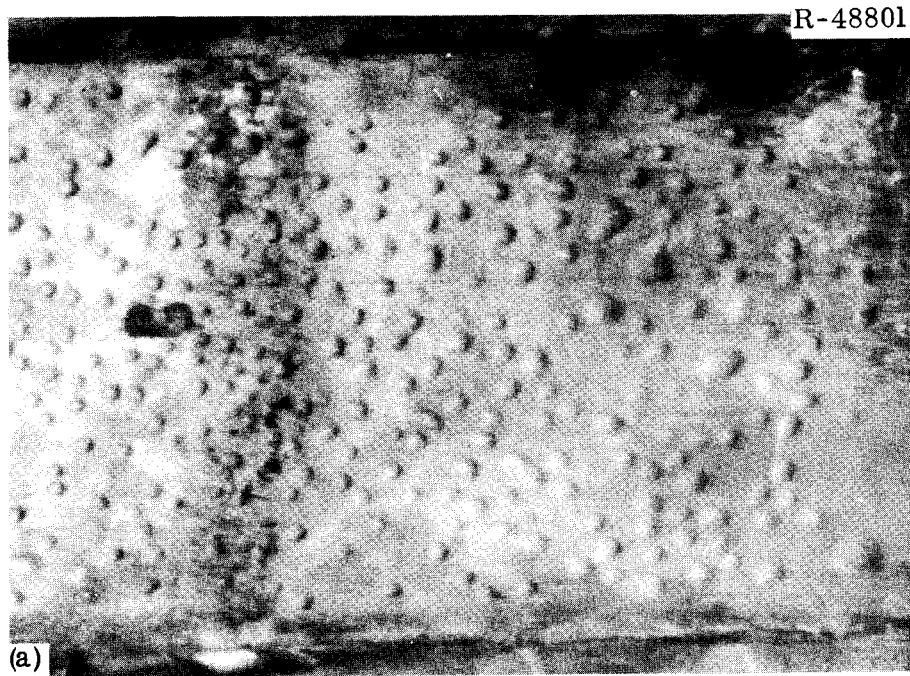


Fig. 36. Sections of an Irradiated HFIR Fuel Plate from Element 21-0 after Heat Treatment for 1 hr at 600°C. (a) Section from upper end of fuel plate. (b) Section from reactor midplane. Approximately actual size.

DISCUSSION

In discussing the results of the postirradiation examination and evaluation of the spent HFIR fuel elements, it is perhaps important to first emphasize that no adverse effects on reactor operations associated with any fuel element have been encountered in the entire operational history of this reactor. Since startup of the HFIR in March 1966, over 60 fuel cores (consisting of over 120 fuel elements) have been operated to their reactivity lifetime at the full design power level of 100 MW without difficulty and with no indications of a fuel element or a fuel plate failure. From an operational viewpoint, therefore, one must conclude that the current HFIR fuel elements perform quite satisfactorily under the present reactor operating conditions. Results of the post-irradiation examination of these four particular spent fuel elements completely support this conclusion. Consequently, we conclude that the useful lifetime of the current HFIR fuel elements is limited only by the reactivity lifetime of these elements and not by irradiation damage. An arbitrary restriction upon the operational lifetime of these fuel elements is therefore both unnecessary and undesirable.

One should not assume, however, that the HFIR fuel elements are completely unaffected by exposure to the reactor environment. Results of the postirradiation examination, for example, clearly show that corrosion, small dimensional changes, and chemical reactions within the fuel dispersion occur during reactor service. Since these effects are an important part of the performance of the HFIR fuel elements, a more detailed evaluation of their significance appears to be warranted for the development of advanced elements.

Dimensional Stability

The postirradiation examination indicates that the dimensional stability of the HFIR fuel elements is quite adequate for the reactor operating requirements. No evidence of significant changes in the length, inner diameter, or outer diameter of fuel assemblies was noted. Corrosion apparently caused the fuel plates to increase slightly in

thickness during irradiation, resulting in a slight corresponding decrease in the plate spacing; however, there were no indications of gross changes in fuel plate spacing, such as would be expected if the individual fuel plates had buckled or warped during reactor service. Irradiation-induced swelling of the fuel dispersion caused less than a 0.001 in. increase in the overall thickness of the fuel plates. As shown in Fig. 37, our irradiation testing program¹⁴ has shown that these particular dispersions can be irradiated to burnup levels of up to about 9×10^{20} fissions/cm³ without swelling. Even at burnup levels as high as 19×10^{20} fissions/cm³, the total core volume increase would only be about 6%. When one considers the rather unique geometry of the HFIR fuel cores and the fuel plate burnup profiles (see Figs. 6 and 7, pp. 10 and 11, respectively), such small thickness increases are not surprising. For example, most areas within these fuel plates are exposed to burnup levels less than 9×10^{20} fissions/cm³; thus, no increase in fuel core thickness would be expected in these areas. In regions exposed to burnups greater than 9×10^{20} fissions/cm³, cores are relatively thin. At the maximum burnup location (at the outer edge of the outer annulus fuel plates) the fuel core is only 0.009 in. thick.

¹⁴A. E. Richt and M. M. Martin, Fuels and Materials Development Program Quart. Progr. Rept. Dec. 31, 1969, ORNL-4520, pp. 266-272.

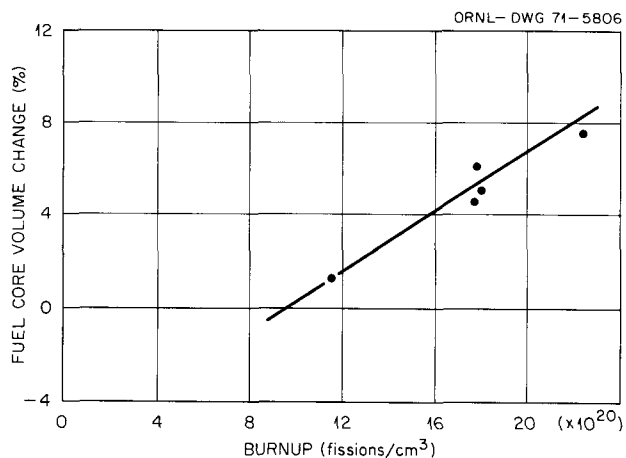


Fig. 37. Experimental Fuel Core Swelling Results for HFIR-Type U₃O₈-Aluminum Dispersions.

Thus, even at the burnup level of 19×10^{20} fissions/cm³, a 6% increase in fuel core thickness should result in only a 0.00054 in. increase in the overall thickness of the fuel plate. Consequently, fuel core swelling does not limit the performance of the current HFIR fuel elements.

Structural Integrity

The overall structural integrity of the current HFIR fuel elements also appears to be quite adequate for the reactor operating conditions. Although the U₃O₈ fuel particles react with the aluminum matrix during irradiation, the reaction does not compromise the integrity of the fuel plate. No indications of fuel core blisters, core-cladding separation, matrix cracking, or any other actual or incipient structural failure of a fuel plate were observed in any region of these fuel plates; thus, the U₃O₈-aluminum fuel dispersions performed satisfactorily at the temperatures and burnup levels encountered in this reactor. Corrosion also appears to be insignificant in that the overall reduction in the thickness of the cladding of the fuel plates is negligible. However, pitting of the cladding and the buildup of a corrosion-product film on the surfaces of the fuel plates may be significant factors in the performance of advanced HFIR fuel elements.

Corrosion

In many respects corrosion appears to be the most important and, unfortunately, the least understood aspect of the irradiation behavior of the HFIR fuel elements. In particular, corrosion apparently is responsible for (1) the only significant dimensional changes found in any of these fuel elements, (2) differences between the in-reactor performance of pretreated and non-pretreated fuel elements, (3) the most damage incurred by these fuel elements, and (4) the only discrepancy between the predicted and actual behavior.

The only significant change in the dimensions of the HFIR fuel elements appears to be a slight increase in the overall thickness of the fuel plates and a corresponding slight decrease in the plate spacing in the coolant channels. These changes result primarily from the buildup

of corrosion-product films on the surfaces of the fuel plates and not from irradiation-induced swelling of the fuel plates. Although these dimensional changes cause no significant problems, they do provide a plausible explanation for the observed differences in the in-reactor behavior of pretreated and non-pretreated HFIR fuel elements. Whenever the reactor operated with pretreated fuel elements, the coolant flow rate gradually decreased and the pressure drop across the elements gradually increased during the fuel cycle. However, no significant changes in either flow rate or pressure drop have been observed during fuel cycles when non-pretreated fuel elements were being used. The oxide film spalled only from the higher performance regions of the pretreated fuel plates.

Probably the two most disturbing aspects of the examination of the spent HFIR fuel elements were (1) the discovery of numerous, shallow pits in the cladding of the fuel plates, and (2) the fact that the corrosion-product films on the surfaces of these plates were considerably thicker than anticipated. However, we doubt that these effects occurred during irradiation; they probably resulted from subsequent corrosion or changes in the oxide film during 9 to 12 month storage in the HFIR pool or during spraying to cool the elements in the hot cells. If these pits and thicker oxide films resulted from storage or hot-cell handling, they have no bearing upon the irradiation behavior of the fuel elements. Since advanced elements would have a longer operational lifetime, pitting could conceivably penetrate the cladding and release fission products to the coolant. The discrepancy between the predicted and actual film thicknesses could be even more significant, for it questions the adequacy of the heat transfer calculations to predict the operating temperatures of the fuel plates. In particular, if the oxide film builds up more rapidly on the plate surfaces, or if the oxide is bayerite instead of boehmite, the fuel-plate temperatures and deflections might exceed safe limits. Since resolution of these questions appears to be important to both the current and advanced fuel-element programs, we recommend effort to determine both the type and thickness of the oxide films on the surface of the HFIR fuel plates be made as soon as is possible after shutdown of the reactor.

Additional Comments

Except for the possible discrepancy in the rate of buildup of the corrosion-product films upon the surfaces of the fuel plates, the current HFIR fuel elements apparently perform in general accord with their anticipated behavior. Gamma-scanning and analytical burnup results, for example, show that the time-integrated power and fission-density distribution within the fuel plates of these elements were in good agreement with that predicted from the core physics calculations. Thus, the nuclear behavior of the elements appears to be remarkably close to that predicted by the reactor designers.

Although the in-reactor performance of the pretreated fuel elements is not typical of that of standard, non-pretreated HFIR fuel elements, the successful operation of the pretreated elements may have some implications concerning the possible irradiation behavior of any advanced HFIR fuel element concepts. Since the oxide film apparently builds up much more rapidly upon the surfaces of the pretreated fuel plates, one would expect that they operated at a higher temperature. In spite of these higher temperatures, however, the fuel plates incurred no significant damage. Thus, the U_3O_8 -aluminum fuel dispersions appear to be capable of operating successfully at temperatures at least somewhat higher than normally encountered in the HFIR. Consequently, the prospects of achieving successful operation of these dispersions under the higher operating temperatures expected in advanced HFIR fuel elements appear to be promising.

CONCLUSIONS

Based upon the results of the postirradiation examination and evaluation of four spent HFIR fuel elements, we conclude the following:

1. The current HFIR fuel elements perform quite satisfactorily throughout their reactivity lifetime under the present operating conditions. The dimensional stability is excellent, and there is nothing to indicate that the elements suffer any type of structural damage that would result in reactor operating problems. Consequently, the useful

lifetime of these fuel elements is limited only by nuclear physics considerations and not by any irradiation-induced damage. An arbitrary limitation upon the operational lifetime of these fuel elements is therefore unnecessary under the present reactor operating practice.

2. Although corrosion does not appear to be a significant problem with the current HFIR fuel elements, additional work will be required to determine if it may limit possible advanced HFIR fuel elements. In particular, we need to resolve some unanswered questions concerning composition and rate of buildup of corrosion-product films upon the surfaces of the current HFIR fuel elements, and determine if the shallow surface pitting found in the postirradiation examination of these elements occurred during reactor service or during postirradiation storage or handling.

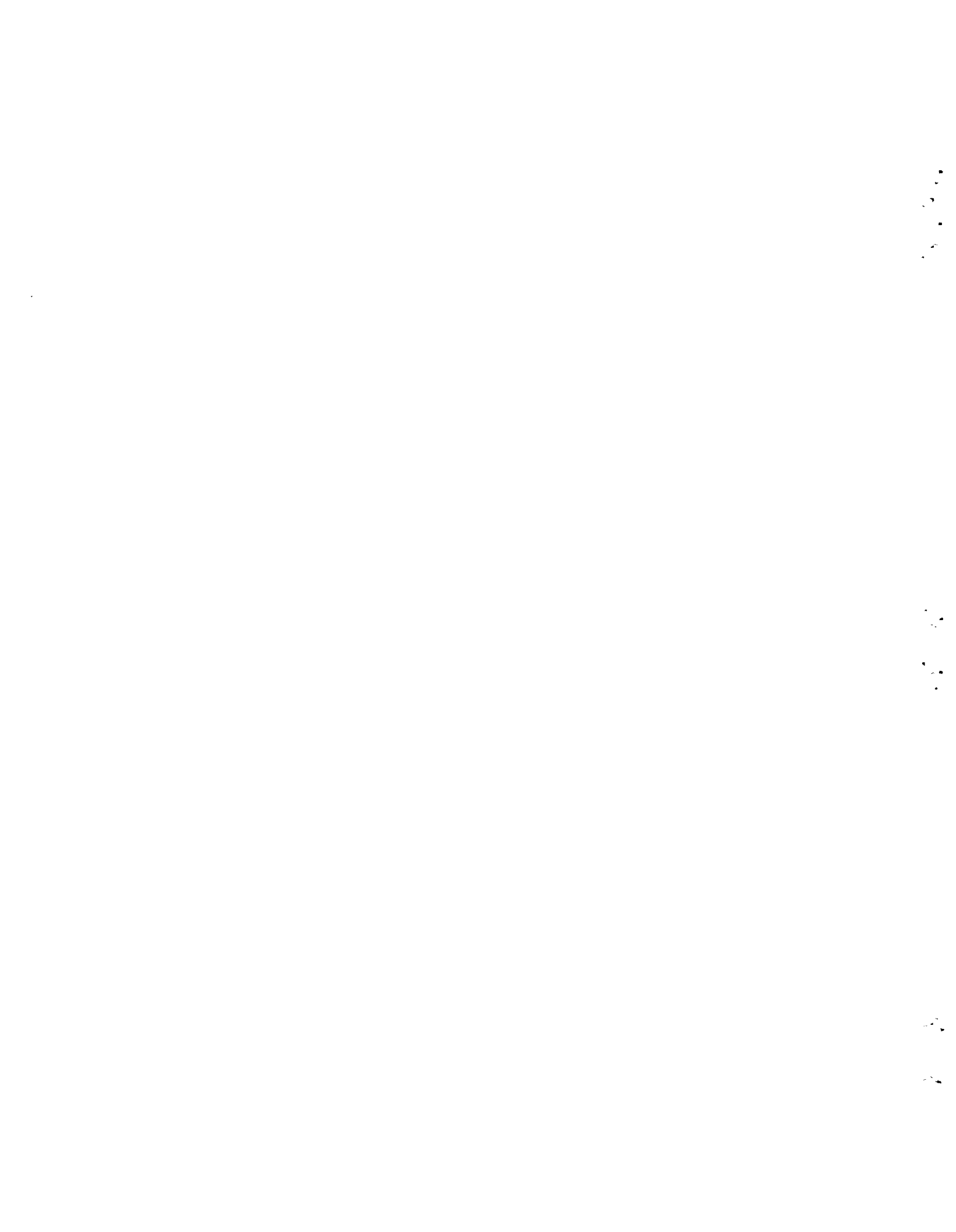
3. Pretreatment of the HFIR fuel elements by immersion in boiling deionized water for 24 hr is undesirable. It results in the buildup of a thicker corrosion-product film on the surfaces of the element during reactor service. Although this thicker film causes no significant damage, it does adversely affect the coolant flow rate and pressure drop through the elements.

4. Postirradiation heat treatment, or so-called blister-annealing tests, appears to be of questionable value for establishing the performance capabilities of U_3O_8 -aluminum dispersion fuel materials.

ACKNOWLEDGMENTS

The authors wish to express their sincere gratitude to the many individuals who participated in and contributed to this work. In particular, special thanks are due to the following people: J. A. Cox, head of the ORNL Operations Division, whose encouragement and support made this work possible; W. R. Martin, for technical guidance and supervision of the evaluation program; T. M. Sims and L. A. Haack, who did the calculations for predicting the burnup, temperature, and oxide film thickness of the HFIR fuel plates; J. C. Griess and R. D. Cheverton, for their many helpful discussions concerning the corrosion behavior of these fuel elements; E. M. King and R. L. Lines, for support and

cooperation in providing hot-cell facilities for the postirradiation examinations; S. E. Dismuke, M. G. Willey, and W. B. Parsley, for assistance in the design, construction, and operation of much of the specialized hot-cell equipment used in the examination program; J. E. Ferguson, G. A. Moore, M. Payne, N. H. Rouse, and J. E. Bacon, for assistance in various phases of the examination program; E. D. Sims and E. H. Lee, for metallographic examination of sections of the irradiated fuel plates; R. E. Eby and J. L. Miller, for the mass spectrographic and x-ray diffraction analyses; Sigfred Peterson, for review and editorial assistance in the preparation of this report.



APPENDIX A

Equipment Used for Examining, Dismantling, and Reassembling
the Irradiated HFIR Fuel Elements

Because of the physical size and unique configuration of the HFIR fuel elements, a considerable amount of specialized equipment was needed to handle, inspect, disassemble, and reassemble the irradiated elements in the hot cells. The following paragraphs briefly describe the design, construction, and operation of some of this equipment.

Fixtures that could be attached to the elements were essential to aid in handling the elements with the in-cell crane or manipulators. The elements were unloaded from and reloaded into the shipping cask by use of the crane and fixtures shown in Fig. A-1, which locked into the upper end adapters of the elements. Bands with a removable bail, shown in Fig. A-2, could also be clamped around the outer surface of the elements to allow them to be handled in a horizontal position. A turntable equipped with a removable cradle (Fig. A-3) was also built to aid in inspection of the elements. The turntable supported the elements and permitted rotation about a vertical axis. The cradle provided support and permitted rotation about a horizontal axis. All other equipment

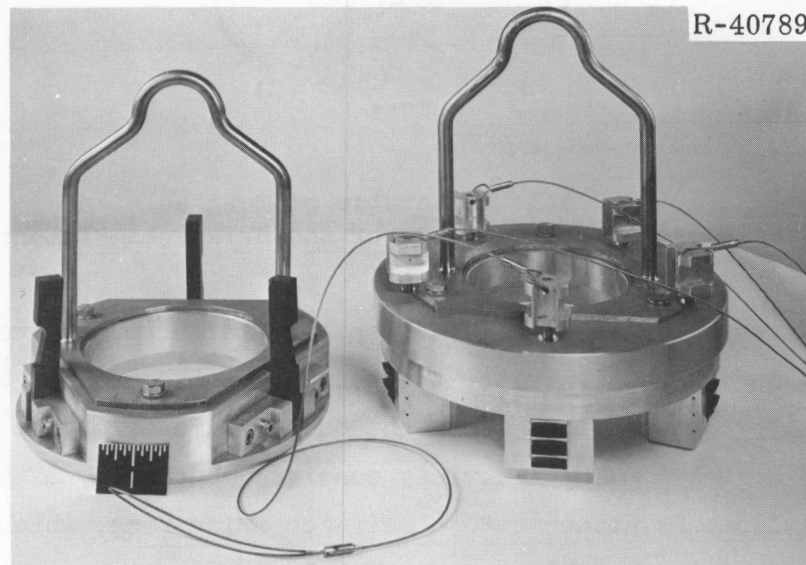


Fig. A-1. Fixtures for Handling HFIR Fuel Elements in the Vertical Position.

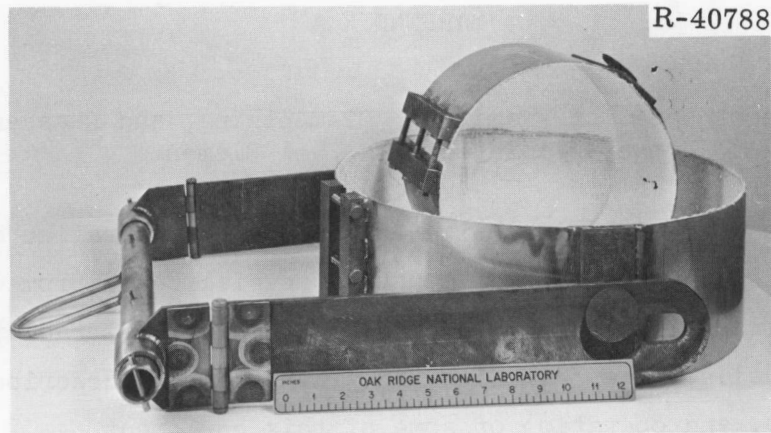


Fig. A-2. Bands and Support Brackets for Handling Elements in Horizontal Position.

ORNL-DWG 69-7294

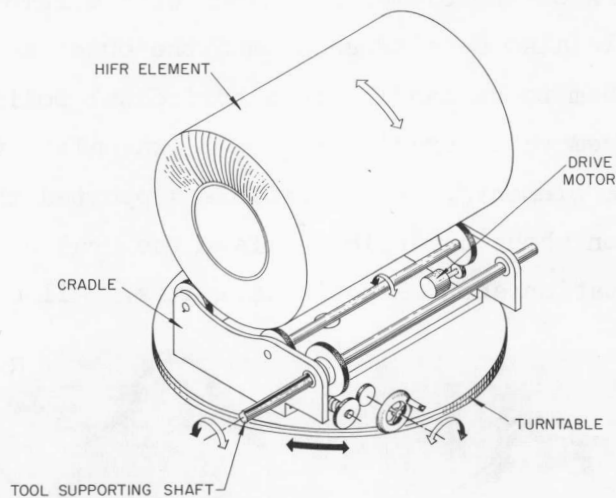


Fig. A-3. Schematic of Turntable and Cradle Used in Examination of the HFIR Fuel Elements.

(except that used for the fuel-plate spacing measurements) was attached to, or used in conjunction with, the turntable, the cradle, or both.

The equipment used to measure the outer diameter of the elements is shown in Fig. A-4. These devices consisted basically of two opposing dial-gage indicators attached to a self-centering ring, which surrounded the elements. This assembly was supported on three legs, which were attached to the turntable while the measurements were being made. Three sets of support legs were required to obtain measurements at the three

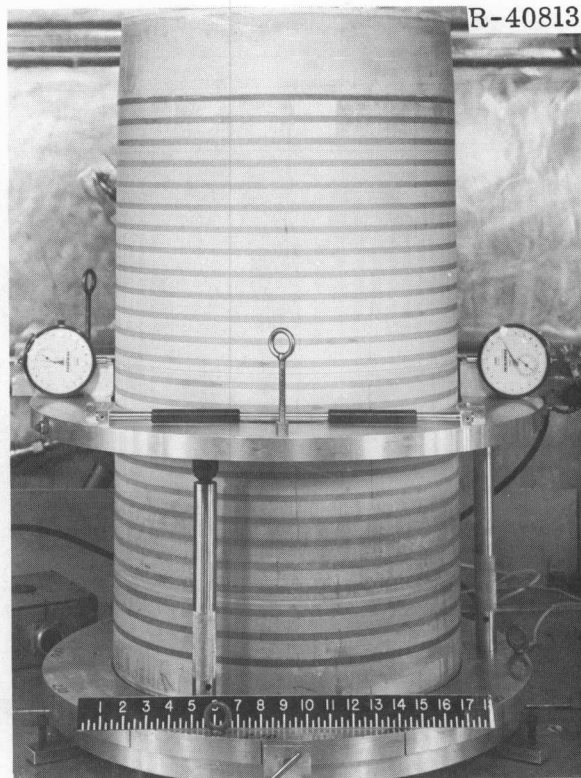


Fig. A-4. Outer Diameter Measurement Equipment.

predetermined axial positions. Each set of legs was equipped with ball transfers to provide ease of movement during centering of the support ring. A set of precision standards was used to periodically calibrate the equipment.

Standard dial bore gages were modified to measure the inner diameter of the elements (Fig. A-5). The gage shaft was extended and equipped with three pre-positioned stops to ensure proper vertical and horizontal positioning of the gage inside the element. These stops rested in a bracket placed across the top adapter of the element during the measurement.

The length of the elements (i.e., distance between the shoulders in the upper and lower end adapters) was measured with the equipment shown in Fig. A-6. Dial-gage micrometers were attached to a steel bar that was equipped with four rollers, two near each end, that rested on the inner side of the element.

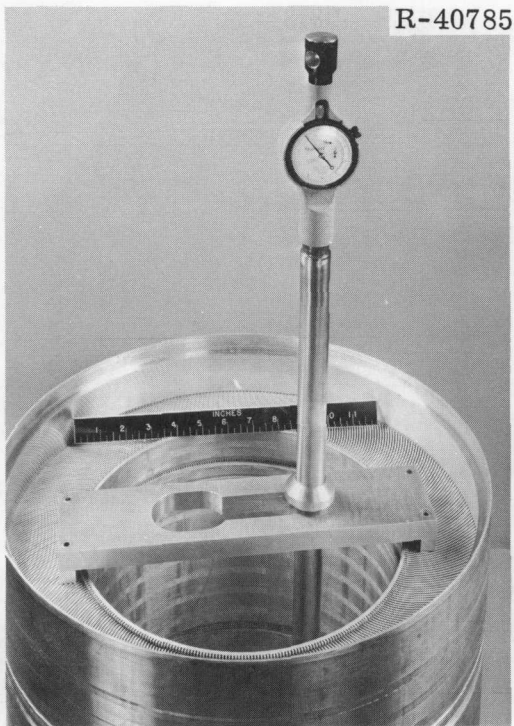


Fig. A-5. Dial Bore Gage, Before and After Modification, for Inside Diameter Measurements.

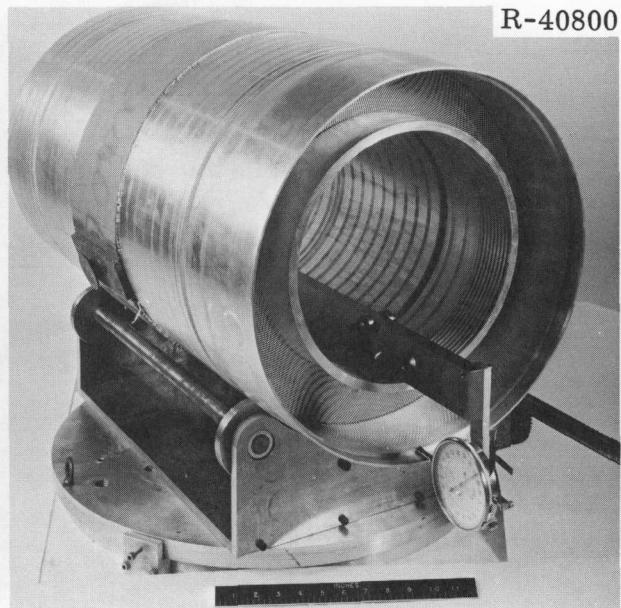


Fig. A-6. Length Measurement Equipment.

The coolant-channel spacings were measured with the equipment shown in Fig. A-7. This apparatus consists of a hand-operated rotary table for indexing, a probe holder, a motor-driven probe extender, and a probe support guide. The probe itself is based upon eddy-current principles¹⁵ and provides a continuous readout of the plate-spacing measurements as it is slowly drawn through the coolant channel.

Individual fuel plates were removed from the irradiated fuel elements by (1) cutting off the element end adapters, (2) milling off the combs at the upper and lower ends of the fuel plates, and (3) slitting through the inner and outer side plates on each side of the desired plate. All cutting was done with high-speed slitting saws (0.030 in. thick) driven by a 10,000-rpm 1/2-hp electrical motor equipped with a flexible drive. The removal of one of the end adapters, milling of the

¹⁵C. V. Dodd, Design and Construction of Eddy-Current Coolant-Channel Spacing Probes, ORNL-3580 (April 1964).

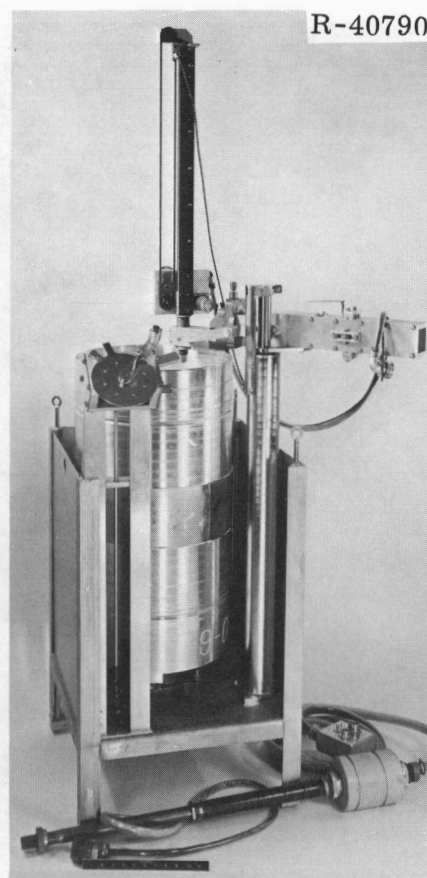
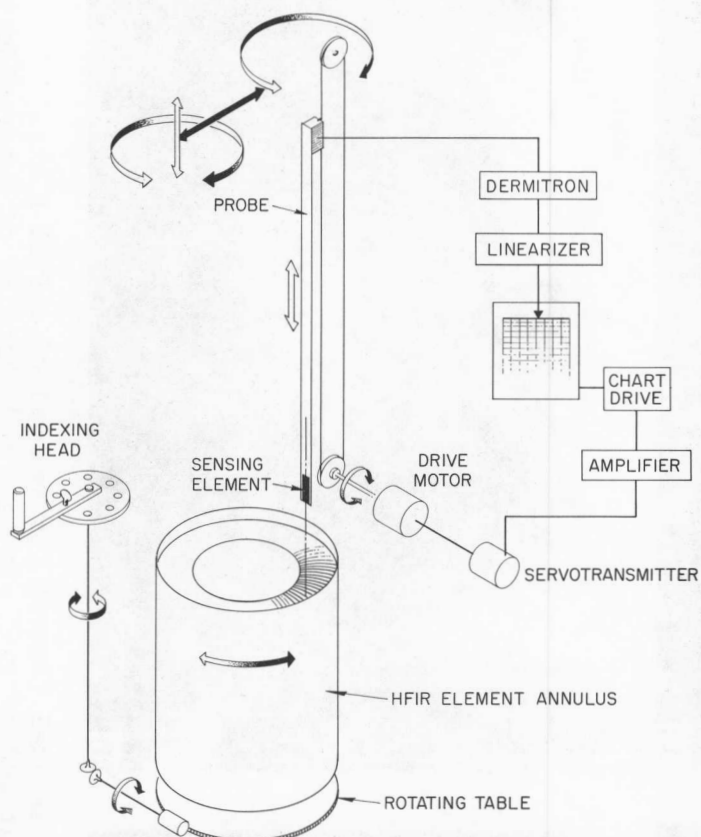


Fig. A-7. Schematic (Left) and Actual Photograph (Right) of Equipment for Coolant-Channel Spacing Measurements.

combs, and slitting through the inner and outer side plates of an irradiated fuel element are shown in Fig. A-8.

To reassemble the irradiated elements into their original configuration after examination, as each fuel plate was removed an aluminum spacer was inserted into the gap in the side plates and manually welded into position. All welding was done with a Heliarc torch held with the master-slave manipulators (Fig. A-9) while the spacers were temporarily held in position by a band placed around the outside of the element. The end adapters were then reattached to the element similarly. An irradiated element after reassembly is shown in Fig. A-10.

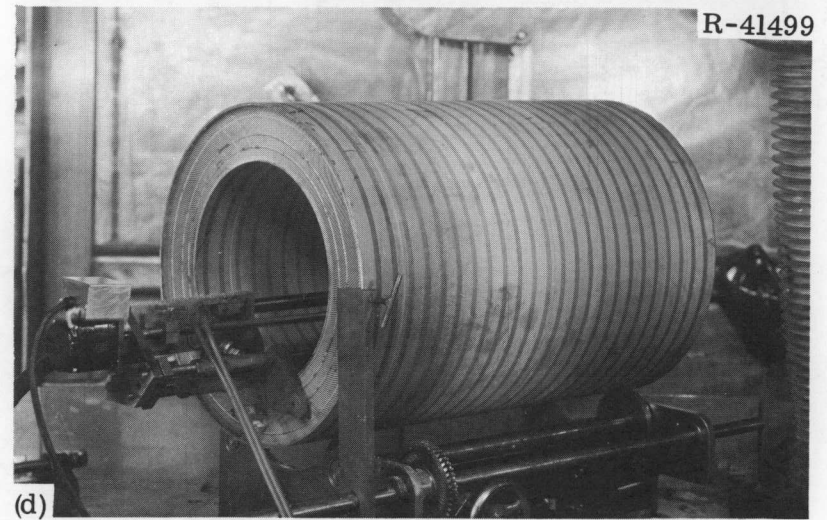
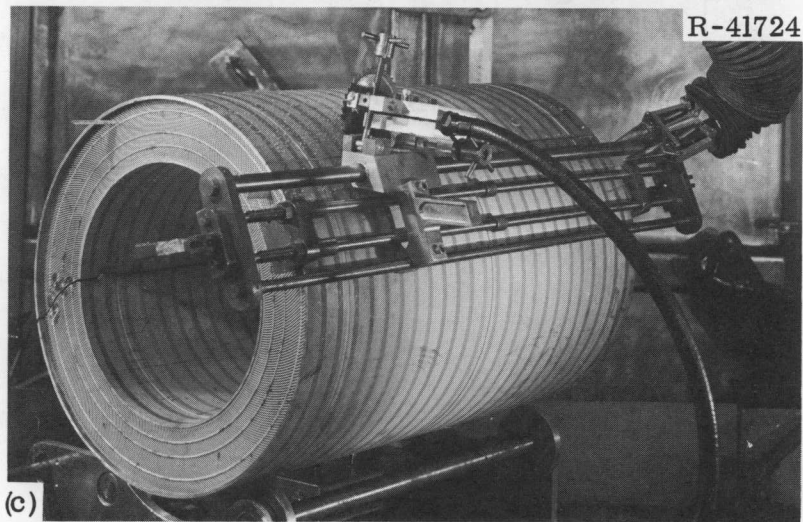
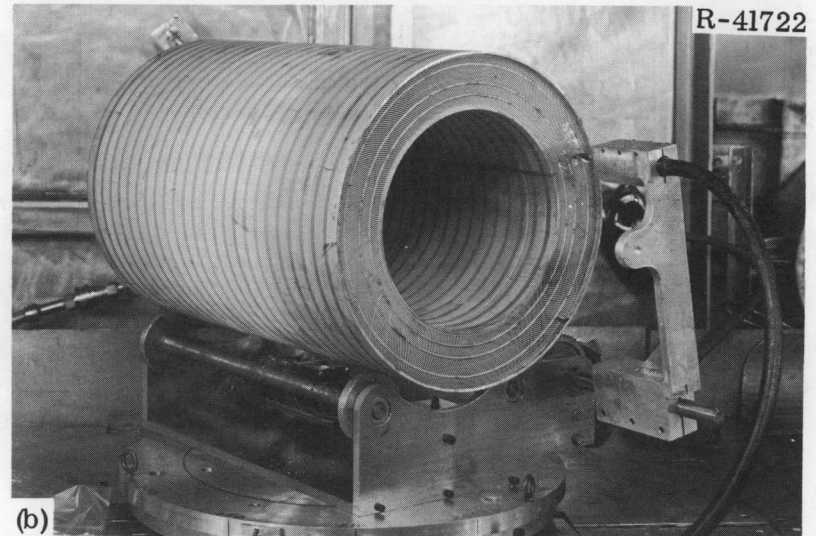
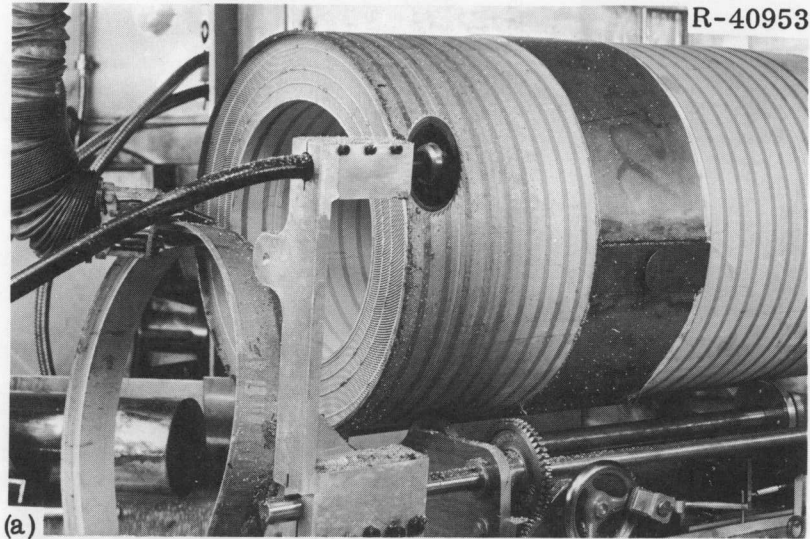


Fig. A-8. Steps in Preparing an Irradiated HFIR Fuel Element for Removal of a Fuel Plate. (a) Removal of end adapter. (b) Milling off comb at end of fuel plates. (c) Slitting of outer side plate. (d) Slitting of inner side plate.

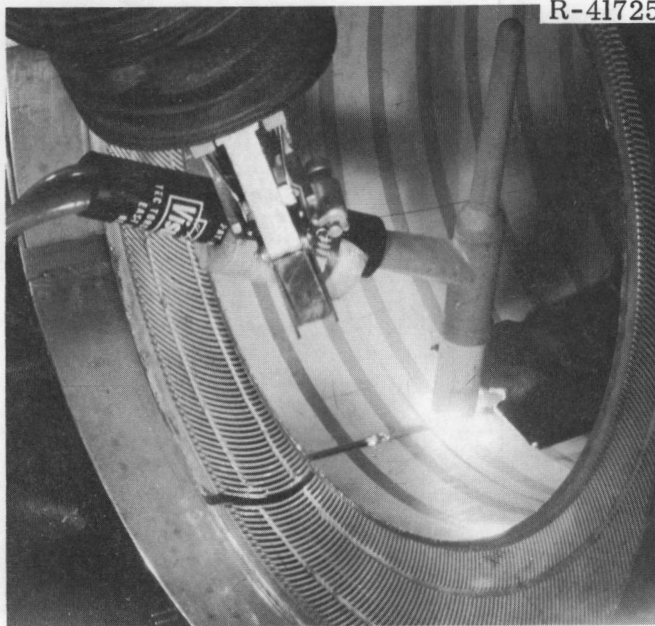


Fig. A-9. Welding Spacers into Gaps in Element Side Plates.

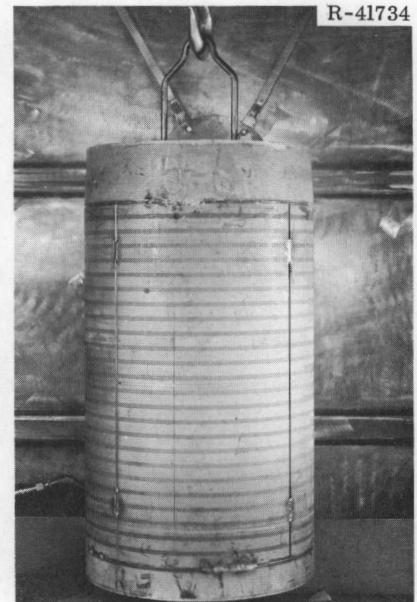
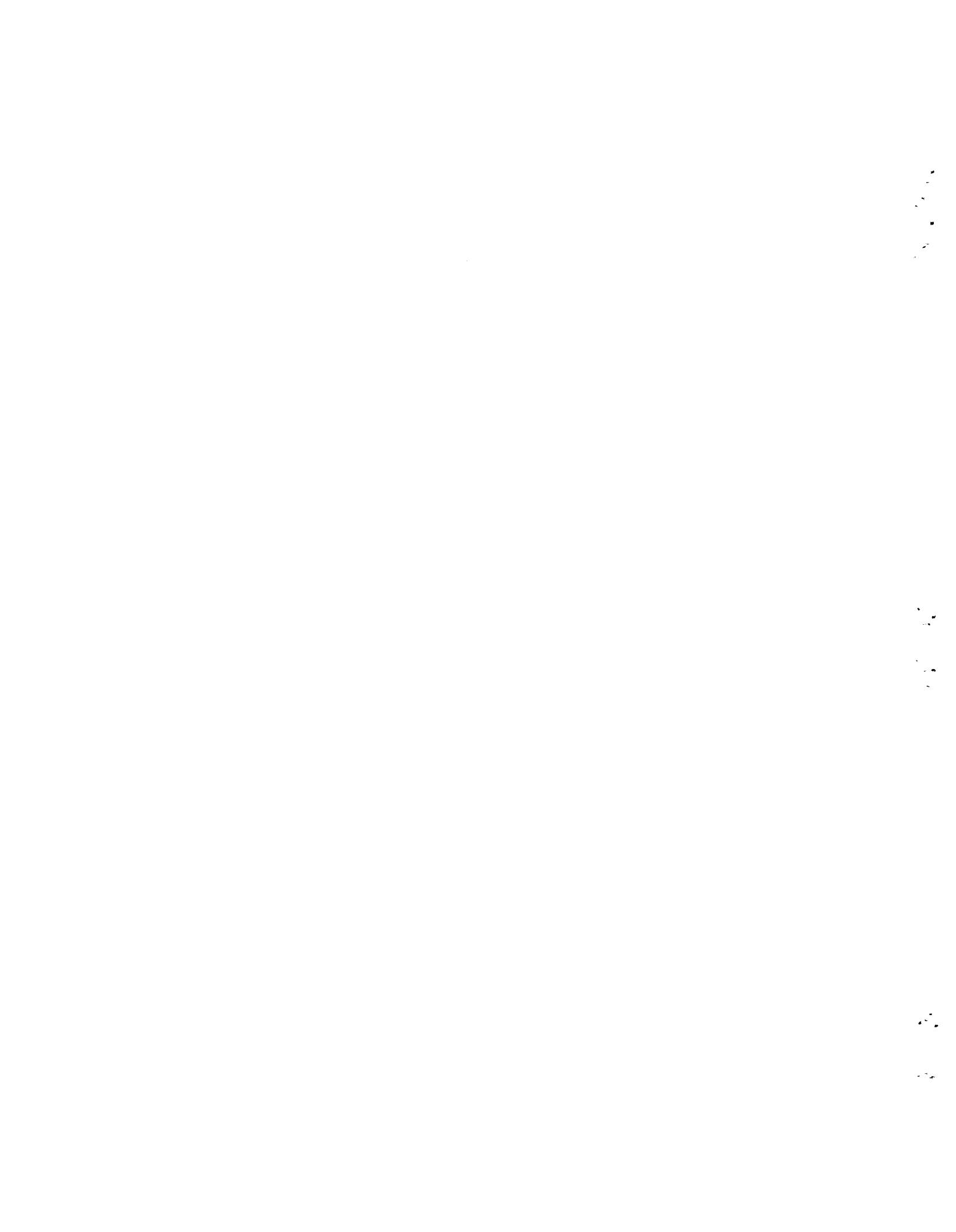


Fig. A-10. Fuel Element After Removal of Four Fuel Plates and Complete Reassembly.

A more detailed description of the design and operation of this specialized equipment has been reported elsewhere.¹⁶

¹⁶W. B. Parsley, "Equipment Used for Examining, Dismantling, and Reassembly of a HFIR Fuel Element," pp. 209-214 in Proceedings of the 17th Conference on Remote Systems Technology, 1969, American Nuclear Society, Inc., Hinsdale, Illinois.



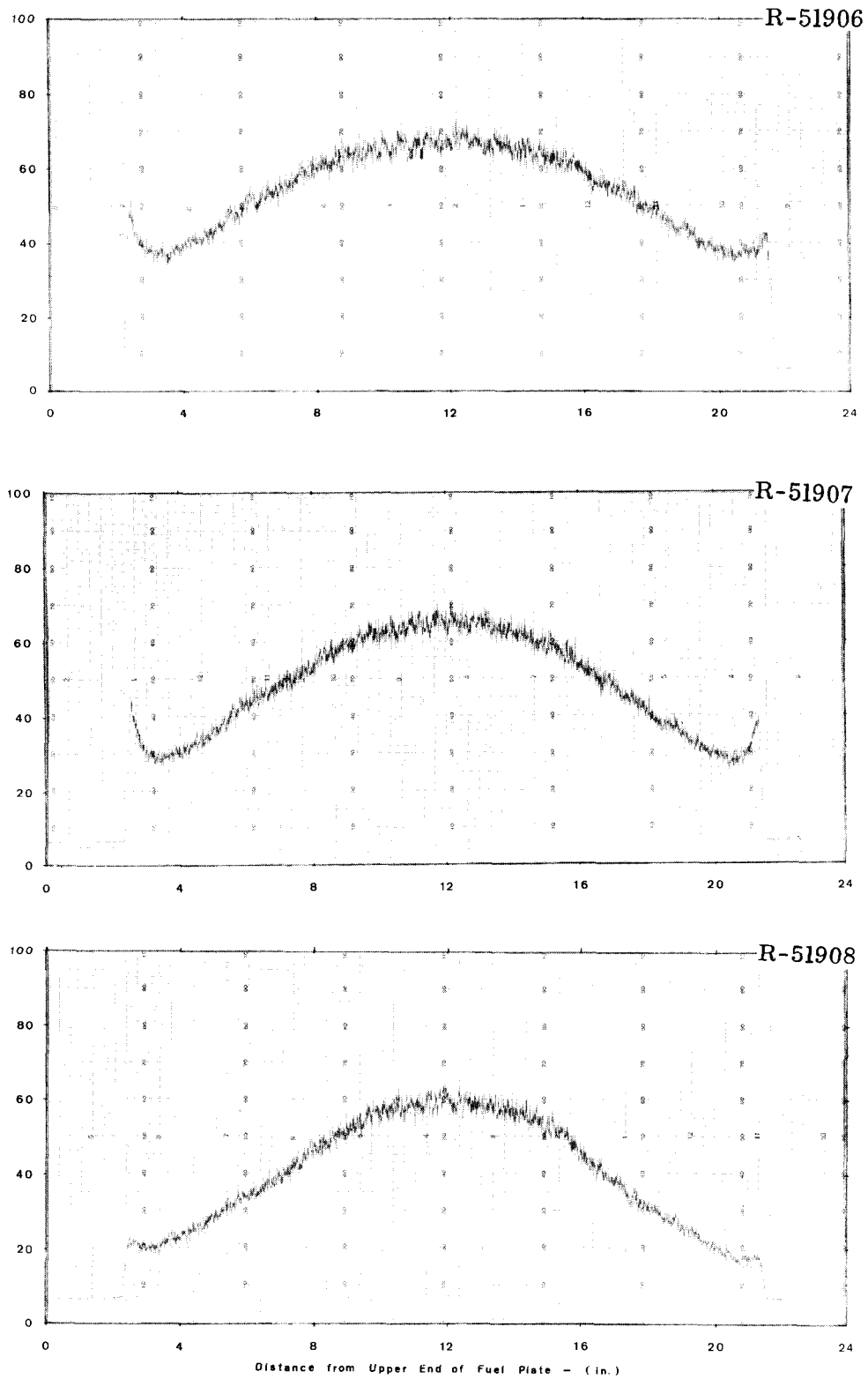
APPENDIX B
Axial Gamma-Activity Scans

Fig. B-1. Typical Axial Gamma-Activity Scans of a Fuel Plate from HFIR Fuel Element 21-0. Scans were made at radial positions 16 cm (top), 18.5 cm (center), and 20 cm (bottom) from the core center line.

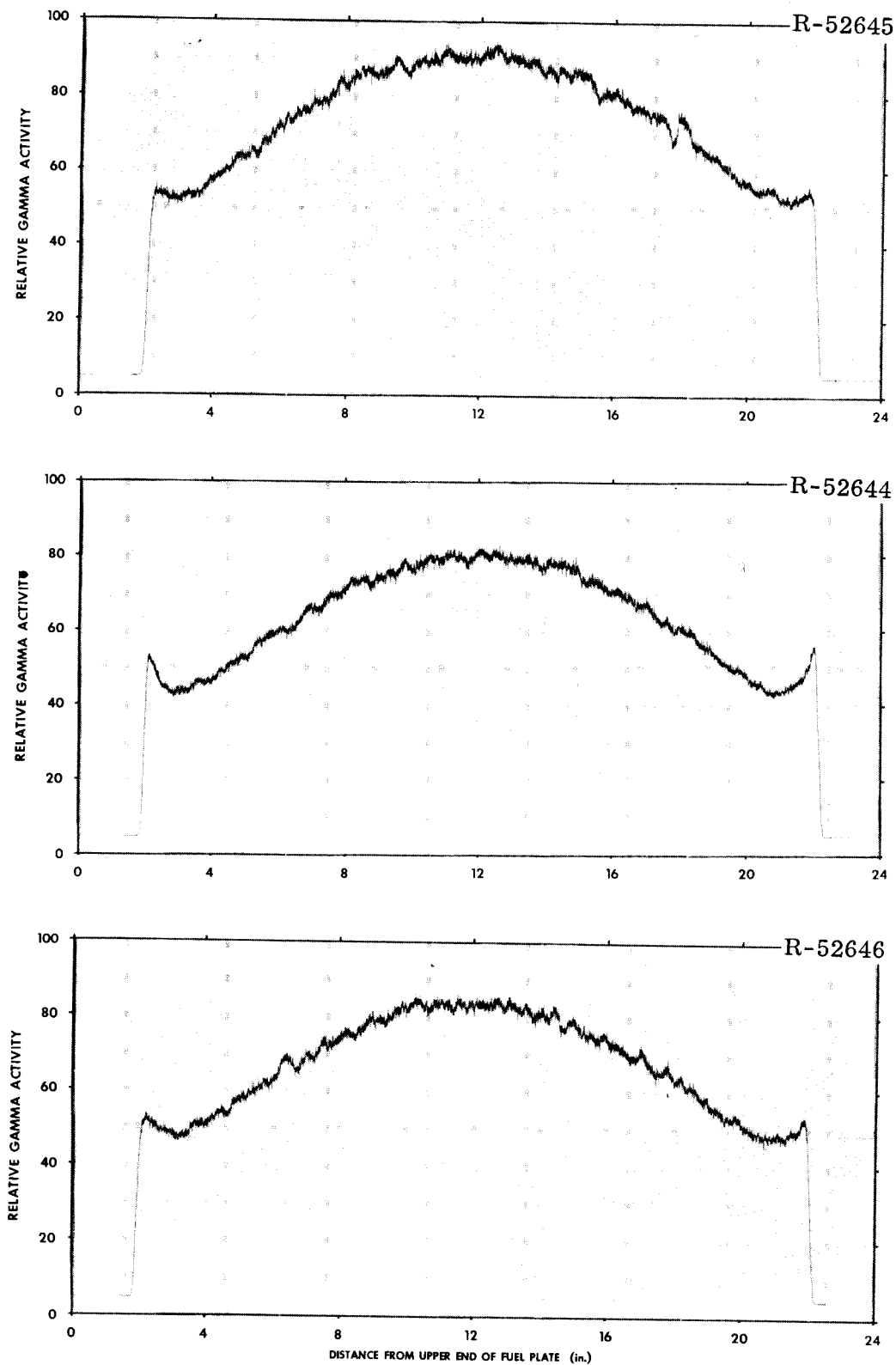


Fig. B-2. Typical Axial Gamma-Activity Scans of a Fuel Plate from HFIR Fuel Element 49-I. Scans were made at radial positions 8 cm (top), 10 cm (center), and 12 cm (bottom) from the core center line.

APPENDIX C

Fuel Plate Thickness Measurements

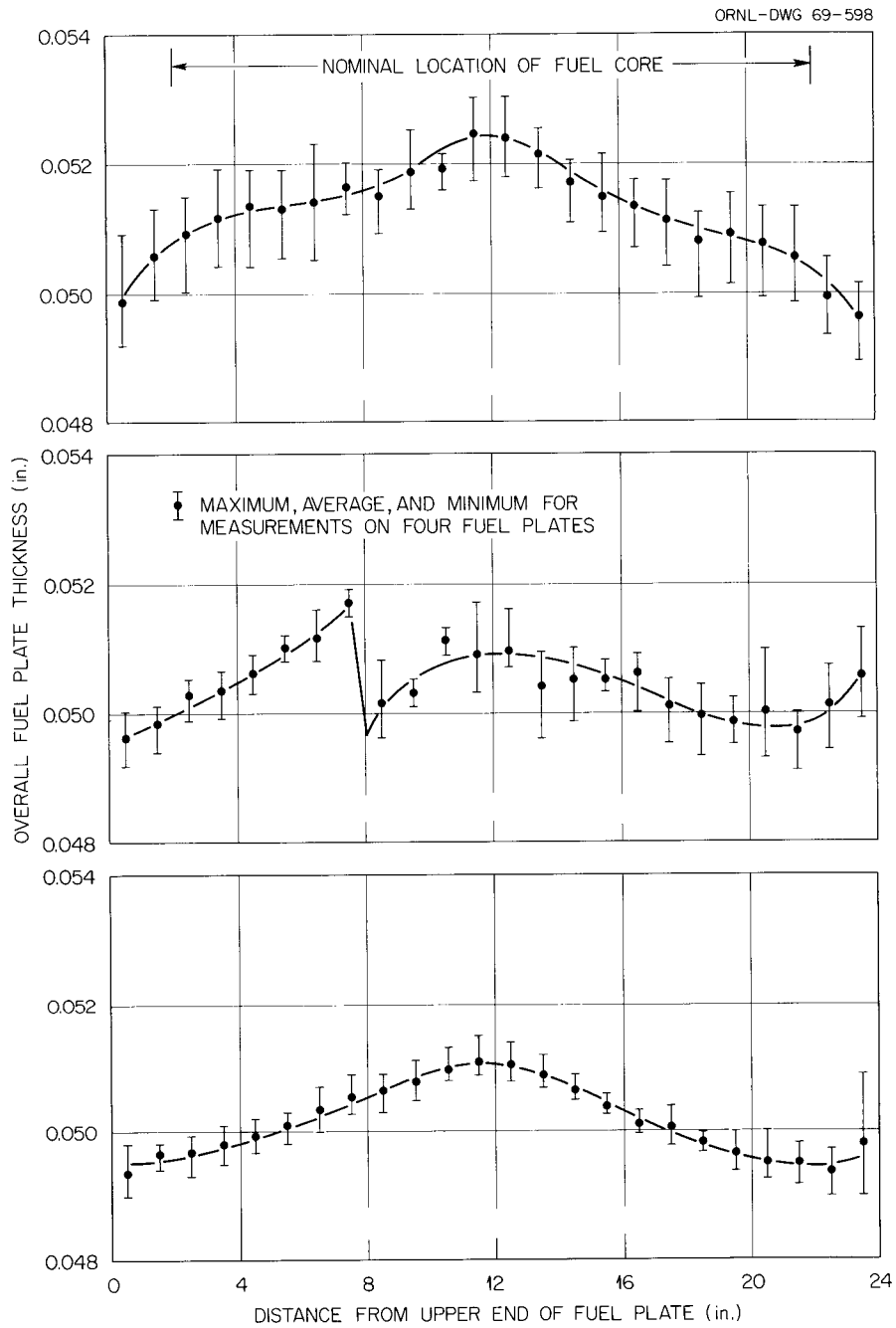


Fig. C-1. Axial Thickness Profiles of Fuel Plates from HFIR Fuel Element 5-0. Near inner edge of plate (top), over fuel-core hump (center), and near outer edge of plate (bottom).

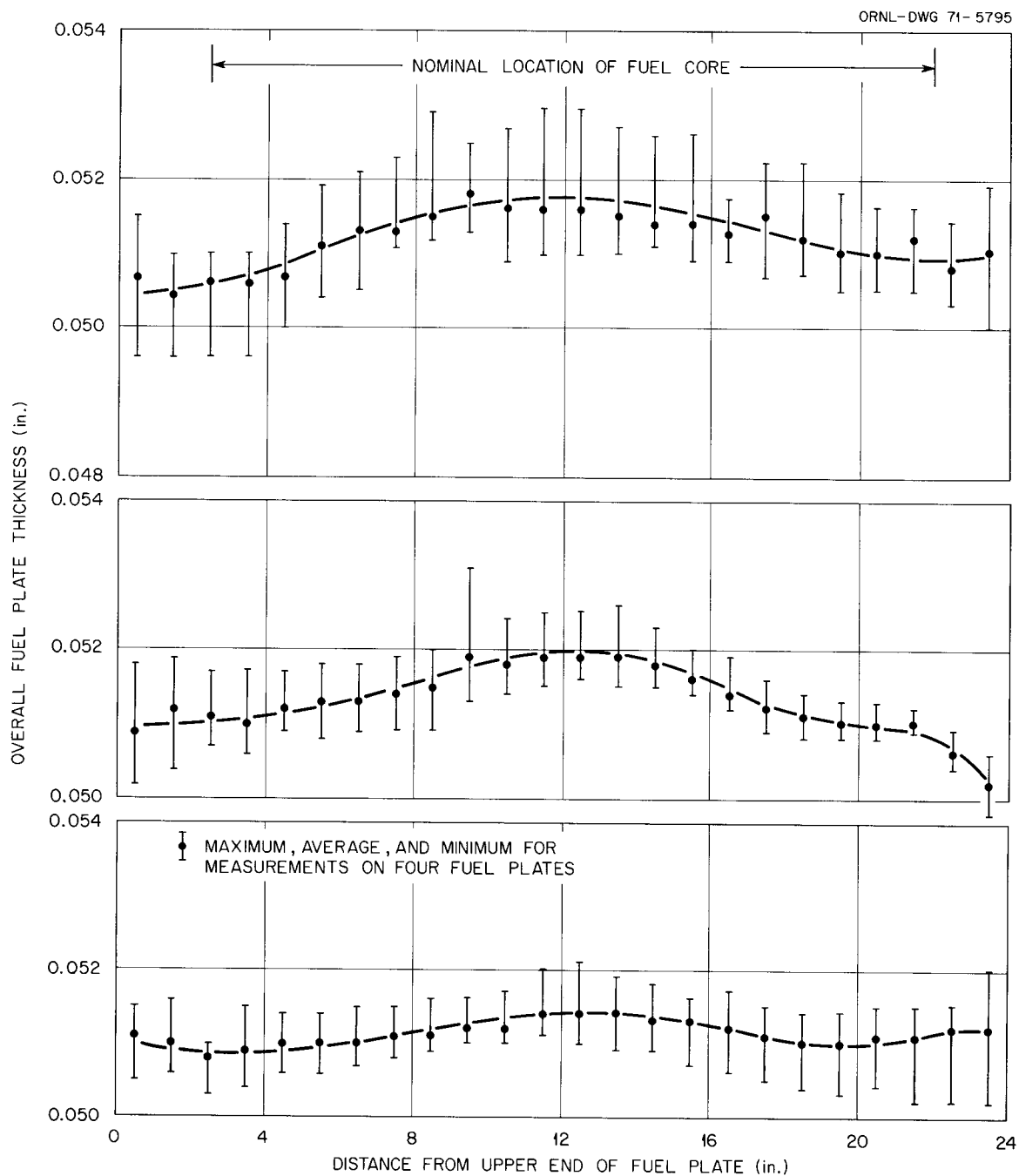


Fig. C-2. Axial Thickness Profiles of Fuel Plates from HFIR Fuel Element 21-0. Near inner edge of plate (top), over fuel-core hump (center), and near outer edge of plate (bottom).

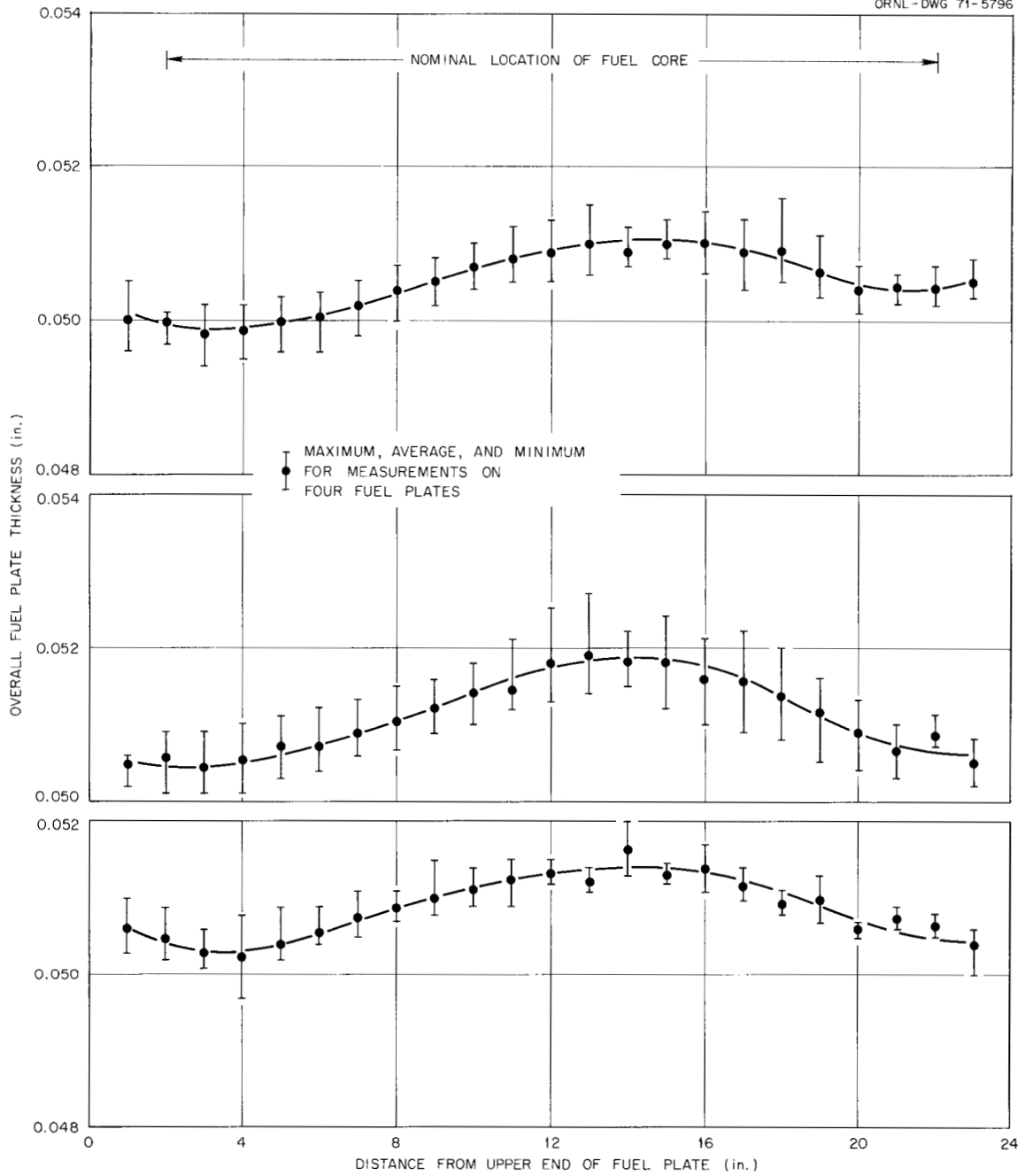


Fig. C-3. Axial Thickness Profiles of Fuel Plates from HFIR Fuel Element 49-I. Near inner edge of plate (top), over fuel-core hump (center), and near outer edge of plate (bottom).

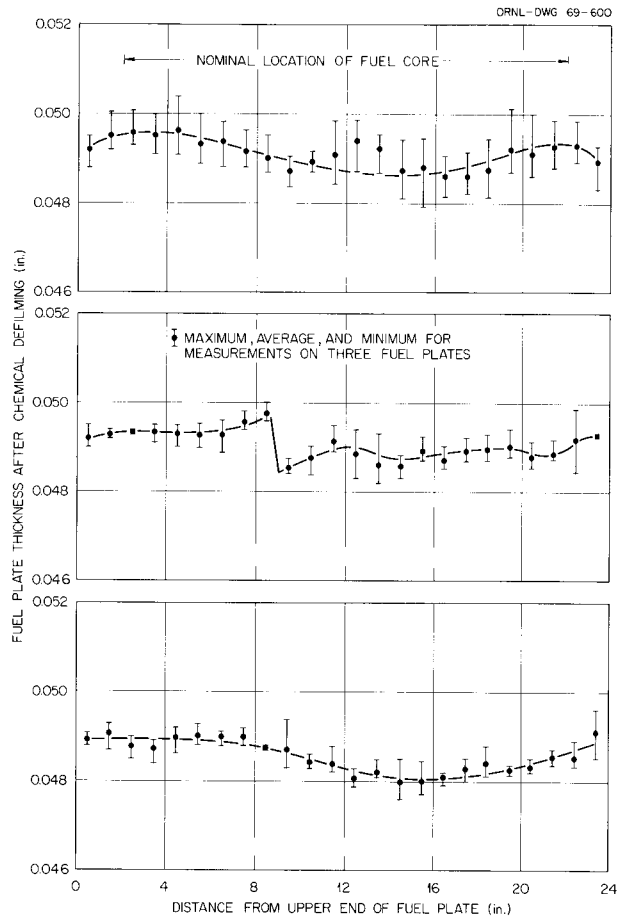


Fig. C-4. Axial Thickness Profiles of Defilmed Fuel Plates from HFIR Fuel Element 5-0. Near inner edge of plate (top), over fuel core hump (center), and near outer edge of plate (bottom).

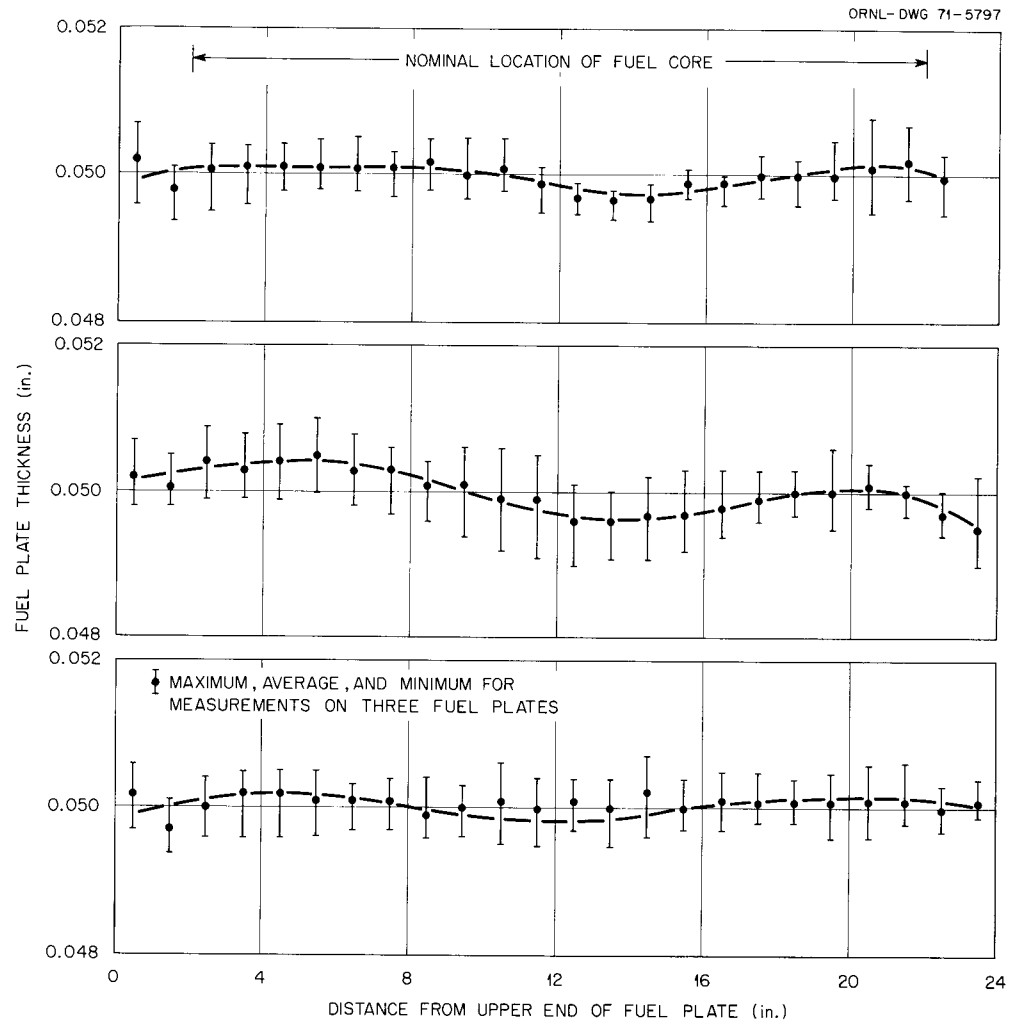


Fig. C-5. Axial Thickness Profiles of Defilmed Fuel Plates from HFIR Fuel Element 21-0. Near inner edge of plate (top), over core hump (center), and near outer edge of plate (bottom).

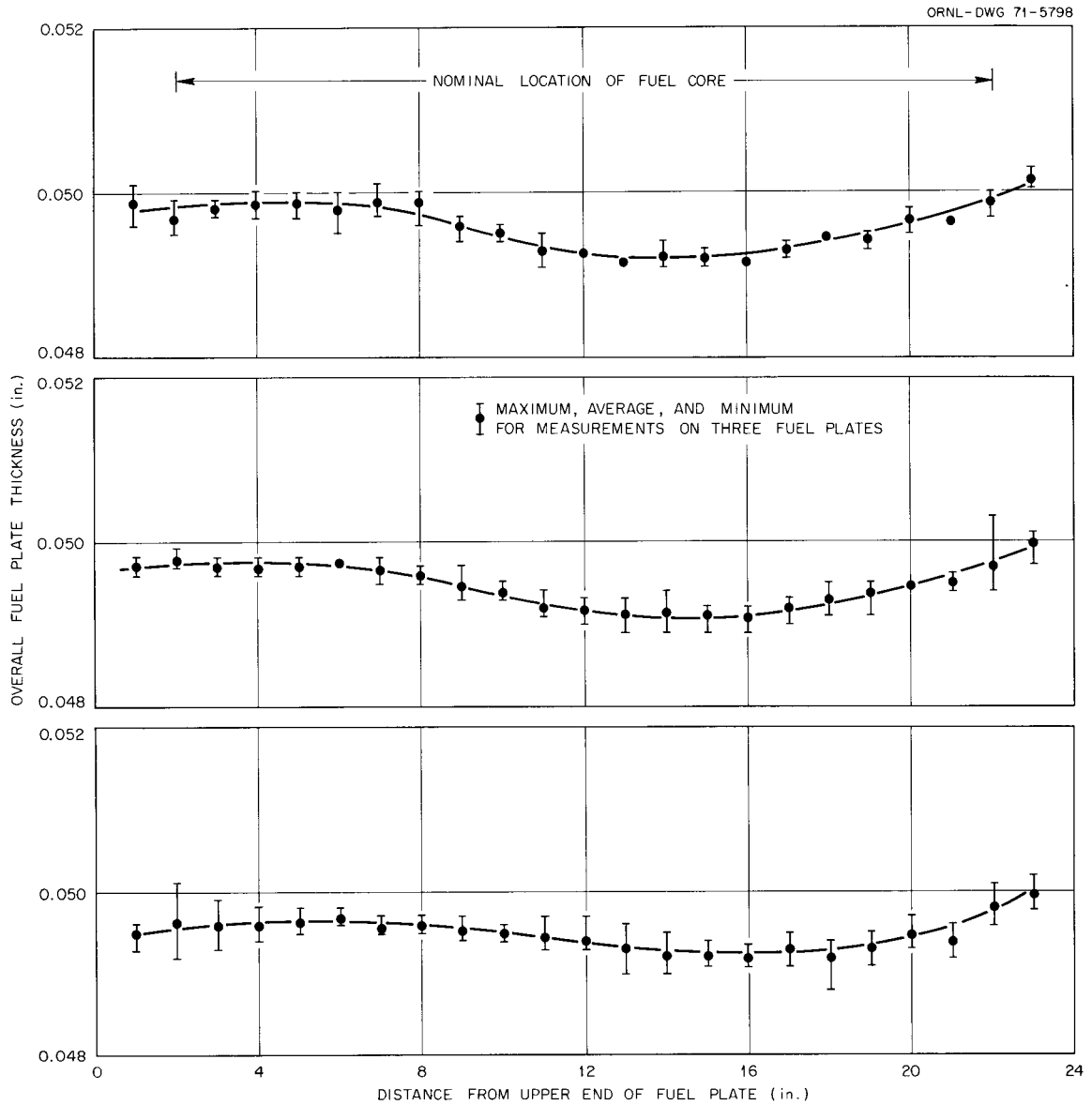


Fig. C-6. Axial Thickness Profiles of Defilmed Fuel Plates from HFIR Fuel Element 49-I. Near inner edge of plate (top), over core hump (center), and near outer edge of plate (bottom).

APPENDIX D

Mass Spectrographic and Burnup Results on Sections
from the Irradiated HFIR Fuel Plates

Table D-1. Mass Spectrographic and Burnup Results on Sections from
Fuel Plate O-111-8 of HFIR Fuel Element 5-0

Specimen	Isotopic Composition, at. %				Specimen Burnup	
	^{234}U	^{235}U	^{236}U	^{238}U	(% of U Atoms)	(fissions/cm ³ of Fuel Core)
						× 10 ²⁰
Preirradiation	0.96	93.21	0.32	5.51		
B-3.25-I	1.10	88.26	4.21	6.43	14.29	4.46
B-3.25-H	1.05	89.68	3.17	6.10	9.66	3.01
B-3.25-O	1.08	88.49	4.12	6.31	12.66	3.83
B-7.75-H	1.06	87.60	4.97	6.37	13.46	4.20
B-12.25-I	1.20	81.65	9.61	7.54	26.84	8.37
B-12.25-H	1.09	85.99	6.28	6.65	17.08	5.33
B-12.25-O	1.32	77.81	12.36	8.51	35.15	10.97
B-16.75-H	1.06	87.86	4.79	6.29	12.37	3.86
B-21.25-I	1.10	87.81	4.57	6.52	15.46	4.82
B-21.25-H	1.03	90.21	2.76	6.00	8.15	2.54
B-21.25-O	1.06	89.68	3.16	6.10	9.67	3.02

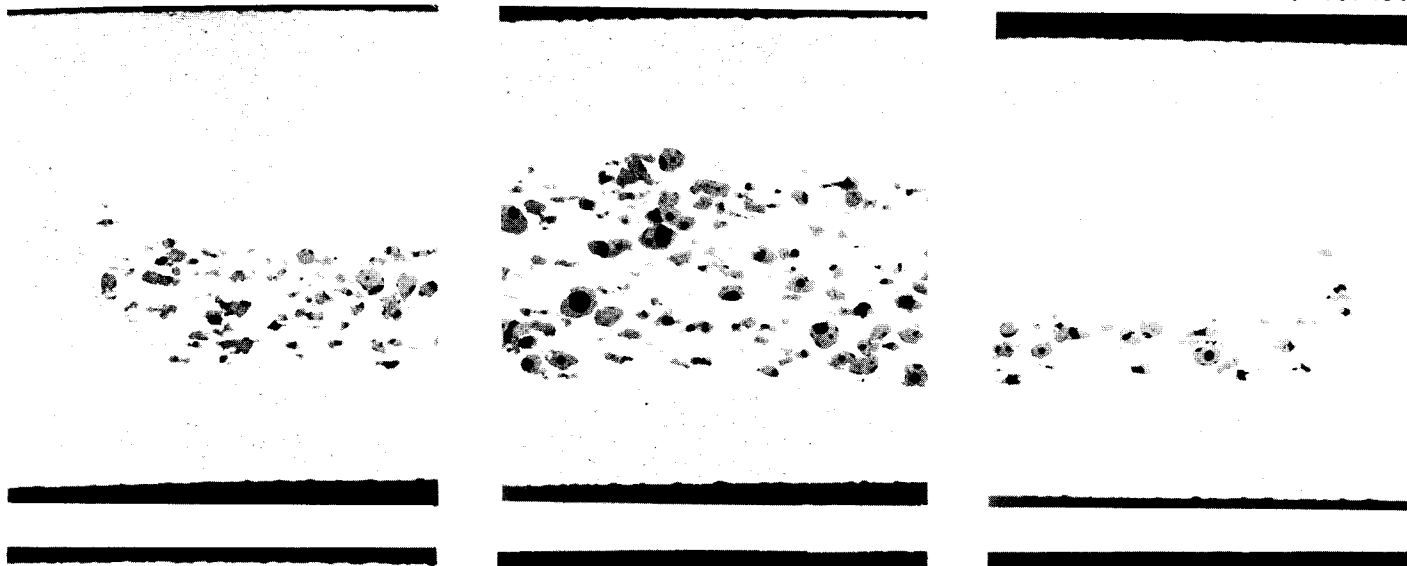
Table D-2. Mass Spectrographic and Burnup Results on Sections from Fuel Plate O-350-I of HFIR Fuel Element 21-0

Specimen	Isotopic Composition, at. %				Specimen Burnup	
	²³⁴ U	²³⁵ U	²³⁶ U	²³⁸ U	(% of U Atoms)	(fissions/cm ³ of Fuel Core)
						× 10 ²⁰
Preirradiation	1.00	93.22	0.33	5.44		
B-3.25-I	1.17	85.45	6.48	6.90	21.07	6.57
B-3.25-H	1.05	89.45	3.43	6.07	10.31	3.22
B-3.25-0	1.10	88.41	4.17	6.32	13.86	4.32
B-7.75-I	1.22	81.69	9.55	7.54	27.72	8.65
B-7.75-H	1.08	86.84	5.64	6.44	15.43	4.81
B-7.75-0	1.24	81.38	9.46	7.92	31.16	9.72
B-12.25-I	1.28	78.08	12.34	8.29	34.22	10.67
B-12.25-H	1.10	85.13	7.02	6.75	20.88	6.51
B-12.25-0	1.39	75.19	14.38	9.04	39.65	12.37
B-16.75-I	1.20	82.14	9.26	7.40	26.36	8.22
B-16.75-H	1.07	87.06	5.46	6.41	15.03	4.69
B-16.75-0	1.27	80.93	10.05	7.75	29.69	9.26
B-21.25-I	1.14	86.60	5.60	6.66	18.24	5.69
B-21.25-H	1.05	90.08	2.97	5.90	7.76	2.27
B-21.25-0	1.07	89.64	3.22	6.07	10.33	3.22

Table D-3. Mass Spectrographic and Burnup Results on Sections from Fuel Plate I-417-24 of HFIR Fuel Element 49-I

Specimen	Isotopic Composition, at. %				Specimen Burnup	
	²³⁴ U	²³⁵ U	²³⁶ U	²³⁸ U	(% of U Atoms)	(fissions/cm ³ of Fuel Core)
						× 10 ²⁰
Preirradiation	1.00	93.24	0.43	5.33		
B-2.75-I	1.44	77.30	12.73	8.53	37.41	8.04
B-2.75-H	1.17	86.17	6.09	6.57	18.82	4.04
B-2.75-0	1.24	83.78	7.88	7.10	24.86	5.34
B-7.25-I	1.64	66.29	21.39	10.68	49.91	10.73
B-7.25-H	1.21	82.16	9.44	7.19	25.77	5.54
B-7.25-0	1.30	79.18	11.70	7.82	31.73	6.82
B-11.75-I	1.72	60.83	25.64	11.81	54.65	11.75
B-11.75-H	1.25	79.18	11.60	7.97	32.96	7.09
B-11.75-0	1.38	74.73	15.17	8.72	38.72	8.32
B-16.25-I	1.68	64.48	22.76	11.08	51.70	11.12
B-16.25-H	1.22	81.76	9.77	7.25	26.38	5.67
B-16.25-0	1.30	78.92	11.90	7.88	32.24	6.93
B-20.75-I	1.41	77.95	12.28	8.36	36.14	7.77
B-20.75-H	1.15	86.77	5.66	6.42	16.93	3.64
B-20.75-0	1.22	84.63	7.26	6.89	21.59	4.64

Specimen M-3
(9 in. above
midplane)



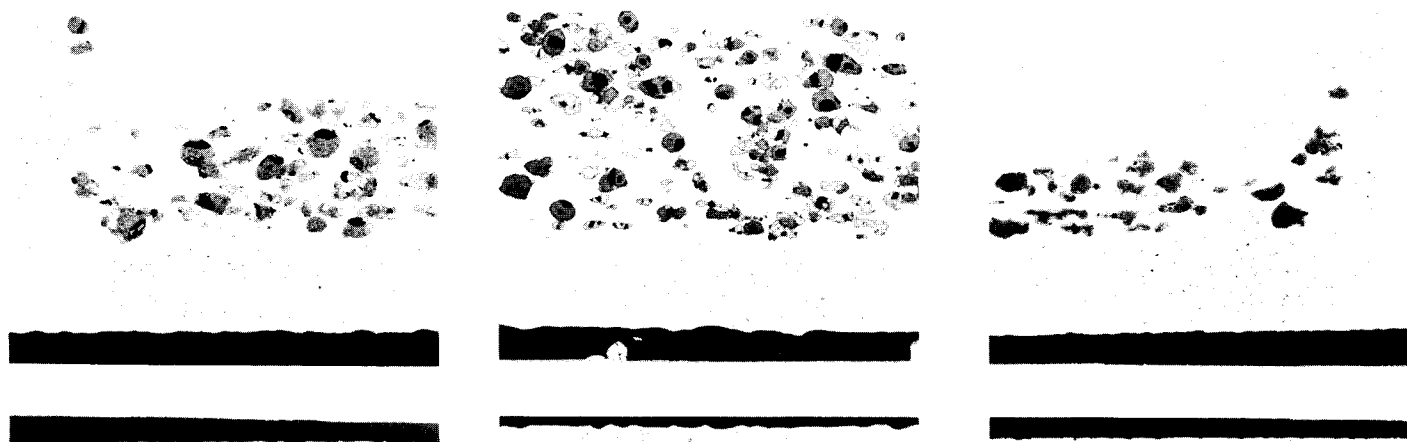
Specimen M-7.5
(4 1/2 in.
above midplane)



Specimen M-12
(midplane)



Specimen M-16.5
(4 1/2 in.
below midplane)



Specimen M-21
(9 in. below
midplane)

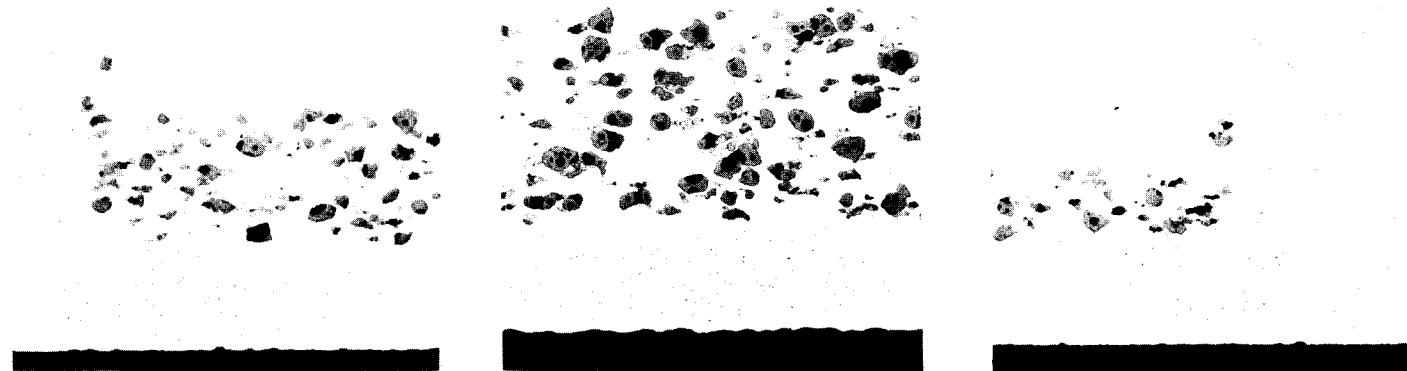
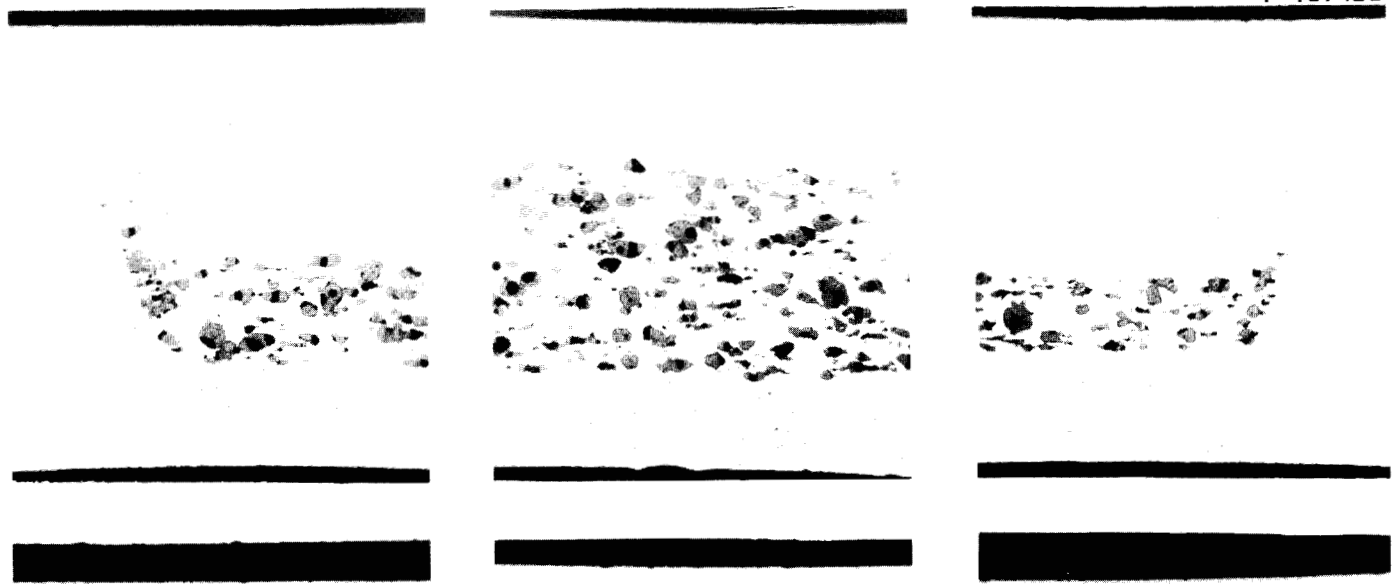
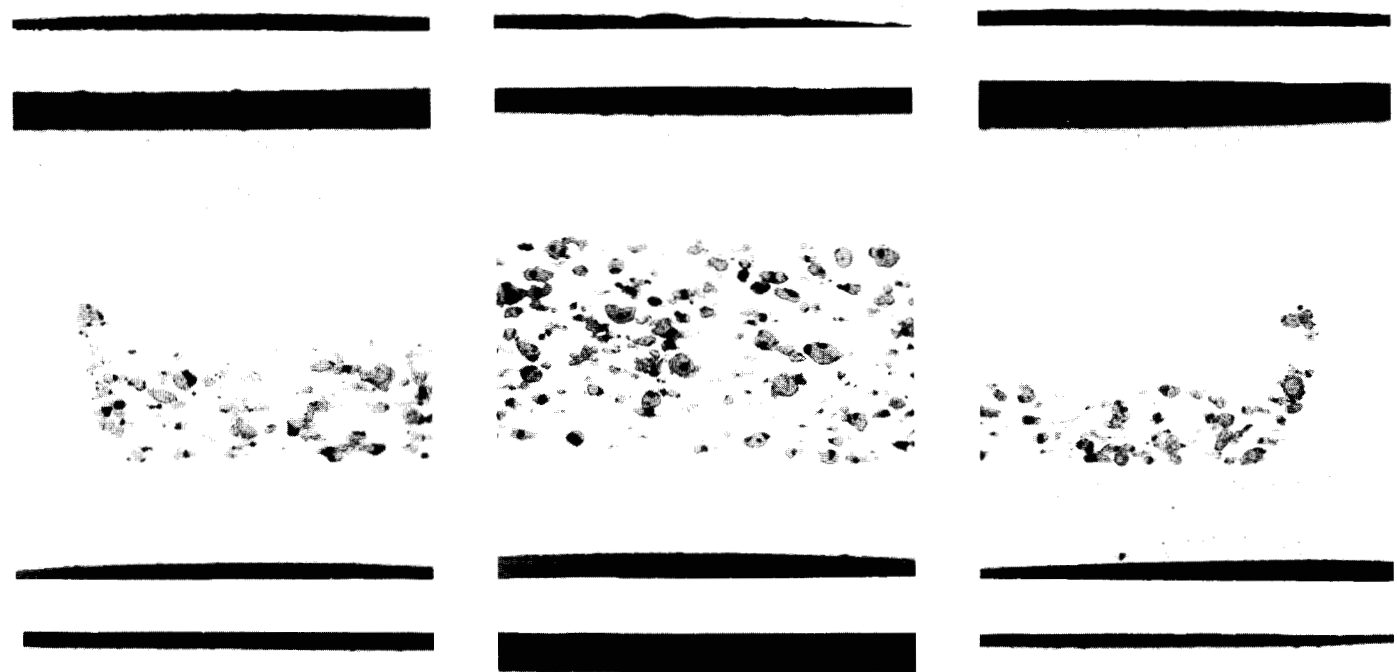


Fig. E-1. Typical Cross Sections of a Fuel Plate from HFIR Fuel Element 5-0. Concave surface of plate is at the bottom edge of all photomicrographs. 50X. As polished. Reduced 5%.

Specimen M-3
(9 in. above
midplane)



Specimen M-7.5
(4 1/2 in.
above midplane)



Specimen M-12
(midplane)



Specimen M-16.5
(4 1/2 in.
below midplane)



Specimen M-21
(9 in. below
midplane)

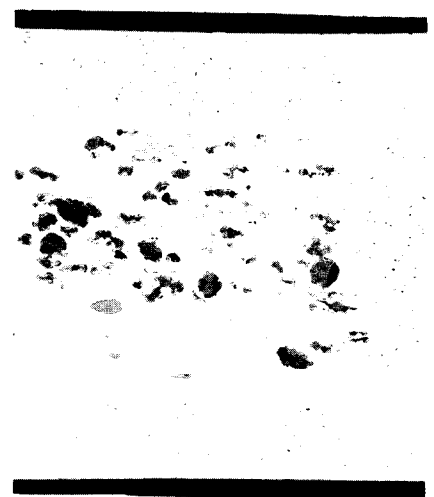
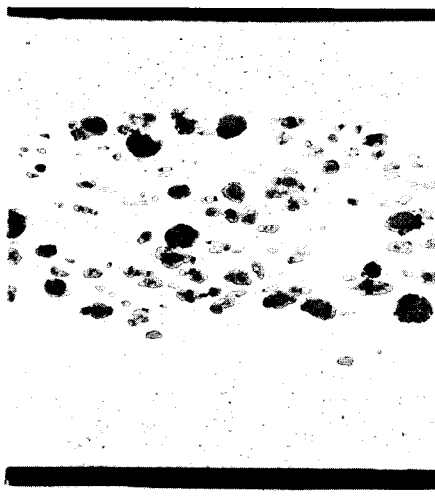


Fig. E-2. Typical Cross Sections of a Fuel Plate from HFIR Fuel Element 21-0. Concave surface of plate is at bottom edge of all photomicrographs. 50X. As polished. Reduced 5%.

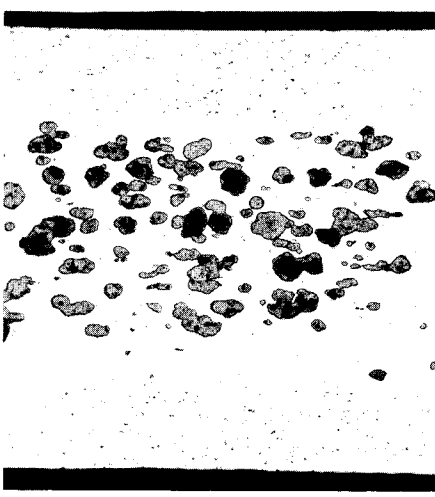
Specimen M-3
(9 in. above
midplane)



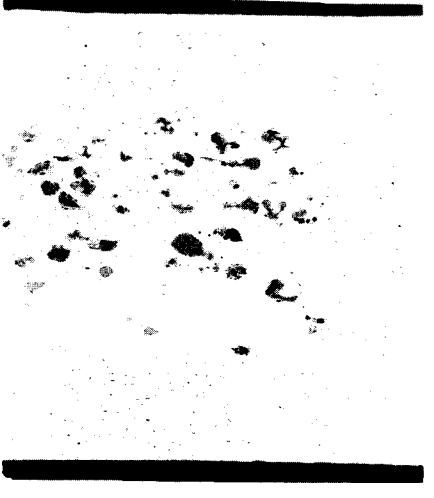
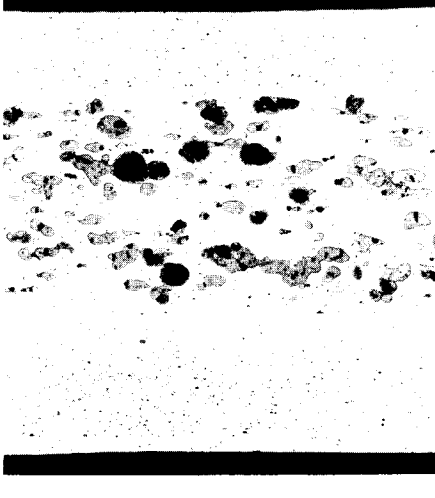
Specimen M-7.5
(4 1/2 in. above
midplane)



Specimen M-12
(midplane)



Specimen M-16.5
(4 1/2 in. below
midplane)



Specimen M-21
(9 in. below
midplane)



Fig. E-3. Typical Cross Sections of a Fuel Plate from HFIR Fuel Element 49-I. Concave surface of plate is at upper edge of all photomicrographs. 50X. As polished. Reduced 5%.

ORNL-4714

UC-25 - Metals, Ceramics, and Materials

INTERNAL DISTRIBUTION

- | | | | |
|--------|-------------------------------|--------|----------------------------------|
| 1-3. | Central Research Library | 55. | M. M. Martin |
| 4. | ORNL - Y-12 Technical Library | 56. | W. R. Martin |
| | Document Reference Section | 57. | R. W. McClung |
| 5-24. | Laboratory Records Department | 58. | R. V. McCord |
| 25. | Laboratory Records, ORNL RC | 59. | J. R. McWherter |
| 26. | ORNL Patent Office | 60. | P. Patriarca |
| 27. | G. M. Adamson, Jr. | 61. | F. L. Peishel |
| 28. | S. Beall | 62. | S. Peterson |
| 29. | R. J. Beaver | 63. | J. W. Reynolds |
| 30. | A. L. Boch | 64-68. | A. E. Richt |
| 31. | W. D. Burch | 69. | M. Rosenthal |
| 32. | C. Cagle | 70. | A. C. Schaffhauser |
| 33. | R. D. Cheverton | 71. | F. M. Sims |
| 34. | T. E. Cole | 72. | T. M. Sims |
| 35. | G. L. Copeland | 73. | G. M. Slaughter |
| 36. | J. A. Cox | 74. | D. B. Trauger |
| 37. | F. L. Culler, Jr. | 75. | J. E. Van Cleve |
| 38. | J. E. Cunningham | 76. | A. M. Weinberg |
| 39. | R. G. Donnelly | 77. | W. J. Werner |
| 40. | J. H. Erwin | 78. | G. D. Whitman |
| 41. | D. E. Ferguson | 79. | F. W. Wiffen |
| 42. | B. E. Foster | 80. | C. M. Adams, Jr.
(consultant) |
| 43. | J. H. Frye, Jr. | 81. | Leo Brewer (consultant) |
| 44. | W. O. Harms | 82. | Walter Kohn (consultant) |
| 45. | R. F. Hibbs | 83. | Jan Korringa
(consultant) |
| 46-48. | M. R. Hill | 84. | Sidney Siegel
(consultant) |
| 49. | E. M. King | | |
| 50. | K. K. Klindt | | |
| 51-53. | R. W. Knight | | |
| 54. | A. L. Lotts | | |

EXTERNAL DISTRIBUTION

85. R. E. Anderson, Space Nuclear Systems Office, AEC,
Washington, DC 20545
86. D. Bailly, AEC, Washington, DC 20545
87. R. D. Baker, Los Alamos Scientific Laboratory, P.O. Box 1663,
Los Alamos, NM 87544
- 88-90. B. J. Beers, Idaho Operations Office, AEC, Idaho Falls, ID 38401
91. W. C. Bills, Idaho Operations Office, AEC, Idaho Falls, ID 38401
92. M. Binstock, Kerr-McGee Corporation, P.O. Box 315, Crescent,
OK 73028
93. H. M. Burte, Air Force Materials Laboratory, Wright-Patterson
Air Force Base, OH 45433
- 94-95. E. G. Case, Director, Division of Reactor Standards, AEC,
Washington, DC 20545

96. W. P. Chernock, Combustion Engineering, Inc., 1000 Prospect Hill Road, Windsor, CT 06095
97. W. C. Compas, United Nuclear Corporation, Grasslands Road, Elmsford, NY 10523
98. D. F. Cope, AEC, RDT, SSR, Oak Ridge National Laboratory
99. J. C. Crawford, Jr., Division of Reactor Development and Technology, AEC, Washington, DC 20545
100. G. W. Cunningham, Division of Reactor Development and Technology, AEC, Washington, DC 20545
101. Defense Materials Information Center, Battelle Memorial Institute, 505 King Ave., Columbus, OH 43209
102. R. P. Denise, Division of Reactor Development and Technology, AEC, Washington, DC 20545
103. N. J. Donahue, AEC, Savannah River Operations Office, P.O. Box A, Aiken, SC 29802
104. E. A. Evans, WADCO Corporation, P.O. Box 1970, Richland, WA 99352
- 105-109. Executive Secretary, Advisory Committee on Reactor Safeguards, AEC, Washington, DC 20545
110. W. C. Francis, Idaho Nuclear Corporation, P.O. Box 1845, Idaho Falls, ID 83401
111. B.R.T. Frost, Argonne National Laboratory, 9700 S. Cass Ave., Argonne, IL 60439
112. P. F. Gast, LMFBR Program Office, Argonne National Laboratory, 9700 S. Cass Ave., Argonne, IL 60439
113. D. C. Goldberg, Westinghouse Astronuclear Laboratory, P.O. Box 10864, Pittsburgh, PA 15236
114. M. J. Graber, Idaho Nuclear Corporation, P.O. Box 1845, Idaho Falls, ID 83401
115. D. H. Gurinsky, Brookhaven National Laboratory, 29 Cornell Ave., Upton, Long Island, NY 11973
116. P. N. Gustafson, Westinghouse, Bettis Atomic Power Laboratory, P.O. Box 79, West Mifflin, PA 15122
117. E. E. Hayes, E. I. du Pont de Nemours and Company, 1007 Market St., Wilmington, DE 19898
118. M. E. Jackson, Argonne National Laboratory, 9700 S. Cass Ave., Argonne, IL 60439
119. R. Jones, AEC, Washington, DC 20545
120. E. E. Kintner, Division of Reactor Development and Technology, AEC, Washington, DC 20545
121. V. Kolba, Argonne National Laboratory, 9700 S. Cass Ave., Argonne, IL 60439
122. C. F. Leitten, Jr., Union Carbide Corporation, Carbon Products Division, P.O. Box 6087, Cleveland, OH 44101
123. M. Levenson, Argonne National Laboratory, 9700 S. Cass Ave., Argonne, IL 60439
124. Library, Westinghouse Atomic Power Division, P.O. Box 355, Pittsburgh, PA 15230
125. Library, USAEC, Room G-049, Washington, DC 20545
126. Library, General Electric Company, 310 DeGuigne Drive, Sunnyvale, CA 94086
127. J. J. Lynch, NASA Headquarters, Code RN, 600 Independence Ave., Washington, DC 20545
128. P. W. McDaniel, Division of Research, AEC, Washington, DC 20545

- 129-131. P. A. Morris, Director, Division of Reactor Licensing, AEC, Washington, DC 20545
132. D. A. Moss, RDT Site Office, AEC, P.O. Box 2108, Idaho Falls, ID 83401
133. P. Murray, Westinghouse Advanced Reactor Division, Waltz Mill Site, P.O. Box 158, Madison, PA 15663
134. M. V. Nevitt, Argonne National Laboratory, 9700 S. Cass Ave., Argonne, IL 60439
135. E. C. Norman, Division of Reactor Development and Technology, AEC, Washington, DC 20545
136. H. Pearlman, Atomics International, P.O. Box 309, Canoga Park, CA 91304
137. J. B. Phillipson, Idaho Nuclear Corporation, P.O. Box 1845, Idaho Falls, ID 83401
138. K. H. Puechl, Manager, NAUS Division, NUMEC, Apollo, PA 15613
139. W. O. Rathbun, AEC, Richland, WA 99352
140. D. Rausch, AEC, Washington, DC 20545
141. W.L.R. Rice, USAEC Scientific Representative, American Embassy, Box 40, FPO, New York, NY 09510
142. L. W. Roberts, Lawrence Radiation Laboratory, P.O. Box 808, Livermore, CA 94550
143. L. S. Rubenstein, AEC, Washington, DC 20545
144. J. Sako, c/o Office of the Assistant Director, Pacific Northwest Laboratories, P.O. Box 999, Richland, WA 99352
145. R. J. Schwinghamer, George C. Marshall Space Flight Center, Huntsville, AL 35800
146. W. F. Sheely, WADCO Corporation, P.O. Box 1970, Richland, WA 99352
147. F. L. Sherman, Texas Instruments, Inc., 34 Forest Street, Attleboro, MA 02703
148. J. M. Simmons, Division of Reactor Development and Technology, AEC, Washington, DC 20545
149. E. E. Sinclair, Division of Reactor Development and Technology, AEC, Washington, DC 20545
150. E. E. Stansbury, Department of Metallurgical Engineering, the University of Tennessee, Knoxville, TN 37901
151. R. H. Steele, Division of Naval Reactors, AEC, Washington, DC 20545
152. D. K. Stevens, Division of Research, AEC, Washington, DC 20545
153. E. F. Sturcken, Savannah River Laboratory, E. I. de Pont de Nemours and Company, Aiken, SC 29801
154. J. A. Swartout, Union Carbide Corporation, 270 Park Ave., New York, NY 10017
- 155-162. Technical Library, Idaho Nuclear Corporation, P.O. Box 1845, Idaho Falls, ID 83401
163. F. H. Tingey, Idaho Nuclear Corporation, P.O. Box 1845, Idaho Falls, ID 83401
164. G. Tuer, Savannah River Laboratory, E. I. du Pont de Nemours and Company, Aiken, SC 29801
165. A. Van Echo, Division of Reactor Development and Technology, AEC, Washington, DC 20545
166. W. R. Voight, Jr., AEC, Washington, DC 20545
167. V. Waller, AEC, Washington, DC 20545

- 168. W. W. Ward, AEC, Washington, DC 20545
- 169. C. Weber, AEC, Washington, DC 20545
- 170. L. J. Weber, Idaho Nuclear Corporation, P.O. Box 1845,
Idaho Falls, ID 83401
- 171. M. S. Wechsler, Ames Laboratory, Iowa State University,
Ames, IA 50010
- 172. S. C. Weaver, U.S. Nuclear, Inc., Oak Ridge, TN 37830
- 173. M. J. Whitman, Division of Reactor Development and Technology,
AEC, Washington, DC 20545
- 174. M. C. Whittels, Division of Research, AEC, Washington, DC 20545
- 175. Laboratory and University Division, AEC, Oak Ridge Operations
- 176. Patent Office, AEC, Oak Ridge Operations
- 177-369. Given distribution as shown in TID-4500 under Metals, Ceramics,
and Materials category (25 copies - NTIS)